Post-transcriptional regulation of the long non-coding RNA HOTAIRM1 involved in cancer

Romane Monnet

Department of Biochemistry

School of Biomedical Sciences

Faculty of Medicine and Health Sciences

McGill University, Montreal

April 2024

A thesis submitted to McGill University in partial fulfillment of the requirements of the degree of Master of Science.

Table of Contents

Abstract

The advent of high-throughput DNA sequencing has led to the emergence of long non-coding RNAs (lncRNAs) as a large class of regulators and effectors of cellular processes with roles in numerous diseases. One such example is HOX antisense intergenic RNA myeloid 1 (HOTAIRM1), which exhibits intriguing duality in cancer as it can act either as a tumor suppressor or an oncogene. Our objective was to investigate its post-transcriptional regulation, in order to set the groundwork for further studies looking into this cancer context-dependent duality. We began by establishing which alternatively spliced HOTAIRM1 isoforms are predominant in our models. We then determined the half-lives of these isoforms, including the effect of isoginkgetin on stability. Next, we verified that the exon-junction complex (EJC) is deposited onto HOTAIRM1. We then investigated the RNA degradation mechanisms affecting HOTAIRM1 and found that a translation-dependent mechanism that is not nonsense-mediated decay (NMD) nor microRNA induced silencing complex (miRISC) is at play. Finally, we explored HOTAIRM1's relationship with miRNAs in the context of cancer, focusing on the miRNAs which bind HOTAIRM1's alternatively spliced exon 2 and how these may be differently expressed in cancer. Overall, this project investigated the post-transcriptional regulation of the alternatively spliced lncRNA HOTAIRM1 to gain a better understanding of its compelling role in cancer as tumor suppressor and oncogene, depending on isoform and cellular context.

Résumé

L'avènement du séquençage de l'ADN à haut débit a conduit à l'émergence des ARNs longs non-codants (ARNlncs) en tant que classe importante de régulateurs et d'effecteurs de processus cellulaires jouant un rôle dans de nombreuses maladies. Un exemple est l'ARN intergénique antisens HOX myéloïde 1 (HOTAIRM1), qui présente une dualité intrigante dans le cancer, puisqu'il peut agir soit comme suppresseur de tumeur, soit comme oncogène. Notre objectif était d'étudier sa régulation post-transcriptionnelle, afin de poser les bases pour d'autres études portant sur cette dualité dépendante du contexte du cancer. Nous avons commencé par établir quelles isoformes résultant de l'épissage alternatif d'HOTAIRM1 sont prédominantes dans nos modèles. Nous avons ensuite déterminé les demi-vies de ces isoformes, y compris l'effet de l'isoginkgétine sur la stabilité. Puis, nous avons vérifié que le complexe de la jonction des exons (EJC) est déposé sur HOTAIRM1. Nous avons ensuite étudié les mécanismes de dégradation de l'ARN affectant HOTAIRM1 et découvert qu'un mécanisme dépendant de la traduction, qui n'est ni la dégradation médiée par le non-sens (NMD), ni le complexe de silençage induit par les microARNs (miRISC), est à l'œuvre. Enfin, nous avons exploré la relation entre HOTAIRM1 et les miARNs dans le contexte du cancer, en nous concentrant sur les miARNs qui se lient à l'exon 2 alternativement épissé de HOTAIRM1 et la façon dont ils peuvent être exprimés différemment dans le cancer. Dans l'ensemble, ce projet a étudié la régulation post-transcriptionnelle de l'ARNlnc HOTAIRM1 alternativement épissé afin de mieux comprendre son rôle dans le cancer en tant que suppresseur de tumeur et oncogène, en fonction de l'isoforme et du contexte cellulaire.

Acknowledgements

Thank you to my supervisor, Dr. Josée Dostie, for warmly welcoming me into your lab, providing feedback on my project, and encouraging me to pursue my interests. Thank you to Dana for the chats and for sharing your experimental and theoretical expertise with me, acquired through many years in the lab. Thank you to Ian for sharing your endless opinions on my experimental designs and for suggesting “Maybe HOTAIRM1 got lost in translation” as my alternative thesis title. Thank you to Rachel for encouraging me every step of the way and for being such a wonderfully kind presence in the lab. Thank you to Xian for helping me out with my oddly timed experiments and for greeting me with a smile every morning. Thank you to all other members of the Dostie lab that I had the pleasure of interacting with (Theodora, Afrida, Natalie, Ali, Chloe, Riley, Laura, Remi) for your help and friendship throughout the years.

Thank you to everyone who’s helped me with this research in one way or another. To members of the Gallouzi lab, with a special mention to Amr, thank you for patiently and passionately teaching me everything you know about benchwork and scientific thinking during my undergraduate research journey, it has truly helped me get to where I am today. To the members of my research advisory committee, Drs. Jerry Pelletier and Marc Fabian, thank you for your insight that allowed my project to grow into what it has become. To my thesis examiner, Dr. Jose Teodoro, thank you for your feedback on this work. To the Défi Canderel initiative, thank you for awarding me the Canderel Graduate Studentship to help fund my studies.

Thank you to all the friends I’ve made along this journey, you have provided a kind, bright and encouraging community during my graduate studies. To my friends from McIntyre 8th and 9th floors (Huang lab, Pelletier lab, Chang lab, Pastor lab, Cockburn lab, Vera Ugalde lab), thank you for the corridor chats, for sharing advice, and for making me laugh every day. To my friends from the Department of Biochemistry, it was a pleasure attending seminars and social events with you. To my friends from the Goodman Cancer Institute, I will cherish our lunchtime discussions in the

atrium. To my fellow teaching assistants, thank you for sharing the ups and downs of teaching with me. To the GCI team, with a special mention to Trina and Anamaria, thank you for providing such a supportive working environment for me to flourish in and explore new interests. To Mario and the rest of the building services team, thank you for keeping our lab spotless and cheering me up after long days at the lab.

Last but not least, thank you to everyone outside of the biochemistry community who has cheered me on from wherever you are. To my parents and grandparents, thank you for your unwavering support and encouragement. To my sisters, thank you for the entertaining calls at lunchtime and during experiment incubations. To my friends from Montreal and beyond, thank you for your friendship over the years and for enthusiastically supporting me and my research endeavours despite never fully understanding what I do.

I have been extremely lucky during my time here and I hope to be surrounded by such wonderful and remarkable individuals as I continue journeying through life!

List of Figures and Tables

Table 1. Existing studies supporting HOTAIRM1's role in multiple cancers by acting as a competing endogenous RNA (ceRNA).

Table 2. Cancer involvement of 7 miRNAs predicted to bind HOTAIRM1's exon 2.

Supplemental data 1. Preliminary knockdown time course for optimization, testing three UPF1 siRNAs over six time points.

Supplemental data 2. Primer pair efficiency testing of novel NORAD, MALAT1, UPF1, GAS5 and 18S rRNA primer pairs.

Supplemental data 3. Comprehensive available list of HOTAIRM1-binding miRNAs.

List of Abbreviations

4sU	4-thiouridine
ACC	Adenoid Cystic Carcinoma
ActD	Actinomycin-D
ARE	AU-rich element
ATCC	American Type Culture Collection
BRIC	5′-BrU immunoprecipitation
BrU	5’-bromouridine
BSA	Bovine Serum Albumin
cDNA	Complementary DNA
ceRNA	Competing endogenous RNA
CESC	Cervical Squamous Cell Carcinoma and Endocervical Adenocarcinoma
CHX	Cycloheximide
CLIP	Crosslinking immunoprecipitation
COMD	Codon optimality-mediated RNA decay
DMEM	Dulbecco’s Modified Eagle Medium
DNA	Deoxyribonucleic acid
DNase	Deoxyribonuclease
dNTP	Deoxynucleoside triphosphates
EEF	Eukaryotic elongation factor
EIF	Eukaryotic initiation factor
EJC	Exon-junction complex
ENCODE	Encyclopedia Of DNA Elements
ER	Estrogen receptor
ERF	Eukaryotic release factor

EU	5’-ethynyluridine
FBS	Fetal Bovine Serum
FT	Flow through
GEPIA	Gene Expression Profiling Interactive Analysis
GTEx	Genotype-Tissue Expression
GWIPS-viz	Genome Wide Information on Protein Synthesis visualized
HM123	HOTAIRM1 spliced variant with exons 1, 2 and 3
HM13	HOTAIRM1 spliced variant with exons 1 and 3
HMu	HOTAIRM1 unspliced variant
HRP	Horseradish peroxidase
HuR	Human antigen R
IgG	Immunoglobulin G
IP	Immunoprecipitation
IRES	Internal ribosomal entry site
IsoG	Isoginkgetin
Kb	Kilobase
KICK	Kidney Chromophobe
KIRC	Kidney Renal Clear Cell Carcinoma
LGG	Low-Grade Glioma
lincRNA	Long intergenic non-coding RNA
lncRNA	Long non-coding RNA
Luc	Luciferase
Luc-i	Intron-containing Luciferase
m6A	N6-methyladenosine
m7G	7-methylguanylate cap
MCS	Multiple cloning site

Met	Methionine
miRNA, miR	Micro RNA
mRNA	Messenger RNA
ncRNA	Non-coding RNA
NGD	No-Go decay
NMD	Nonsense-mediated decay
NSD	Non-Stop decay
ORF	Open reading frame
PBS	Phosphate buffered saline
PCR	Polymerase chain reaction
PDB	Protein data bank
PIC	Pre-initiation complex
PROMPT	Promoter upstream transcript
PTC	Premature termination codon
RA	Retinoic acid
Ribo-Seq	Ribosome profiling sequencing
RIP	RNA immunoprecipitation
RNA	Ribonucleic acid
RNase	Ribonuclease
RNC-Seq	Ribosome-nascent chain complex sequencing
RNP	Ribonucleoprotein
RPMI	Roswell Park Memorial Institute 1640 Medium
rRNA	Ribosomal RNA
RT-qPCR	Reverse transcription quantitative polymerase chain reaction
SDS-PAGE	Sodium dodecyl sulphate polyacrylamide gel electrophoresis
siNC	siRNA negative control

siRNA	Small interfering RNA
smFISH	Small molecule fluorescent in situ hybridization
snoRNA	Small nucleolar RNAs
snRNP	Small nuclear ribonucleoprotein
SOC	Super Optimal broth with Catabolite repression
TAE	Tris-Acetate-EDTA
TBE	Tris-Borate-EDTA
TCGA	The Cancer Genome Atlas
tRNA	Transfer RNA
UTR	Untranslated region
UV	Ultraviolet
UVM	Uveal Melanoma

Introduction

Non-coding RNAs (ncRNAs)

The central dogma of molecular biology proposes that the main goal of RNA is to act as an intermediate between DNA, which carries the genetic information, and proteins, which act as cellular effectors (1). These RNAs, termed messenger RNAs (mRNAs), have been extensively studied over the past decades. The discovery of H19, the first eukaryotic non-coding RNA (ncRNA), eventually prompted further investigation regarding the existence of ncRNAs (2,3). The sequencing of the human genome and the discovery of pervasive transcription in the early 2000s led to further developments in this field, and it was later shown that mRNAs constitute only a small fraction of the total amount of RNA inside cells, with the vast majority of the human genome being non-coding (4). Indeed, small ncRNAs such as microRNAs (miRNAs), small interfering RNAs (siRNAs), transfer RNAs (tRNAs), small nucleolar RNAs (snoRNAs), ribosomal RNAs (rRNAs) and long non-coding RNAs (lncRNAs) are abundantly present in cells (Figure 1) (4). Instead of encoding proteins, ncRNAs function directly as structural, catalytic or regulatory molecules (5).

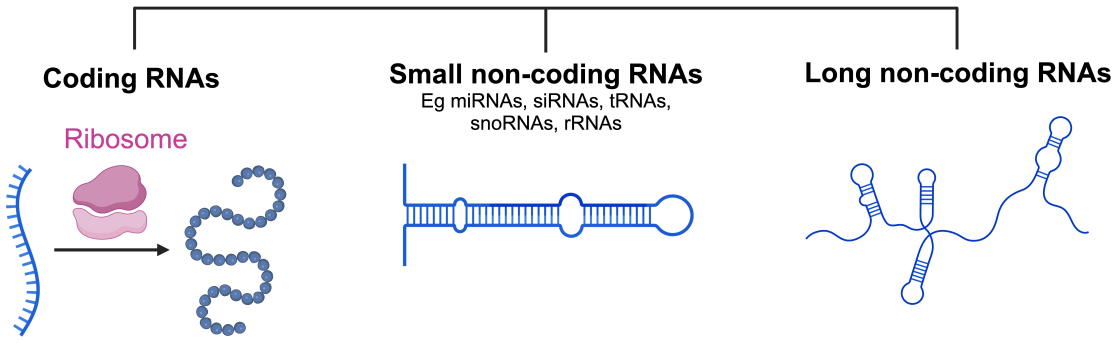

Figure 1. Types of coding and non-coding RNAs. Coding mRNAs, translated by ribosomes into peptides; small ncRNAs e.g. miRNAs, siRNAs, tRNAs, snoRNAs and rRNAs; long ncRNAs. Adapted from Joshi and Rajender, 2020 (6,7).

Long non-coding RNAs (lncRNAs)

The biological advances made possible by high-throughput sequencing and the efforts of large-scale international consortia have helped propel the field of lncRNAs (8,9). The Encyclopedia of DNA Elements (ENCODE) has helped identify numerous novel lncRNAs, although many are still awaiting functional validation (10,11). Other studies and consortia found that approximately 80% of the human genome is transcribed, although many genes are tissue-specific during development, and these are not all expressed at once (11-13). Estimates for the number of lncRNAs in the human genome range from 9,000 to 70,000, with only a minor portion of those having been studied (3,10).

LncRNAs are defined as transcripts over 200 nucleotides in length that do not have established protein coding potential (14). The arbitrary limit of 200 nucleotides was set to distinguish them from short non-coding RNAs (14). Although they are defined as lacking protein coding potential, as determined by the presence of extremely short open reading frames (ORFs) and the low abundance of corresponding peptides, some of them have recently been shown to encode micropeptides (15-19). Most lncRNAs are capped, meaning they feature a 7-methylguanylate cap (m^7G) linked to the first nucleotide via a 5' to 5' triphosphate linkage (20,21). The majority of lncRNAs are also polyadenylated, as a series of adenosine monophosphates are added to their 3' end to constitute the polyA tail (21). In addition, many lncRNAs are spliced, a process that will be reviewed in further detail later. LncRNAs can form stable or transient associations with DNA, RNA or proteins (21). They are a heterogeneous group with respects to their evolutionary origin; transcription mechanism, with most of them produced by RNA Polymerase II except a few which are produced from RNA Polymerase III; cellular function; spatial and temporal expression, exhibiting high tissue-specificity and tight regulation during development; and intracellular localization, as they may be strictly nuclear, strictly cytoplasmic or found in both, while some lncRNAs even co-localizing with protein partners in specific subcellular compartments (22).

LncRNAs can be classified according to three main characteristics. Firstly, they can be grouped depending on their relative positions to nearby protein coding genes (22). They may be sense lncRNAs (e.g. BAN, sense to *BCAM*), antisense lncRNAs (e.g. HOTAIRM1, antisense to *HOXA* genes) or intronic lncRNAs (e.g. PCA3, within *PRUNE2*) (23-25). In all three of these cases, their proximity to protein coding genes suggests that they possibly function through a mechanism that affects the transcription of genes nearby, working in cis (22). They may also be intergenic lncRNAs (lincRNAs, e.g. PCAT-1) which have their own promoters and polyA signals, work in trans, and require transportation and localization, although these are rare (22,26). Secondly, lncRNAs can be classified according to their mechanism of action (22). They may play roles in signaling, in response to cellular stimuli to activate genetic expression machinery (e.g. LINK-A) (27). They may act as decoys, to sponge up functional protein factors (e.g. MALAT1) (28). They may act to guide RNA-protein complexes to specific cellular localizations (e.g. NeST) (29). They may also act as scaffolds to help in the assembly of functional protein-RNA complexes (e.g. lincRNA-Cox2) (29). Thirdly, they can be classified according to the cellular processes they are involved in (22). Indeed, they may perform roles in chromatin regulation, transcriptional regulation, splicing, translation, RNA and protein modification, degradation, or act as competing endogenous RNAs (ceRNAs) (30).

HOX transcript antisense intergenic RNA myeloid 1 (HOTAIRM1)

The lncRNA HOX transcript antisense intergenic RNA myeloid 1 (HOTAIRM1) is located in the *HOXA* gene cluster, on chromosome 7, between the *HOXA1* and *HOXA2* genes to which it is antisense (31). It is most highly expressed in cells of myeloid lineage, in fetal brain, and in colon tissues (32). It plays a role in in normal development through its implication in myelopoiesis and neural differentiation and has also been widely shown to be implicated in disease states such as cancer (31,33-47).

HOTAIRM1 is composed of 3 exons, separated by 2 introns (Figure 2A). Due to its weak splicing acceptor site on exon 2 (48), three splicing isoforms are widely observed: the unspliced variant, HMu, with a total size around 4 kilobases (kb); the spliced variant containing all three exons, HM123, whose size is approximately 1 kb (RefSeq NR_038366); and the spliced variant lacking the second exon, HM13, with a size around 0.8 kb (RefSeq NR_038367) (Figure 2B).

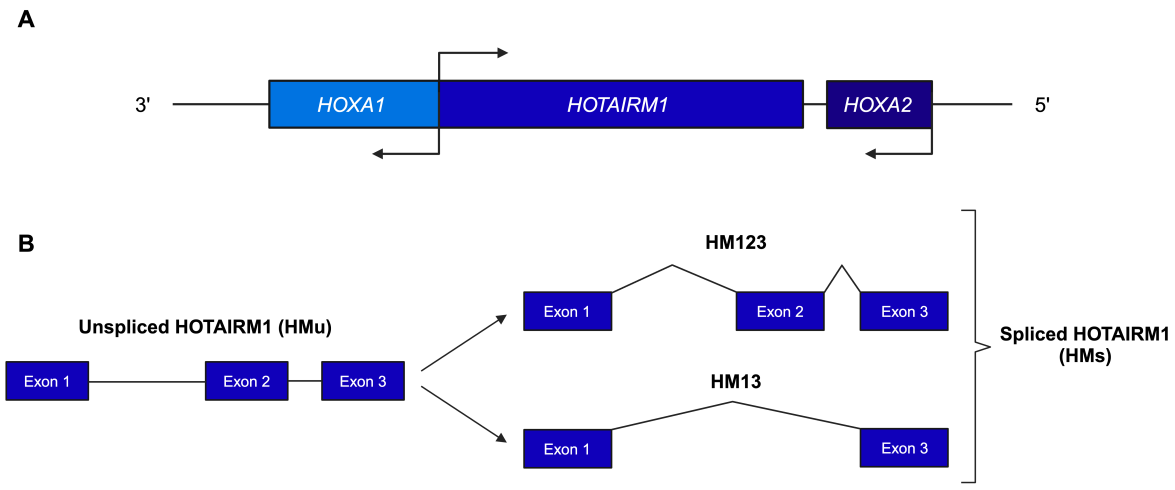

Figure 2. General features of HOTAIRM1. (A) The *HOTAIRM1* gene is located within the *HOXA* gene cluster, between and antisense to the *HOXA1* and *HOXA2* genes. Adapted from Wang and Dostie, 2017 (46). (B) Main isoforms of HOTAIRM1, with unspliced HOTAIRM1 (HMu) yielding spliced HOTAIRM1 (HMs) variants HM123 and HM13. Adapted from Hamilton et al., 2020 (7,43).

HOTAIRM1's involvement in cancer

Multiple groups have focused their research on HOTAIRM1's involvement in cancer. Intriguingly, some studies have shown its involvement as an oncogene, while others have shown that it rather acts as a tumor suppressor.

As an oncogene, it has been shown to be implicated in breast cancer, thyroid cancer, endometrial cancer, glioma, non-small cell lung cancer, hepatocellular carcinoma, and osteosarcoma. Indeed, HOTAIRM1 promotes tamoxifen endocrine resistance in ER-positive

breast cancer cells (34); its genomic amplification drives anaplastic thyroid cancer progression via repressing miR-144 biogenesis (35); it promotes cell proliferation, migration and invasion in endometrial cancer (36); it promotes malignant progression of transformed fibroblasts in glioma stem-like cells remodeled microenvironment via regulating the miR-133b-3p/TGFβ axis (49); it has been implicated in glioma by increasing malignancy, tumor growth and invasion, decreasing tumor sensitivity to temozolomide, acting as a sponge for miR-129-5p and miR-495-3p, sequestering G9a/EZH2/Dnmts away from the *HOXA1* gene, and regulating long-range chromatin interactions within *HOXA* cluster genes (37-39); it promotes cell proliferation and invasion in human glioblastoma by upregulating SP1 via sponging miR-137 (50); it increases migration and invasion in glioblastoma cells (51); it drives cell glycolysis metabolism and tumor progression via the miR-498/ABCE1 axis in non-small cell lung cancer (52); it promotes lenvatinib resistance by downregulating miR-34a and activating autophagy in hepatocellular carcinoma (53); and it promotes aerobic glycolysis and proliferation in osteosarcoma via the miR-664b-3p/Rheb/mTOR pathway (54) (Table 1).

As a tumor suppressor, it was found to be implicated in gastric cancer, ovarian cancer, papillary thyroid cancer, renal cell carcinoma, and colorectal cancer. Indeed, HOTAIRM1 inhibits cell progression in gastric cancer by regulating the miR-17-5p/PTEN axis (40); suppresses cell proliferation and invasion in ovarian cancer by facilitating ARHGAP24 expression via sponging of miR-106a-5p (41); regulates cell proliferation and invasion in papillary thyroid cancer through the miR-107/TDG axis (42); inhibits the hypoxia pathway in clear cell renal cell carcinoma (43), and has been implicated in colorectal cancer by sponging the endogenous miR-17-5p/BTG3 axis in 5-fluorouracil resistant colorectal cancer cells and inhibiting cell proliferation (44,45) (Table 1).

Moreover, data from the Gene Expression Profiling Interactive Analysis (GEPIA), which analyzed RNA sequencing expression data of 9,736 tumors and 8,587 normal samples from The Cancer Genome Atlas (TCGA) and the Genotype-Tissue Expression (GTEx) projects, shows that

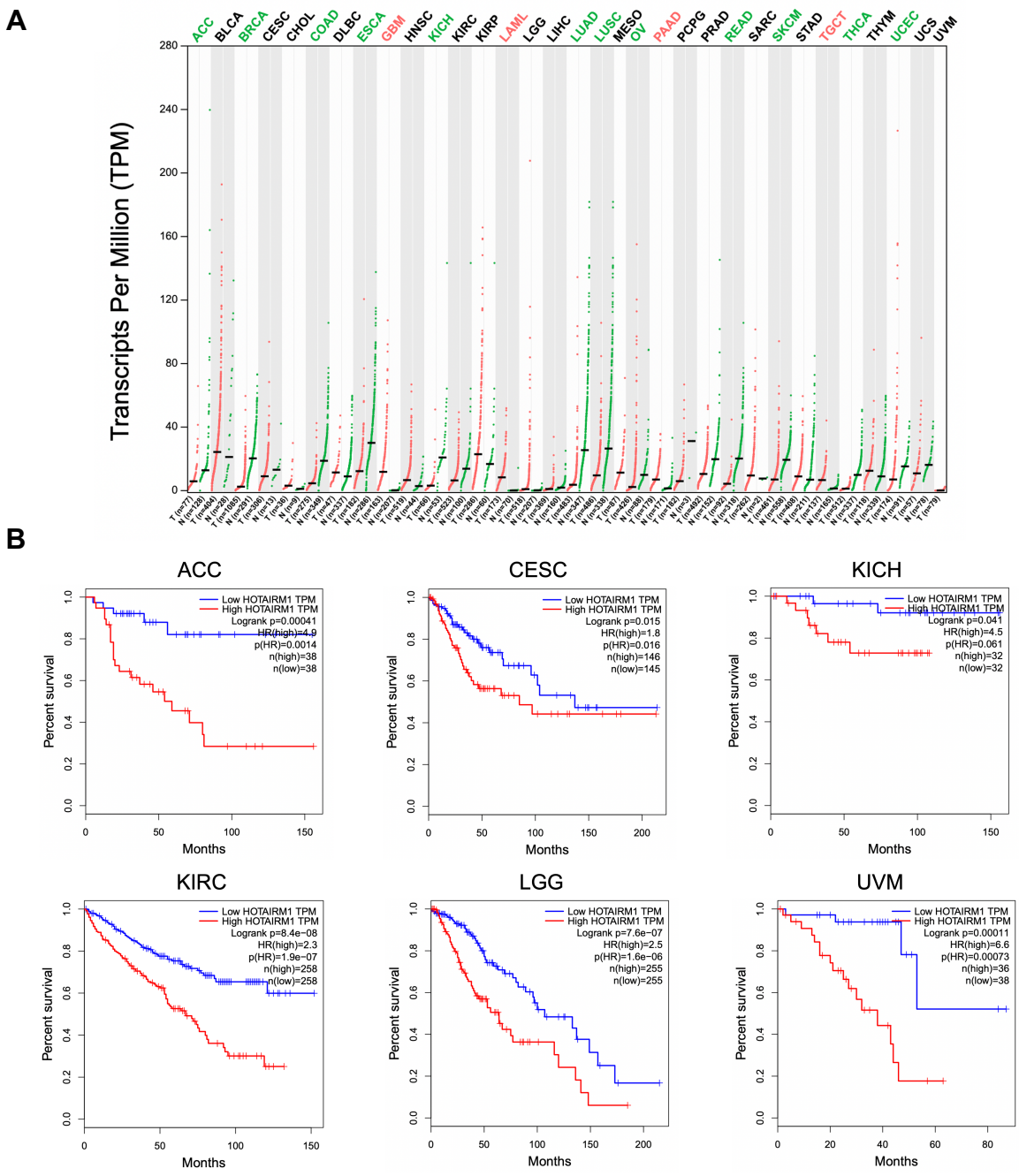

Figure 3. HOTAIRM1's involvement in cancer. Data obtained from GEPIA (55). (A) HOTAIRM1 transcripts per million (TPM) per cancer subtype in tumor tissue (T, red dots) compared to normal tissue (N, green dots). (B) Kaplan-Meier plots highlighting HOTAIRM1's involvement in survival in Adenoid Cystic Carcinoma (ACC), Cervical Squamous Cell Carcinoma and Endocervical Adenocarcinoma (CESC), Kidney Chromophobe (KICH), Kidney Renal Clear Cell Carcinoma (KIRC), Low-Grade Glioma (LGG) and Uveal Melanoma (UVM).

HOTAIRM1 is differentially expressed (either up- or down-regulated) in many cancers (Figure 3A) and Kaplan-Meier plots highlight its implication in cancer survival (Figure 3B) (32,55,56).

Table 1. Existing studies supporting HOTAIRM1's role in multiple cancers by acting as a competing endogenous RNA (ceRNA).

Cancer	HOTAIRM1 expression	miRNA	Target	Reference
Glioma	↑ Increased	miR-129-5p	Unknown	(37)
		miR-495-3p	Unknown	(37)
		miR-133b-3p	TGFB	(49)
Glioblastoma		miR-137	SP1	(50)
		miR-153-50	SNAI2	(51)
Non-small cell lung cancer		miR-498	ARCE1	(52)
Hepatocellular carcinoma		miR-34a	Beclin-1	(53)
Osteosarcoma		miR-664-30	Rheb	(54)
Ovarian cancer	↓ Decreased	miR-17-5p	PTEN	(40)
Gastric cancer		miR-106a-5p	ARHGAP24	(41)
Papillary thyroid cancer		miR-107	TDG	(42)
Colorectal cancer		miR-17-5p	BTG3	(45)

Translation of lncRNAs

Translation is the process whereby RNAs, composed of nucleotides, are used to produce proteins, also known as polypeptides, composed of amino acids (57). This is performed by the ribosome, a macromolecule containing rRNAs and proteins (57). Translation occurs in three phases: initiation, during which the ribosome assembles on the target RNA with the help of eukaryotic initiation factors (EIFs); elongation, during which the ribosome proceeds along the nucleotide chain and produces the peptide chain with the help of eukaryotic elongation factors (EEFs); and termination upon reaching a stop codon, during which the ribosome detaches from

the RNA transcript and releases the polypeptide with the help of eukaryotic release factors (ERFs) (57). Briefly, the pre-initiation complex (PIC) scans through the secondary structures of the 5' untranslated region (UTR) until an AUG initiation codon is reached, at which point elongation occurs until a stop codon is reached (58). Translation induces a switch in cap-binding protein composition, from the nuclear cap-binding proteins CBP80 and CBP20 to the cytoplasmic cap-binding protein EIF4E (59).

Although lncRNAs are generally considered as a class of RNAs without protein-coding potential, there is increasing evidence pointing to some of them encoding micropeptides (15-19,60). The first evidence for lncRNAs with coding abilities came from a study by Ruiz-Orera et al. showing that the majority of lncRNAs expressed in human cells were bound by ribosomes, and that the ribosomal conservation pattern was consistent with translation of micropeptides (61). The emergence of high-throughput technologies like ribosome-nascent chain complex sequencing (RNC-Seq) and ribosome profiling sequencing (Ribo-Seq) has helped propel the field by demonstrating that many lncRNAs have short ORFs and encode micropeptides (60,62,63). Moreover, the majority of lncRNAs are bound by the m^7G cap, hence they can initiate translation through a cap-dependent mechanism (64). In addition, lncRNAs containing internal ribosome entry sites (IRESs) can be translated in a cap-independent manner (65). Interestingly, a study by Ji et al. estimated that 40% of lncRNAs and pseudogene RNAs expressed in human cells are translated (66). The same study showed that lncRNAs which get translated are mostly found in the cytoplasm, while lncRNAs which do not get translated are mostly located in the nucleus (66).

HOTAIRM1 is no exception, and there is evidence that HOTAIRM1 may be undergoing translation. Firstly, mass spectrometry of HOTAIRM1-bound proteins has identified nuclear cap binding protein subunit 1 (NCBP1, also known as CBP80), nuclear cap binding protein subunit 3 (NCBP3, also known as CBP20) and EIF4E, indicating that it is likely capped and could undergo cap-dependent translation initiation (67). Secondly, the fact that we observe both nuclear (NCBP1 and NCBP3) and cytoplasmic (EIF4E) cap-binding proteins in this dataset indicates that at least

one pioneer round of translation occurred for this switch to take place (59,67). Thirdly, analysis of the HOTAIRM1 transcript using the NCBI's Open Reading Frame Finder identified many ORFs in the transcript (68). Finally, analysis and visualization of Ribo-seq data obtained through ribosome profiling using the Genome Wide Information on Protein Synthesis visualized (GWIPS-viz) genome browser revealed that HOTAIRM1 appears to be ribosome-bound, which is yet another indicator of its potential for translation (69).

Post-transcriptional regulation: RNA stability and degradation

RNA degradation can occur either in a normal context as a regulated and continuous turnover mechanism, or in an abnormal context linked to quality control surveillance pathways that detect and degrade defective RNA transcripts (70). RNA-destabilizing mechanisms rely on three types of RNA-degrading enzymes (RNases): endonucleases, 5' exonucleases and 3' endonucleases, which degrade RNA internally, from the 5' end and from the 3' end, respectively (70). Human RNAs have evolved to avoid 5' exonuclease activity thanks to their m^7G protective cap, which can be removed by decapping proteins to allow 5' exonucleases to act (71). They have also evolved to avoid 3' exonuclease activity by the exosome complex thanks to their polyA tail, which undergoes progressive deadenylation, thus providing a timing mechanism to confer a specific half-life to the transcript (72). The best characterized stabilizing and destabilizing elements are AU-rich elements (AREs) which are bound by various proteins and serve to stabilize or destabilize the transcript, often in response to intracellular or extracellular signals (73). Select mechanisms of RNA destabilization and degradation, namely nonsense-mediated decay (NMD) and the miRNA induced silencing complex (miRISC), will be discussed later.

Post-transcriptional regulation, including transcript stability, is one particularly poorly understood aspect of lncRNAs (74). It is generally assumed that lncRNAs are less stable than mRNAs, as demonstrated by the existence of promoter upstream transcripts (PROMPTs) and

other highly unstable lncRNAs in humans (70,75). However, it is now recognized that lncRNAs have a wide diversity of half-lives (74).

Methods to determine RNA half-lives include the use of transcriptional inhibitors such as Actinomycin-D (ActD), a small molecule which intercalates into GC-rich DNA sequences and inhibits RNA polymerases from transcribing, α-amanitin and 5,6-dichloro-1-D-ribofuranosyl-benzimidazole (DRB), as well as metabolic pulse labelling of RNA transcripts using uridine analogs like 4-thiouridine (4sU), 5-ethynyluridine (EU) or 5-bromouridine (BrU) (76,77). In all cases, cells are treated at a given moment and collected over time to obtain a decay curve (76).

Splicing and the exon-junction complex (EJC)

Splicing is the process by which newly transcribed RNAs undergo maturation upon removal of their introns and splicing back of the exons (78). This is performed by the spliceosome, a complex of small nuclear ribonucleoproteins (snRNPs) (78). Notable differences in lncRNA splicing as compared to mRNA splicing include higher alternative splicing, meaning most exist in a very large number of potential isoforms, and less efficient and less specific splicing (79,80).

During the process of splicing, which occurs in the nucleus, a protein complex known as the exon-junction complex (EJC) gets deposited onto the RNA transcript, 20 to 24 nucleotides upstream from the exon-exon junction (81-83). It acts as a sequence-independent marker of exon-exon junctions and provides position-specific memory of the splicing event (81-83). It remains stably bound to the transcript during nuclear export and in the cytoplasm, only leaving upon translation of the transcript (81-83).

The EJC is made up of three core invariable proteins: Eukaryotic translation Initiation Factor 4A3 (EIF4A3, also known as DDX48), Mago Homolog (MAGOH), and RNA Binding Motif Protein 8A (RBM8A, also known as Y14) (82,84-86). EIF4A3 is the main RNA-binding protein in this complex, it is an ATP-dependent RNA helicase from the DEAD-box family which also exhibits ATPase activity (84). MAGOH and RBM8A act as a heterodimer that inhibits EIF4A3's ATPase

activity (81,87). In addition to these core proteins, the EJC is composed of peripheral proteins such as CASC3, PYM1, UPF proteins, factors from the ASAP and PSAP complexes, and others, which join the complex transiently throughout the RNA's lifespan (88).

The EJC was shown to have roles in splicing, as EJC proteins prevent the use of cryptic 5' and 3' splice sites; RNA export from the nucleus, by associating with RNA export factors such as ALYREF; subcellular localization; translation, by binding the PYM1, SKAR and CASC3 factors which then recruit translation machinery; and NMD, by associating with UPF3B (81).

Ribosome-mediated disassembly is the predominant EJC removal mechanism (89). In this translation-dependent event, translating ribosomes physically remove EJCs they encounter from the transcript, causing a conformational change in EIF4A3 and the dissociation of the complex (89). PYM1-mediated disassembly is the minor EJC removal mechanism. In this translation-independent event, PYM1 binds the MAGOH-RBM8A dimer and removes it, causing EIF4A3 to adopt an open conformation and detach itself from RNA (90,91). Since PYM1 is a ribosome-associated factor, both ribosome-mediated and PYM1-mediated disassembly may occur cooperatively (89-91).

In a recent study by Chuang et al., two experiments hinted at the fact that the EJC is likely deposited onto HOTAIRM1. Firstly, following transfection with FLAG-RBM8A, crosslinking, immunoprecipitation, and RNA sequencing, they identified HOTAIRM1 as one of their numerous hits (67). Secondly, to validate findings from the sequencing output, they performed transfection with FLAG-EIF4A3 or FLAG-RBM8A, and FLAG immunoprecipitation followed by end-point PCR identified HOTAIRM1 bound to RBM8A but not to EIF4A3 (67). However, it is important to note that these experiments are presented as single replicates, and the authors recommend verification of identified factors by additional methods (67).

Nonsense-mediated decay (NMD)

NMD is a translation-dependent RNA degradation mechanism (92). It is both a quality control mechanism to degrade RNA transcripts with aberrant premature termination codons (PTCs) and a regulatory mechanism used by some transcripts to regulate their levels in a normal context (92). In most transcripts, the stop codon is within the last exon, such that translating ribosomes displace all EJCs. In some cases however, a stop codon occurs before the last EJC, leading to the interaction between ERFs recruited during translation termination and the remaining EJC(s) (89,92). If a termination codon is at least 50 nucleotides upstream from the remaining EJC, this induces NMD, which ultimately leads to endonuclease-mediated degradation, decapping and 5' exonuclease degradation, and deadenylation and 3' exonuclease degradation (93).

Since lncRNAs exhibit many of the characteristics known to initiate NMD, such as the presence of EJCs downstream from a termination codon or long 3' UTRs after a short ORF, it stands to reason that they may be undergoing NMD-mediated degradation (94). In fact, a study by Wery et al. used ribosomal analysis to show that lncRNAs with actively translated short ORFs and long 3' UTRs are responsive to NMD (94). The lncRNA GAS5 has also been experimentally shown to be regulated by NMD under normal conditions (95).

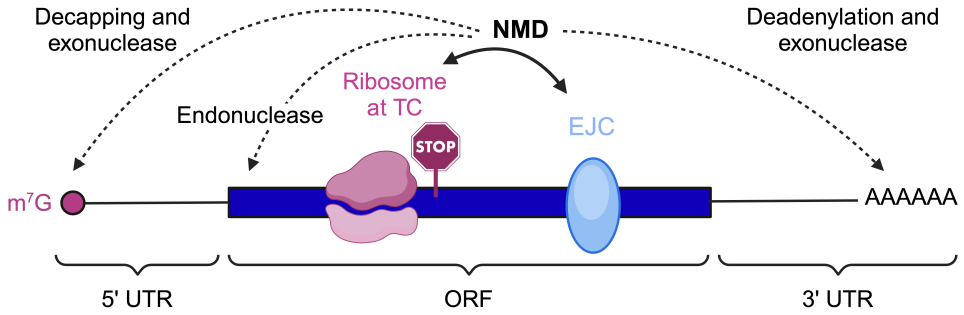

Figure 4. The RNA degradation mechanism nonsense-mediated decay (NMD). When a translating ribosome reaches a termination codon (TC) while there are one or more exon-junction complexes (EJCs) remaining donwstream on the transcript, these interact and induce degradation of the RNA transcript by endonuclease activity, decapping and 5' exonuclease activity, and deadenylation and 3' exonuclease activity. Adapted from Hwang et al., 2021 (7,96).

MicroRNA-induced silencing complex (miRISC)

MicroRNAs (miRNAs) are small ncRNAs involved in RNA silencing and post-transcriptional gene regulation, and it is estimated that approximately 60% of human genes are under regulation by miRNAs (97). MiRNAs can associate with Argonaute proteins such as AGO2 to form the miRNA induced silencing complex (miRISC) (98). The miRISC is then recruited to RNA transcripts via complementary binding between both RNA species, most often in the 3' UTR of mRNAs in humans (98). In cases where complementarity between the miRNA and the RNA target is high, which is rare in humans, the Argonaute protein can slice the target transcript, allowing 5' and 3' exonuclease degradation (98). In cases where there is partial complementarity, there is no slicing but instead decreased translation as well as increased 5' and 3' exonuclease degradation due to decapping and deadenylation (98). There are disagreements within the miRISC field regarding the balance between translational repression and RNA decay. Intriguingly, one study estimated that 48% of transcripts undergo translational repression exclusively, 29% undergo decay only, and 23% undergo both (99,100). For the transcripts that undergo both, evidence points towards a model in which miRNAs induce translational repression before RNA

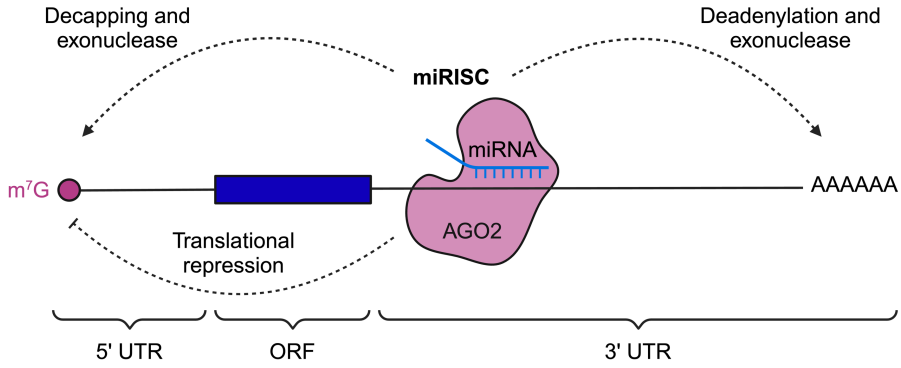

Figure 5. Overview of RNA degradation and translational repression caused by the microRNA-induced silencing complex (miRISC). MicroRNAs bound to AGO2 form the miRISC. Complementary binding between the miRNA and the target RNA recruits AGO2 to the transcript, which causes translational repression, decapping and 5' endonuclease activity, and deadenylation and 3' exonuclease activity. Adapted from Kuzuoğlu-Öztürk et al., 2016 (7,101).

decay occurs (102,103). The effect of miRNAs on translational repression occurs predominantly at the translation initiation stage, though there has been some evidence of it happening post-initiation (104).

Rationale and Objectives

Given the growing evidence pointing towards HOTAIRM1's role in multiple cancers, either as an oncogene or tumor suppressor, as well as the high impact of post-transcriptional regulation on lncRNAs' ability to perform their respective functions, our study aimed to address multiple aspects of HOTAIRM1's post-transcriptional regulation.

Aim 1: Determine HOTAIRM1's stability and half-life

As it has been shown that lncRNAs exhibit an extremely wide spectrum of half-lives when compared to mRNAs, we were particularly interested in investigating HOTAIRM1's stability and half-life as part of its post-transcriptional regulation. Indeed, knowledge on whether it is a short- or long-lived RNA would yield precious insight into its possible roles and functions in cellular contexts. Specifically, we were curious to investigate whether different isoforms, namely the HMu, HM123 and HM13 variants, would exhibit vastly different half-lives. This was considered particularly important as different cell lines and tissues, hence different cancer types as well, express different HOTAIRM1 isoforms.

Aim 2: Investigate destabilizing mechanisms affecting HOTAIRM1

In addition to establishing HOTAIRM1's half-life under normal conditions, we were interested in the RNA destabilizing and degrading mechanisms affecting this transcript's turnover. Due to the high involvement of alternative splicing on HOTAIRM1, we began by investigating whether inhibition of splicing would affect its half-life. Next, we studied whether translation was broadly

involved in its post-transcriptional regulation, before seeing whether specific translation-dependent mechanisms such as NMD were affecting its levels. Furthermore, we investigated whether miRISC independently affects HOTAIRM1 levels, as well as whether NMD and miRISC work jointly to affect its stability.

Aim 3: Elucidate potential links between HOTAIRM1 and miRNAs

Given the abundance of experimental data highlighting the repercussions of interactions between lncRNAs and other ncRNAs such as miRNAs, we were intrigued by the links between HOTAIRM1 and miRNAs. We were especially interested in miRNAs which have been previously implicated in cancer and those binding HOTAIRM1's exon 2, as this exon is alternatively spliced in a cell type-dependent manner.

Overall, we hypothesized that context-dependent alternative splicing of HOTAIRM1 and available miRNA pool may affect HOTAIRM1's half-life and post-transcriptional regulation through various RNA destabilizing mechanisms, which could potentially explain its intriguing dual role in cancer as either oncogene or tumor suppressor.

Materials and Methods

Cell culture

HEK293T and NCCIT cell lines were purchased from the American Type Culture Collection (ATCC, Cat # CRL-3216 and # CRL-2073, respectively). HEK293T cells were cultured in Dulbecco's Modified Eagle Medium (DMEM; Gibco) supplemented with 10% Fetal Bovine Serum (FBS; Gibco). NCCIT cells were cultured in Roswell Park Memorial Institute 1640 Medium (RPMI; Gibco) supplemented with 10% Fetal Bovine Serum (FBS; Gibco). Gene induction and cell differentiation were performed by adding all-trans retinoic acid (RA; Sigma-Aldrich) to 10 µM. Cells were collected at various induction times as specified in the figures. Cells counts were measured using a hematocytometer. Trypsin-EDTA (0.25% Trypsin, 0.53 mM EDTA; Wisent, Cat # 325-045-EL) was used to detach cells from plates. All cells were grown at 37°C in 5 % CO_2 atmosphere.

Cloning and plasmid constructs

The pcDNA3.1(+) plasmid was a kind gift from Dr. Jose Teodoro (McGill University). A 3xFLAG oligonucleotide was ordered from Integrated DNA Technologies (IDT) and the sequence was inserted into the pcDNA3.1(+) backbone using *NheI* and *HindIII*. The EIF4A3 and RBM8A cDNA sequences were obtained from plasmids generated by our lab, pcMYC-EIF4A3 and pcMYC-Y14, respectively. The MAGOH complementary DNA (cDNA) sequence was obtained from the MAGOH (RefSeq NM_002370) Human Tagged ORF Clone (OriGene, Cat # RC203863). This was done through polymerase chain reaction (PCR), with the following primers (Invitrogen).

Primer	Sequence
EIF4A3_PCR (forward)	5’-GAACGGATCCATGGCGAC-3’
EIF4A3_PCR (reverse)	5’-GCATGCTCGAGTCAGATAAGATC-3’
MAGOH_PCR (forward)	5’-GGAAAGCTTATGGAGAGTGACTTTTATC-3’
MAGOH_PCR (reverse)	5’-GATCAGAATTCCTAGATTGGTTTAATCTTGAAG-3’
RBM8A_PCR (forward)	5’-GATAAGCTTGCGGACGTGCTAGATCTTC-3’
RBM8A_PCR (reverse)	5’-GATATGAATTCGTCAGCGACGTCTCCGG-3’

The PCR products, along with the pc3xFLAG plasmid, were digested with *BamHI* and *XhoI* for EIF4A3, *HindIII* and *EcoRI* for MAGOH, and *HindIII* and *EcoRI* for RBM8A, and inserted into pc3xFLAG. All cloning was performed in XL1-Blue bacteria, rendered chemically competent using the calcium chloride method (105). Plasmid transformation into bacteria was performed by incubating on ice for 30 minutes, heat shocking at 37°C for 3 minutes, returning to ice for 5 minutes, and growing in Super Optimal broth with Catabolite repression (SOC) medium at 37°C for 45 minutes. All bacterial cultures were grown at 37°C in LB medium with 100 µg/mL ampicillin or on LB-agar with 100 µg/mL ampicillin. Miniprep, midiprep and maxiprep procedures were performed using PureLink HiPure Plasmid Kits (Invitrogen) as per manufacturer’s instructions. Cloning was validated by agarose gel electrophoresis, western blot analyses and Sanger sequencing. Agarose gels contained ethidium bromide, agarose-D1-LE, and Tris-Acetate-EDTA (TAE) or Tris-Borate-EDTA (TBE) buffers. For Sanger sequencing, samples were sent to the Génome Québec sequencing facility and processed according to platform guidelines.

Small interfering RNA (siRNA) constructs

The knockdowns of UPF1 and AGO2 were performed with small interfering RNA (siRNA). A negative control (siNC) was also used. The siRNA sequences are described below. Knockdowns were validated by western blot analyses.

siRNA	Sequence
siNC	Silencer ® Select Negative Control No. 1 siRNA (Invitrogen, Cat # 4390843)
siUPF1.1	5'-CGAAGGCACUAUCAAAGCATT-3'
siUPF1.2	5'-CAGCGGAUCGUGUGAAGAATT-3'
siUPF1.3	5'-CAACGGACGUGGAAAUACUTT-3'
siAGO2	5'-GGUCUAAAGGUGGAGAUAATT-3'

Transient transfections of plasmids or siRNA

For cloning validation in HEK293T, 0.6 million cells were plated per well in 6-well plates and forward transfected the next day with 2.5 µg of plasmid (pcFLAG-GFP, pc3xFLAG, pc3xFLAG-EIF4A3, pc3xFLAG-MAGOH and pc3xFLAG-RBM8A) using the Lipofectamine 2000 transfection reagent (Invitrogen, Cat # 11668019). For RIP experiments in NCCIT, 3.5 million cells were plated in 10 cm dishes and reverse transfected with 12.5 µg of pc3xFLAG-EIF4A3, pc3xFLAG-MAGOH and pc3xFLAG-RBM8A using the Lipofectamine STEM transfection reagent (Invitrogen, Cat # STEM00015). For knockdown experiments in NCCIT, 0.5 million cells were plated per well in 6-well plates and transfected with 10 µM of siRNA using Lipofectamine RNAiMAX transfection reagent (Invitrogen, Cat # 13778150). All Lipofectamine reactions were performed in OptiMEM Reduced Serum Medium (Gibco, Cat # 31985062). For Luciferase assay experiments in NCCIT, 0.35 million cells were plated per well in 6-well plates and transfected with 1.5 µg of CMV-LUC2CP/intron/ARE (AddGene, Plasmid # 62858) or CMV-LUC2CP/ARE (AddGene, Plasmid # 62857) using JetPRIME transfection reagent (PolyPlus, Cat # 114-01).

Cycloheximide (CHX) time course experiment

HEK293T and NCCIT cells were seeded at 0.35 million cells per well in 6-well plates. Gene induction and cell differentiation were performed 6 hours post-plating by adding 10 µM all-trans retinoic acid (RA; Sigma-Aldrich). Cells were treated with 50 µg/mL of cycloheximide (CHX; 100

mg/mL in DMSO, Thermo Scientific) 52 hours post-plating and collected using Trypsin-EDTA (Wisent, Cat # 325-045-EL) at indicated time points. Following a PBS wash, total RNA was extracted from cells using TRIzol and RT-qPCR was performed as described below.

Actinomycin-D (ActD) pulse-chase experiment

NCCIT cells were seeded at 0.35 million cells per well in 6-well plates. Gene induction and cell differentiation were performed 6 hours post-plating by adding 10 µM all-trans retinoic acid (RA; Sigma-Aldrich). For isoginkgetin (IsoG; Sigma Aldrich, Cat # 416154) experiments, cells were treated 48 hours post-plating with 30 µM of isoG. Cells were then treated with 5 µg/mL of actinomycin-D (ActD; Invitrogen, Cat # A7592) 52 hours post-plating and collected using Trypsin-EDTA (Wisent, Cat # 325-045-EL) at indicated time points. Following a PBS wash, total RNA was extracted from cells using TRIzol and RT-qPCR was performed as described below.

Exogenous RNA immunoprecipitation (RIP)

NCCIT cells were transiently transfected with 3xFLAG-EIF4A3, 3xFLAG-MAGOH or 3xFLAG-RBM8A as described above, RA-induced 6 hours post-plating, and treated with 50 µg/mL of cycloheximide (CHX; 100 mg/mL in DMSO, Thermo Scientific) 47 hours post-plating. Following a PBS wash, cell pellets were lysed 48 hours post-plating in 1 mL lysis buffer (10 mM HEPES pH 7.5, 200 mM NaCl, 2.5 mM MgCl2, 0.5% NP-40 Tergitol, 0.5% Triton X-100, 0.5 mM DTT, 1X Protease Inhibitor Cocktail (Sigma-Aldrich, Cat # P8340), 1 mM PMSF, and 0.1 U/mL RiboLock RNase Inhibitor (Thermo Scientific, Cat # EO0382)) by incubating on ice 15 minutes, shearing through a 23 G needle (20 strokes), sonicating on a Covaris M220 Focused-Ultrasonicator (50W PIP; 10% Duty Factor; 200 Cycles per Burst; 7°C bath temperature; 30s time), and shearing again with a 23 G needle (20 strokes). Lysates were centrifuged at 14,000 rpm for 15 minutes at 4°C to pellet debris. Each RIP used the equivalent of 5 million cells in a final volume of 500 µL, with 10% set aside as input (for western blotting or RT-qPCR). Magnetic Protein G Dynabeads (Invitrogen,

Cat # 10003D) were washed with 5 mg/mL Bovine Serum Albumin (BSA) three times at room temperature, incubated with 5 µg of antibodies against the FLAG epitope (Sigma-Aldrich, Cat # F1804) or a control IgG (Abcam, Cat # ab12073) for 3 hours at 4°C on an end-over-end rotor, and washed again with BSA solution three times at 4°C. Cell lysates were incubated with antibody-conjugated beads for 4 hours at 4°C on an end-over-end rotor. Flow through was set aside (for western blotting or RT-qPCR), then beads were washed with lysis buffer three times for 5 mins at 4°C on end-over-end rotor. Elution was performed using 50 µL lysis buffer supplemented with 3xFLAG peptide (100 µg/mL; APExBIO, Cat # A6001). Sample was collected for western blotting or RT-qPCR. For all samples (input, flowthrough, and pulldown), RNA was extracted using TRIzol and RT-qPCR was performed as described below, and protein was extracted using Laemmli buffer and western blotting was performed as described below.

Endogenous RNA immunoprecipitation (RIP)

NCCIT cells were RA-induced 6 hours post-plating and treated with 50 µg/mL of cycloheximide (CHX; 100 mg/mL in DMSO, Thermo Scientific) 47 hours post-plating. Following a PBS wash, cell pellets were lysed 48 hours post-plating in 1 mL lysis buffer (10 mM HEPES pH 7.5, 200 mM NaCl, 2.5 mM MgCl2, 0.5% NP-40 Tergitol, 0.5% Triton X-100, 0.5 mM DTT, 1X Protease Inhibitor Cocktail (Sigma-Aldrich, Cat # P8340), 1 mM PMSF, and 0.1 U/mL RiboLock RNase Inhibitor (Thermo Scientific, Cat # EO0382)) by incubating on ice 15 minutes, shearing through a 23 G needle (20 strokes), sonicating on a Covaris M220 Focused-Ultrasonicator (50W PIP; 10% Duty Factor; 200 Cycles per Burst; 7°C bath temperature; 30s time), and shearing again with a 23 G needle (20 strokes). Lysates were centrifuged at 14,000 rpm for 15 minutes at 4°C to pellet debris. Each RIP used the equivalent of 5 million cells in a final volume of 500 µL, with 10% set aside as input (for western blotting or RT-qPCR). Magnetic Protein G Dynabeads (Invitrogen, Cat # 10003D) or Protein A Dynabeads (Invitrogen, Cat # 10002D) were washed with 5 mg/mL Bovine Serum Albumin (BSA) three times at room temperature, incubated with 5 µg of antibodies

targeting EIF4A3 (Atlas Antibodies, Cat # HPA021878) or RBM8A (Sigma-Aldrich, Cat # 05-1511) for 3 hours at 4°C on an end-over-end rotor, and washed again with BSA solution three times at 4°C. Cell lysates were incubated with antibody-conjugated beads for 4h at 4°C on an end-over-end rotor. Flow through was set aside (for western blotting or RT-qPCR), then beads were washed with lysis buffer three times for 5 mins at 4°C on end-over-end rotor. Sample was collected for western blotting or RT-qPCR. For all samples (input, flowthrough, and pulldown), RNA was extracted using TRIzol and RT-qPCR was performed as described below, and protein was extracted using Laemmli buffer and western blotting was performed as described below.

RNA extraction

TRIzol reagent (Invitrogen, Cat # 15596026) was used to extract total RNA from cells as per the manufacturer's protocol. Molecular biology grade glycogen (Thermo Scientific, Cat # R0561) was added to aid with precipitation for low abundance samples (RNA immunoprecipitation samples). The resulting RNA pellets were resuspended in RNAse-free water (Wisent, Cat # 809-115-CL) and quantified using a NanoDrop2000 Spectrophotometer (Thermo Scientific). 1 µg of total RNA was treated with RNase-free DNaseI (New England Biolabs, Cat # M0303S) for 15 minutes at 37°C. DNaseI was deactivated for 5 minutes at 75°C.

Complementary DNA (cDNA) generation through reverse transcription

1 µg of RNA was annealed to Random Hexamer Primer (Thermo Scientific, Cat # SO142) at 65°C for 5 mins in the presence of dNTPs (Invitrogen). RNA was then reverse transcribed using SuperScript III Reverse Transcriptase (Invitrogen, Cat # 18080093), adding DTT (Invitrogen, Cat # 18080093) and First-Strand Synthesis Buffer present (Invitrogen, Cat # 18080093), at 55°C for 70 mins followed by 70°C for 15 mins for enzyme deactivation.

Quantitative PCR (qPCR)

qPCR was performed using SsoFast EvaGreen Supermix (Bio-Rad, Cat # 1725204) and a BioRad CFX96 Real-Time PCR System. Data was analyzed using the ΔΔCt method, normalizing expression to 18S ribosomal RNA (18S rRNA; for Actinomycin-D experiments), to input (for RNA immunoprecipitation experiments), or to Phosphoglycerate Kinase 1 (PGK1; for all other experiments). The sequences of primers used for RT-qPCR are described below.

RNA target	Primer sequence
Total HOTAIRM1 (forward)	TAGTTATTGACCTGGAGACTGGTAGC
Total HOTAIRM1 (reverse)	TCAGTGCACAGGTTCAAGCC
Spliced HOTAIRM1 (forward)	AGGGAAGGTAGGGAGCAAACCTATG
Spliced HOTAIRM1 (reverse)	GTTGATGGGTTCAGGCAAAACAGAC
Unspliced HOTAIRM1 (forward)	CTGGAGCTGGTCTCTTTCAACG
Unspliced HOTAIRM1 (reverse)	CCTTTCTAGCATAAGAGCCC
PGK1 (forward)	CAAGAAGTATGCTGAGGCTG
PGK1 (reverse)	TGATGGTGATGCAGCCCCTA
18S rRNA (forward)	GTAACCCGTTGAACCCCATT
18S rRNA (reverse)	CCATCCAATCGGTAGTAGCG
GAPDH (forward)	CCCAGCAAGAGCACAAGAGG
GAPDH (reverse)	TGGTACATGACAAGGTGCGG
NORAD (forward)	GAATGACAGGCCACGTTTGG
NORAD (reverse)	TACGTCGGCAACCTCTTTCC
GAS5 (forward)	TGGACAGTTGTGTCCCCAAG
GAS5 (reverse)	CGTTACCAGGAGCAGAACCA
MALAT1 (forward)	CTGACCCAGGTGCTACACAG
MALAT1 (reverse)	CGTTAGCGCTCCTTCCTTCT
UPF1 (forward)	CACCTCCTACCTGAACAGGAC
UPF1 (reverse)	GTGATGATGCCAATCTGGTCCG
GAPDH intron 1 (forward)	GAAGCTGAGTCATGGGTAGTTG

GAPDH intron 1 (reverse)	CGGTGACATTTACAGCCTGG
GAPDH exons 1-2-3 (forward)	CGGAGTCAACGGATTTGGTC
GAPDH exons 1-2-3 (reverse)	CTTCCCGTTCTCAGCCTTGA

Primer pair efficiency testing

To verify efficiency of all new qPCR primer pairs, qPCR was performed on total gDNA and cDNA from the cell line of interest using five 8-fold serial dilutions. Results were analyzed using CFX Manager and CFX Maestro software, validating primer pairs whose E-value is above 85% and below 115%.

Western blotting

Whole cell extracts were boiled for 15 minutes at 95°C in Laemmli buffer (62.5 mM Tris-HCl pH 6.8, 2% SDS, 7.5% glycerol, 5% β-mercaptoethanol, 0.04% bromophenol blue). Protein samples were resolved by uniform sodium dodecyl sulphate polyacrylamide gel electrophoresis (SDS-PAGE) with a hand-cast 4% stacking gel (0.125 M Tris-HCl pH 6.8, 4% Acryl./0.44% Bis-Acryl., 0.1% SDS, 0.033% APS, 0.2% TEMED) and a variable percentage resolving gel (0.38 M Tris-HCl pH 9.1, 8% to 12.5%of Acryl./0.3% Bis-Acryl., 0.1% SDS, 0.08 % APS, 0.1% TEMED). The EZ-Run Pre-stained Rec Protein Ladder was used to monitor progression and assess band size (Fisher BioReagents, Cat # BP3603500). The gel was run for 20 minutes at 80 V, then for 1 hour at 100 V in a Mini-PROTEAN Tetra Cell (Bio-Rad, Cat # 1658001), with a Mini Trans-Blot Module (Bio-Rad, Cat # 1703935). The gel was transferred onto a 0.45 µm nitrocellulose membrane (Thermo Scientific, Cat # 88018) with 10% methanol using a Hoefer TE77X semi-dry transfer unit at 20 V for 1 hour. Ponceau S staining was performed on membranes for 5 minutes on a rocking platform (Thermo Scientific, Cat # A40000279), washed with ddH_2O, and removed with PBST (PBS, 0.1% Tween-20). Membranes were blocked in 5% skim milk in PBST for 2 hours at room temperature on a rocking platform. Membranes were washed in PBST before incubating with

primary antibodies in 5% skim milk in PBST overnight at 4°C on a rocking platform. Membranes were washed in PBST before incubating with horseradish peroxidase (HRP) conjugated secondary antibodies in 5% skim milk in PBST for 2 hours at room temperature. Membranes were washed in PBST before using chemiluminescence to reveal protein bands with the western Lightning Plus-ECL Enhanced Chemiluminescence reagent (Revvity, Cat # NEL105001EA) as per the manufacturer's instructions. For visualization, film exposure or a ChemiDoc imaging system were used. Quantification was performed with ImageJ, by using the analyze gel rectangular tool, delineating plots, measuring area with the wand (tracing) tool, and comparing to reference gene EEF2 or HuR (106).

Antibody	Manufacturer and Cat #	Dilution
Anti-FLAG-M2 (primary)	Sigma-Aldrich, Cat # F1804	1:2000
Anti-UPF1 (primary)	Bethyl Laboratories, Cat # A301-902A-T	1:10000
Anti-AGO2, clone C34C6 (primary)	Cell Signaling Technology, Cat # 2897	1:1000
Anti-EIF4A3 (primary)	Atlas Antibodies, Cat # HPA021878	1:1000
Anti-MAGOH, clone F-6 (primary)	Santa Cruz Biotechnology, Cat # sc-271365	1:500
Anti-RBM8A, clone 4C4 (primary)	Sigma-Aldrich, Cat # 05-1511	1:500
Anti-EEF2 (primary)	Cell Signaling Technology, Cat # 2332	1:2000
Anti-HuR, clone 3A2 (primary)	Kind gift from Dr. Imed Gallouzi (King Abdullah University of Science and Technology)	1:10000
Anti-mouse (secondary, HRP-conjugated)	AffiniPure rabbit anti-mouse IgG (Jackson ImmunoResearch Laboratories, Cat # 315-035-003)	1:2500
Anti-rabbit (secondary, HRP-conjugated)	AffiniPure goat anti-rabbit IgG (Jackson ImmunoResearch Laboratories, Cat # 111-035-003)	1:2500

Luciferase assay

0.35 million NCCIT cells were plated per well in a 6-well plate and transfected the next day with 1.5 µg plasmid (CMV-LUC2CP/intron/ARE “Luc-i”, AddGene Cat # 62858, and CMV-LUC2CP/ARE “Luc”, AddGene Cat # 62857) using JetPRIME (PolyPlus Sartorius) as per the manufacturer’s instructions. The next day, cells were induced with 10 µM all-trans retinoic acid (RA; Sigma-Aldrich). The fourth day, cells were treated with 30 µM isoginkgetin (IsoG; Sigma Aldrich, Cat # 416154) for 4 hours. Cells were then lysed and collected using Passive Lysis Buffer form the Dual-Luciferase Assay Kit (Promega) by shaking on a rocking platform at room temperature for 20 minutes. Total protein was quantified using a Bradford assay, measuring absorbance at OD = 595 nm (Bio-Rad, Cat # 5000006). 8 µg of total protein was added to 100 µL Luciferase Assay Reagent II and Firefly Luciferase activity was recorded in triplicates.

Results

HOTAIRM1 is spliced alternatively and with cell-type specificity in HEK293T and NCCIT

Since HOTAIRM1 is known to be spliced alternatively and with cell-type specificity (see discussion for an in-depth review of known spliced and unspliced isoforms and their expression in various cell lines), we began by investigating which variants are predominant in our cell lines of interest, namely the human embryonic kidney cell line HEK293T and the human pluripotent embryonal carcinoma cell line NCCIT which can differentiate in response to retinoic acid (RA) (107). We found that, in the HEK293T cell line, spliced HOTAIRM1 (HMs) is the major isoform compared to unspliced HOTAIRM1 (HMu), with an estimated 91% of the lncRNA in its spliced form as compared to 9% in the unspliced form (Figure 6A). We also found that, in the NCCIT cell line, there is a drastic increase in HOTAIRM1 levels upon RA exposure. Indeed, levels of HOTAIRM1 increased over 300-fold regardless of the isoform when treated with RA for 2 days

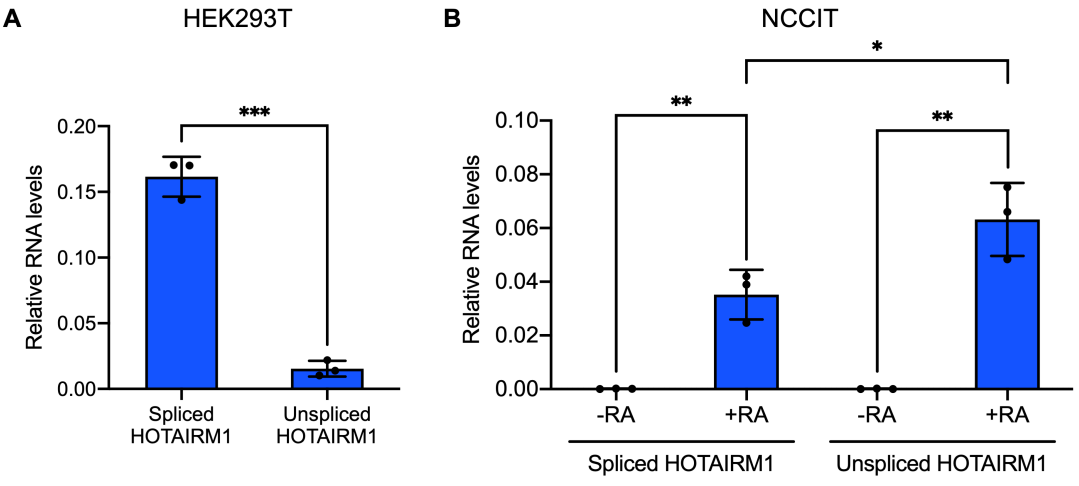

Figure 6. HOTAIRM1 is spliced alternatively and with cell-type specificity. Total RNA from HEK293T cells (A) and untreated (-RA) and RA-induced (+RA) NCCIT cells (B) was quantified. Unpaired t-test, P-value = 0.0001 (HEK293T), P-value = 0.0028 (HMs in NCCIT), P-value = 0.0013 (HMu in NCCIT), P-value = 0.0421 (HMs vs HMu in NCCIT). Experiments were performed in triplicate technological measurements from three biological replicates and standard deviations are shown.

(Figure 6B). Moreover, in the RA-treated cells, inversely to HEK293T cells, HMu is the major isoform compared to HMs, with approximately 64% of the lncRNA in its unspliced form as compared to 36% in the spliced form (Figure 6B). These preliminary findings shed light on the HOTAIRM1 variants present in our models and were instrumental in guiding our experimental design choices throughout this project.

Determining the half-lives of HOTAIRM1 isoforms HMs and HMu

In order to better understand how HOTAIRM1 functions in the cell, we then determined its half-life using the transcriptional inhibitor Actinomycin-D (ActD) in a time course experiment (Figure 7A). We aimed to identify how stable the HOTAIRM1 transcript is, and how much of its expression relies on constant expression from its promoter. We also wanted to see whether HMs and HMu exhibit differences in their stability. 18S ribosomal RNA (rRNA) was chosen as a relative control due to its incredibly high stability, with a half-life around 72 hours, ensuring that it does not negatively impact the accuracy of our half-life measurements (108). Our 24-hour time course in RA-induced NCCIT cells revealed that HMs is more stable, with a half-life around 10 hours, while the half-life of HMu is approximately 1.5 hours (Figure 7B). However, we were concerned that the apparent lower stability of HMu may in fact be due to the combination of transcription inhibition and conversion into HMs through splicing, which would make the half-life appear as lower than it is. Hence, we decided to repeat this experiment in the presence of a splicing inhibitor to rule out this possibility.

Isoginkgetin stabilizes HOTAIRM1 isoforms HMs and HMu

To investigate whether these differences in half-life between HOTAIRM1 isoforms may be due to conversion of HMu into HMs upon transcriptional inhibition, we repeated the time course in the presence of the splicing inhibitor isoginkgetin (isoG) (109).

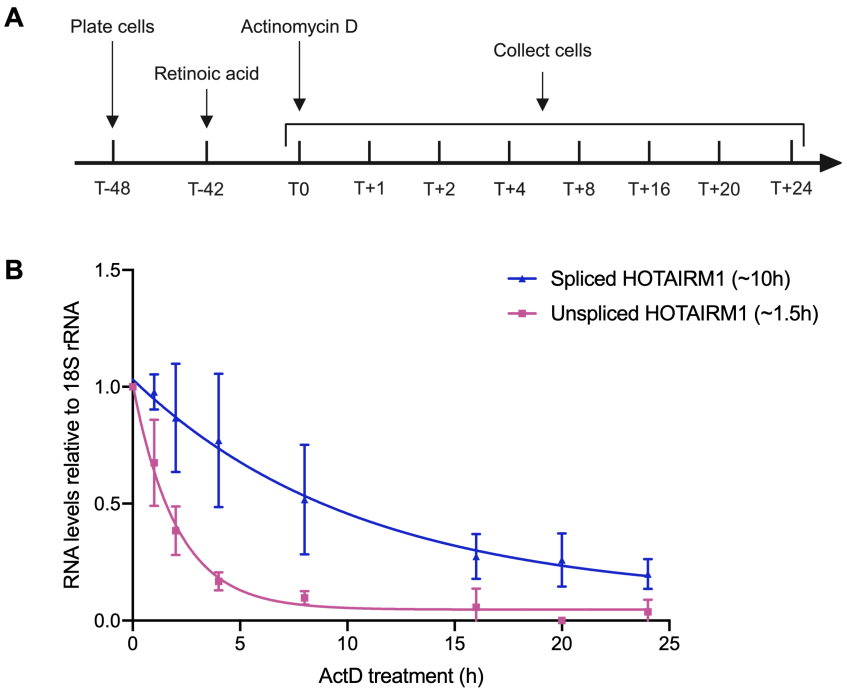

Figure 7. Determining the half-lives of HOTAIRM1 isoforms. (A) Temporal schematic showing how NCCIT cells were treated with RA for 42 hours and the transcriptional inhibitor Actinomycin D (ActD) for up to 24 hours. (B) Total RNA levels of spliced and unspliced HOTAIRM1 over time were quantified. Experiments were performed in triplicate technological measurements from three biological replicates and standard deviations are shown.

We performed a 24-hour ActD time course in RA-induced NCCIT cells with simultaneous isoG treatment (Figure 8A). This revealed that HMs is once again more stable than HMu (Figure 8B). Strikingly, isoG treatment significantly stabilized the HOTAIRM1 transcript, with the half-life increasing from 10 hours to over 24 hours for HMs and from 1.5 hours to 2 hours for HMu (Figure 8B). The stabilizing effect of splicing inhibition hints towards a splicing-dependent destabilizing mechanism at play in HOTAIRM1's post-transcriptional regulation.

We then verified the efficacy of isoG in inhibiting splicing by two methods. First, we performed a Luciferase assay where NCCIT cells were transfected with plasmids encoding either an intronless Luciferase gene (Luc) or an intron-containing Luciferase gene (Luc-i) (Figure 9A), submitted them to RA and isoG treatment, and quantified light emission (Figure 9B) (110). We

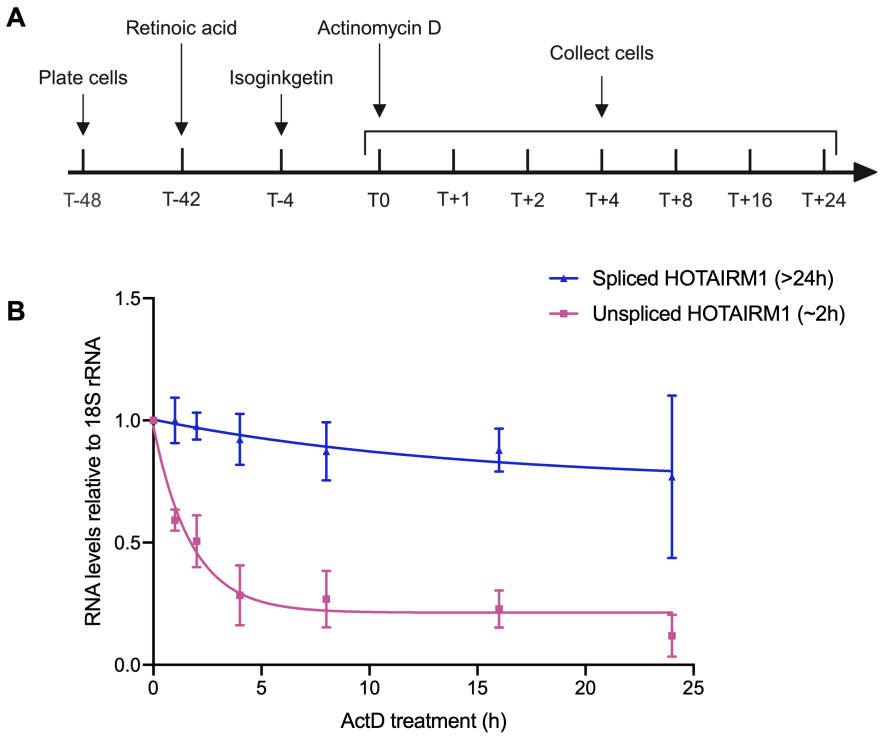

Figure 8. Isoginkgetin stabilizes HOTAIRM1. (A) Temporal schematic showing how NCCIT cells were treated with RA for 42 hours, isoG for 4 hours, and the transcriptional inhibitor Actinomycin D (ActD) for up to 24 hours. (B) Total RNA levels of spliced and unspliced HOTAIRM1 over time were quantified. Experiments were performed in triplicate technological measurements from three biological replicates and standard deviations are shown.

were expecting the Luc condition to express bright luminescence regardless of isoG, and the Luc-i condition to show decreased luminescence when treated with isoG. Instead, we observed decreased light emission for both Luc and Luc-i upon isoG treatment (Figure 9C). This indicates that, at least for transiently transfected transcripts, the effect is not absolutely selective. We also observed higher luminescence with the Luc-i gene both under -isoG and +isoG conditions compared to the Luc gene (Figure 9C), the implications of which are canvassed in the discussion. Since the Luciferase assay did not allow us to conclude that isoG was selectively inhibiting splicing, we also quantified the levels of spliced GAPDH and unspliced GAPDH in response to

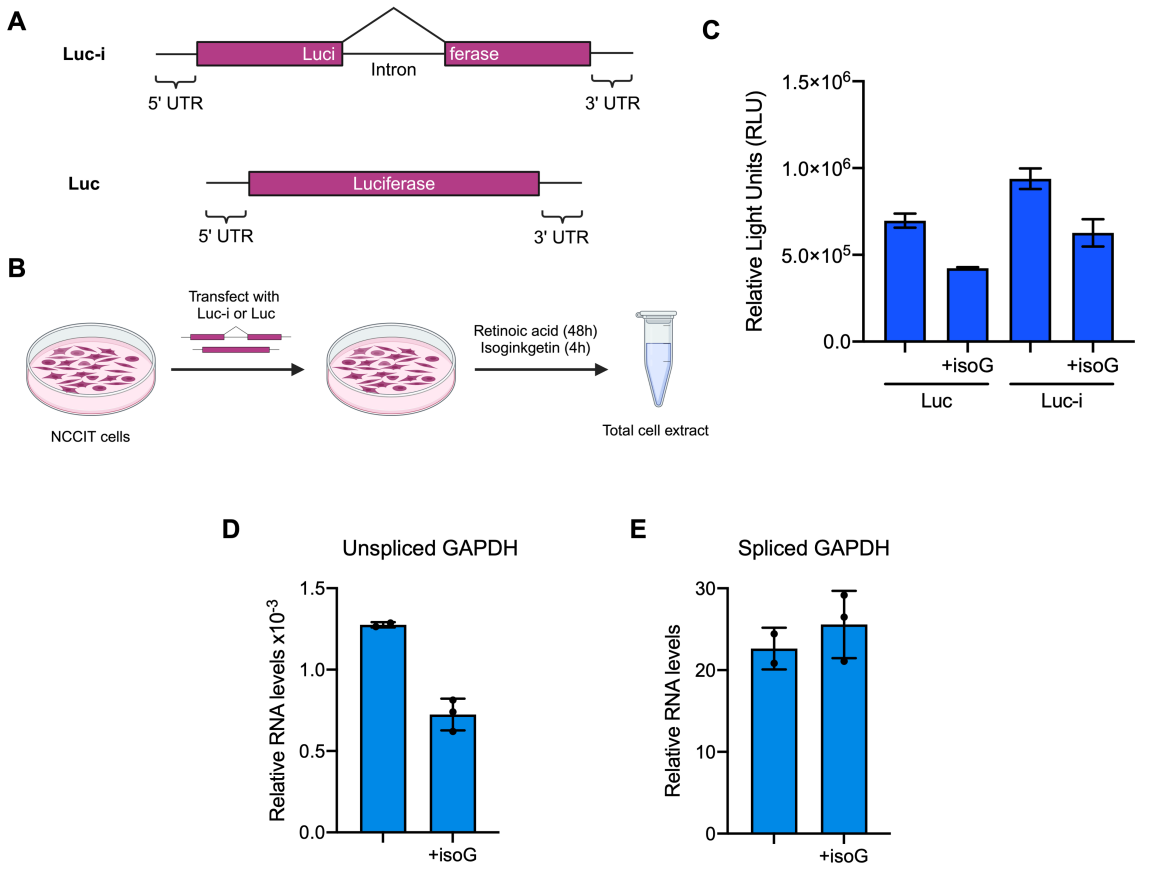

Figure 9. Effect of isoginkgetin on splicing inhibition. (A) Schematic showing the intron-containing Luciferase (Luc-i) and intronless Luciferase (Luc) sequences. Adapted from Younis et al., 2010 (110). (B) Temporal schematic showing transfection with Luc-i or Luc followed by RA and isoG treatment (7). (C) Relative Light Units (RLU) from Luc and Luc-i, with and without isoG treatment. Experiments were performed in triplicate technological measurements from one biological replicates and standard deviations are shown. (D, E) Total RNA levels of unspliced GAPDH (D) and spliced GAPDH (E) with and without isoG treatment. Experiments were performed in triplicate technological measurements from three biological replicates and standard deviations are shown.

isoG treatment. We chose an amplicon spanning the junctions of exons 1, 2 and 3 for spliced GAPDH and an amplicon within intron 1 for unspliced GAPDH. We were expecting to observe decreased levels of spliced GAPDH and increased levels of unspliced GAPDH in response to isoG. However, we observed no significant difference in the levels of spliced GAPDH and decreased levels of unspliced GAPDH upon treatment with isoG (Figures 9D and 9E). This indicates that, at least for GAPDH, the isoG drug has a blanket effect on transcript levels. Taken

together, these two methods to assess efficacy of isoG indicate that, in RA-induced NCCIT cells, this small molecule does not seem to successfully inhibit splicing, though further investigation is needed. Thus, the stabilizing effect of isoG on HOTAIRM1's half-life is likely due to a mechanism unrelated to splicing.

Cycloheximide-mediated translational inhibition increases HOTAIRM1 levels

After determining the half-life of HOTAIRM1 under normal conditions and under splicing repression, we set out to investigate whether processes related to translation may be impacting HOTAIRM1's stability. To do so, we inhibited translation using cycloheximide (CHX) in HEK293T cells and in RA-induced NCCIT cells in an 8-hour time course experiment (Figure 10A). In both cell lines, we observed a gradual increase in total HOTAIRM1 levels with increased CHX treatment time (Figures 10B and 10C). Specifically, we reached an approximately 2-fold increase in HOTAIRM1 levels after 8 hours of treatment in both cell lines. Similarly, levels of our positive control GAS5, a lncRNA which is known to be sensitive to NMD, gradually increased with longer CHX treatment (Figures 10B and 10C) (95). In contrast, levels of our GAPDH negative control, which has never been found destabilized by NMD in spite of extensive investigation, were not affected by CHX treatment (Figures 10B and 10C). While CHX-mediated stabilization of HOTAIRM1 and GAS5 achieved similar levels in HEK293T cells, HOTAIRM1 was interestingly more strongly stabilized by CHX treatment than GAS5 in RA-induced NCCIT cells. Taken together, these results indicate that HOTAIRM1's stability is influenced by translation-dependent mechanisms, with particularly strong effects in the NCCIT cell line.

The exon-junction complex is deposited onto HOTAIRM1

We next sought to determine which translation-dependent processes might be involved in regulating HOTAIRM1 stability. One such possible mechanism is through nonsense-mediated decay (NMD). Since NMD relies on the exon-junction complex (EJC), we thus explored whether

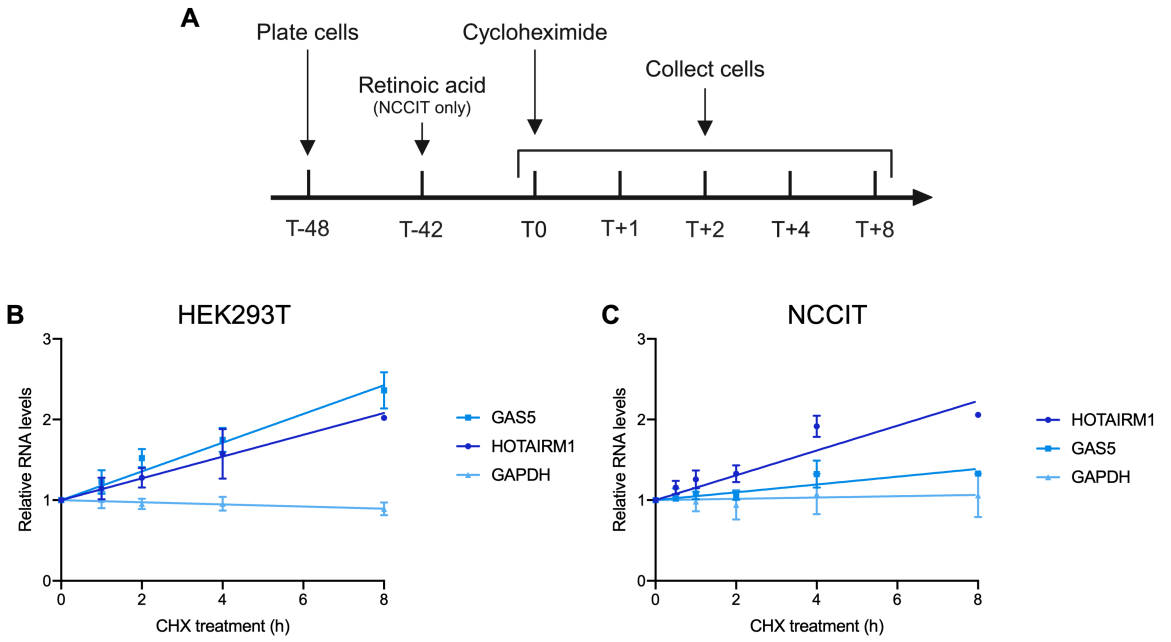

Figure 10. Cycloheximide-mediated translational inhibition increases HOTAIRM1 levels. (A) Temporal schematic showing how NCCIT cells were treated with RA for 42 hours, and how both HEK293T and NCCIT cells were treated with the translational inhibitor cycloheximide D (CHX) for up to 8 hours. (B, C) Total RNA levels of HOTAIRM1, GAS5 and GAPDH over time were quantified in HEK293T (B) and NCCIT (C) cells. Experiments were performed in triplicate technological measurements from three biological replicates and standard deviations are shown.

the EJC gets deposited onto HOTAIRM1. This was doubly interesting to us as it would complement our investigation of HOTAIRM1's alternative splicing and yield further insight on HOTAIRM1's splicing.

We began by constructing plasmids encoding 3xFLAG-tagged EJC factors EIF4A3, MAGOH or RBM8A. Using the Protein Data Bank (PDB), we first determined whether tagging at the N or C terminus would be preferred and opted for the N terminus due to its protrusion from the EJC protein folding structure (Figures 11A and 11B) (87,111,112). We then introduced the 3xFLAG sequence into the pcDNA3.1(+) plasmid vector in the upstream portion of its multiple cloning site (MCS) followed by the EIF4A3, MAGOH or RBM8A sequences downstream from the tag (Figure

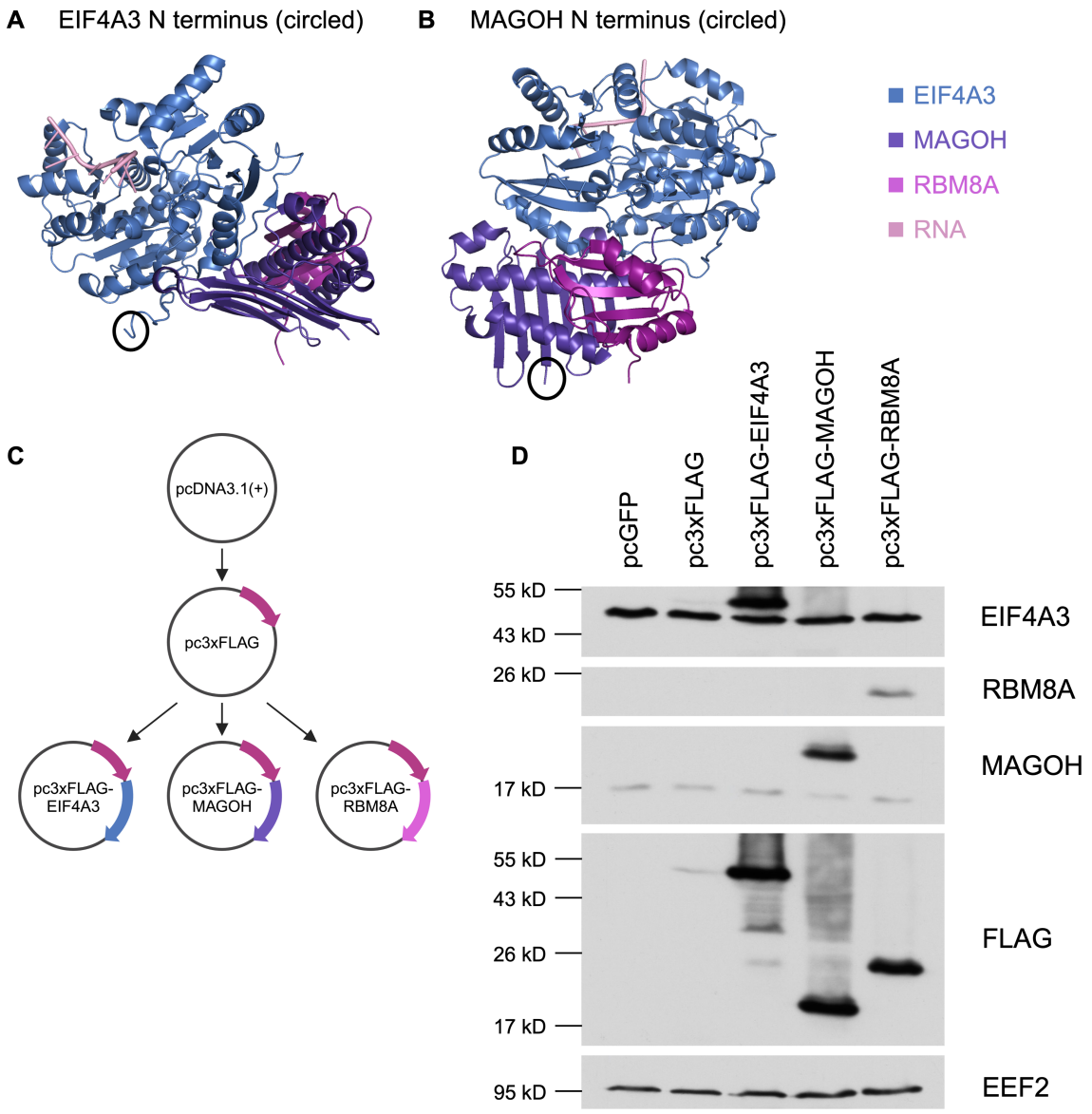

Figure 11. Cloning of plasmid constructs containing 3xFLAG-tagged EJC factors EIF4A3, MAGOH and RBM8A. (A, B) EIF4A3 and MAGOH N termini highlighted within the EJC as per the crystal structure determined by Bono et al., 2006 (87,112). EIF4A3 is shown in blue, MAGOH is shown in purple, RBM8A is shown in dark pink, RNA is shown in light pink (C) Schematic of the cloning workflow, with sequential insertion of the 3xFLAG within pcDNA3.1(+) followed by insertion of the EIF4A3, MAGOH and RBM8A downstream from the 3xFLAG (7). (D) Western blot confirmation of successful expression of 3xFLAG-tagged EJC factors, by probing for the FLAG as well as EIF4A3, MAGOH and RBM8A. EEF2 is used as a control.

11C). After verifying the cloning accuracy in our plasmids by Sanger sequencing, we confirmed the expression of our tagged proteins 3xFLAG-EIF4A3, 3xFLAG-MAGOH and 3xFLAG-RBM8A by western blotting, probing with anti-EIF4A3, anti-MAGOH, anti-RBM8A, anti-FLAG, and the eukaryotic elongation factor EEF2 as control (Figure 11D).

Following transfection of RA-induced NCCIT cells with these 3xFLAG-tagged EJC constructs, we treated the cells with the translational inhibitor CHX for one hour (Figure 12A). The purpose of this treatment was to favour retention of EJC onto transcripts, as the process of translation removes this complex (89). RNA immunoprecipitation (RIP) using FLAG-targeting antibody was performed on total cell extracts and samples were subjected to protein and RNA analysis (Figure 12A). We first confirmed the success of the immunoprecipitation (IP) by western blotting. We observed the presence of FLAG-tagged EJC constructs (3xFLAG-EIF4A3, 3xFLAG-MAGOH and 3xFLAG-RBM8A, respectively) in input, FLAG IP and IgG flowthrough (FT) samples, but not in IgG IP nor FLAG FT samples (Figure 12B). As these results confirmed the success of the IP, we then turned to the investigation of RNA transcripts which immunoprecipitate along with EJC factors. We found enrichment of HOTAIRM1 in all FLAG IPs (3xFLAG-EIF4A3, 3xFLAG-MAGOH and 3xFLAG-RBM8A), as compared to IgG IPs and to the NORAD transcript, an intronless and thus EJC-deficient lncRNA, both of which acted as negative controls (Figures 12C, 12D and 12E).

Overall, this exogenous RIP with FLAG-tagged constructs indicated that the EJC gets deposited onto HOTAIRM1, which allowed us to continue our investigation of HOTAIRM1's links to NMD and splicing. However, we were equally interested in performing an endogenous RIP with antibodies directly targeting the EJC factors, as these have the advantage of targeting the RNPs in a cellular context (113).

To complement the previously described exogenous RIP, we performed an endogenous RIP using antibodies directly targeting the EJC factors, using a similar experimental design to the exogenous RIP (Figure 13A). Following extensive troubleshooting, we determined that none of

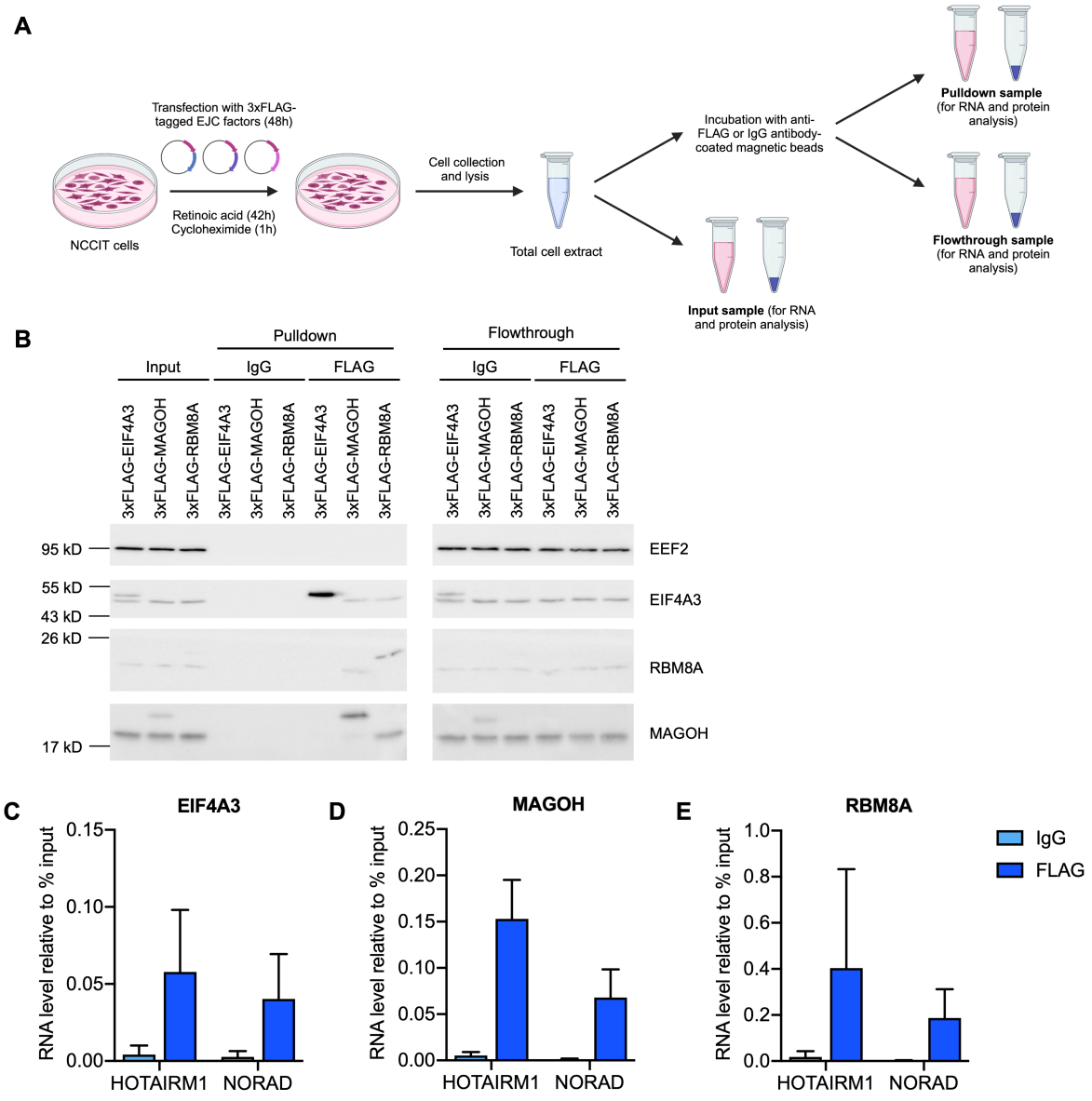

Figure 12. Exogenous RNA immunoprecipitation shows that the exon-junction complex is deposited onto HOTAIRM1. (A) Schematic of the experimental workflow showing transfection of 3xFLAG-tagged EJC factors into NCCIT cells, induction with RA, treatment with cycloheximide (CHX), collection of total cell extract, pulldown with anti-FLAG antibody-coated magnetic beads, followed by analysis of protein and RNA (7). (B) Western blot confirmation of successful immunoprecipitation by probing for FLAG. EEF2 is used as a negative control for pulldown. (C) RNA quantification of levels of HOTAIRM1 and NORAD in pulldown samples relative to input. Experiments were performed in triplicate technological measurements from three biological replicates and standard deviations are shown.

the commercially available MAGOH antibodies are suitable for IP, while antibodies targeting EIF4A3 and RBM8A yielded partial results. We were able to perform a successful IP, and even obtained co-IP of EIF4A3 and MAGOH in the RBM8A pulldown, indicating that the interactions between the three core EJC components remain intact throughout the IP protocol (Figure 13B). RNA analysis of transcripts that IP with endogenous EJC factors unfortunately showed highly inconsistent results (not shown). Nevertheless, the exogenous RIP provides us with sufficient evidence of EJC deposition onto HOTAIRM1, and we thus continued our investigation of HOTAIRM1's links to NMD and splicing.

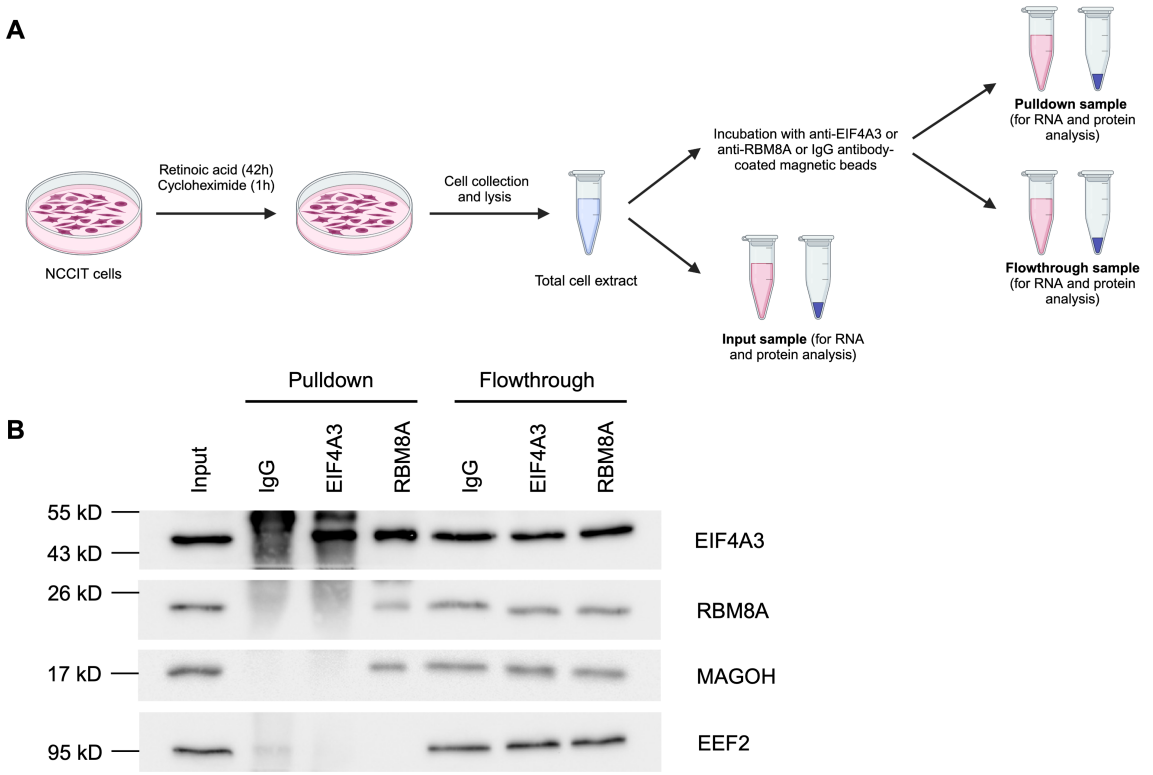

Figure 13. Endogenous immunoprecipitation of EJC factors shows co-IP. (A) Schematic of the experimental workflow showing induction of NCCIT cells with RA, treatment with cycloheximide (CHX), collection of total cell extract, pulldown with anti-EIF4A3 and anti-RBM8A antibody-coated magnetic beads, followed by analysis of protein and RNA (7). (B) Western blot confirmation of successful IP and co-IP by probing for EIF4A3, MAGOH and RBM8A. EEF2 is used as a negative control for pulldown.

NMD inhibition through UPF1 knockdown does not impact HOTAIRM1's stability

Upon uncovering evidence that HOTAIRM1's stability is influenced by translation-dependent mechanism(s), with particularly strong effects in the NCCIT cell line, and that the EJC is deposited onto HOTAIRM1, we then turned to the investigation of NMD as a potential HOTAIRM1-destabilizing mechanism. We performed knockdown of UPF1, a central and essential component of the NMD machinery, to shut down this process (92). We designed three small interfering RNAs (siRNAs) targeting distinct regions of the UPF1 transcript, termed siUPF1.1, siUPF1.2 and siUPF1.3, and employed them independently from each other to rule out off-target effects such as knockdown of other genes. To optimize our protocol, we performed preliminary time course experiments where we looked at knockdown efficiency with all three siRNAs every 12 hours for a total of 72 hours (Supplemental data 1). Based on these results, we opted to use siUPF1.1 and siUPF1.3 in a 48-hour knockdown. We verified the success of the UPF1 knockdown by western blotting (Figure 14A) which we quantified relative to the stably expressed EEF2 protein and observed an ~80% knockdown efficiency (Figure 14B). We then quantified RNA levels of HOTAIRM1 – our gene of interest –, GAS5, an NMD-sensitive control whose levels were expected to increase upon UPF1 knockdown, and MALAT1, an NMD-insensitive control whose levels were expected to remain constant despite knockdown of UPF1 (95,114). We observed a marked increase in GAS5 levels and no significant change in MALAT1 levels, confirming the success of UPF1 knockdown in achieving NMD inhibition (Figure 14C). Moreover, we did not notice any significant changes in HOTAIRM1 levels relative to MALAT1 in UPF1 knockdown conditions, implying that HOTAIRM1's stability is not dependent on NMD (Figure 14C). We thus turned our attention to other RNA-destabilizing mechanisms.

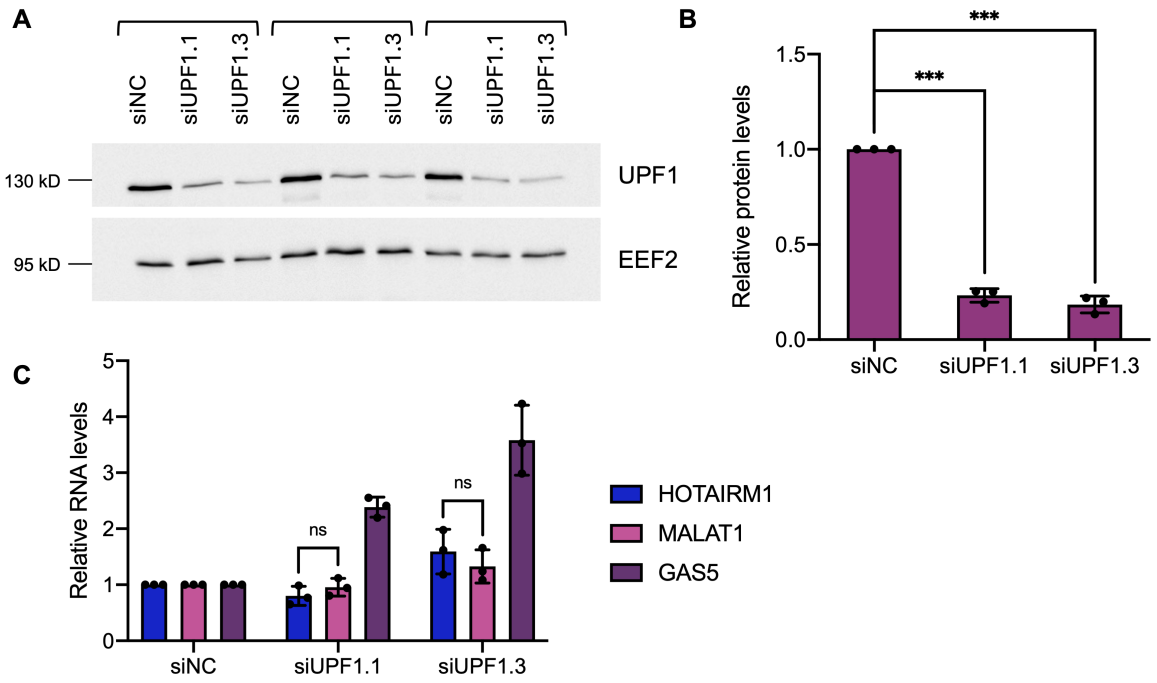

Figure 14. NMD inhibition through UPF1 knockdown does not impact HOTAIRM1 levels. (A) Western blot confirmation of successful knockdown, comparing the non-coding siRNA control (siNC) to two UPF1-targeting siRNAs (siUPF1.1 and siUPF1.3). EEF2 is used as a control. (B) Quantification of UPF1 protein levels from the western blot, relative to EEF2 levels. Welch's t-test, P-value = 0.0007 (siUPF1.1) and P-value = 0.0010 (siUPF1.3) (C) Quantification of RNA levels for HOTAIRM1, NMD-insensitive MALAT1, and NMD-sensitive GAS5. Welch's t-test, P-value = 0.2469. Experiments were performed in triplicate technological measurements from three biological replicates and standard deviations are shown.

MiRISC inhibition through AGO2 knockdown does not influence HOTAIRM1's stability

The next translation-related process that we investigated in relation to HOTAIRM1's stability was the miRNA-induced silencing complex (miRISC). We performed knockdown of AGO2, a central and essential component of the miRISC machinery, to shut down this process (98). We verified the success of the AGO2 knockdown by western blotting (Figure 15A) which we quantified relative to the stably expressed HuR protein to observe an ~65% knockdown efficiency (Figure 15B). We then quantified RNA levels of HOTAIRM1, as well as GAS5 and MALAT1, and observed no significant changes relative to GAS5 nor MALAT1 in the AGO2 knockdown condition, implying that HOTAIRM1's stability is not dependent on miRNA-induced silencing (Figure 15C). We were

however still interested in seeing whether NMD and miRISC may be working in partnership to affect HOTAIRM1's post-transcriptional regulation.

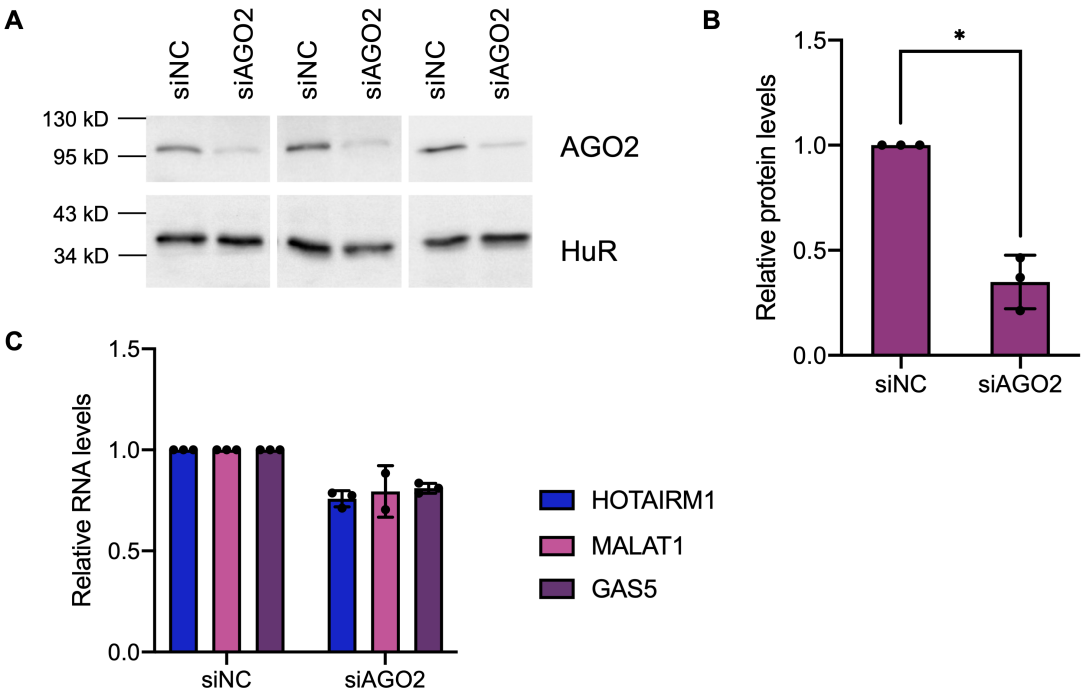

Figure 15. MiRISC inhibition through AGO2 knockdown does not influence HOTAIRM1 levels. (A) Western blot confirmation of successful knockdown, comparing the non-coding siRNA control (siNC) to an AGO2-targeting siRNAs (siAGO2). HuR is used as a control. (B) Quantification of AGO2 levels from the western blot, relative to HuR levels. Welch's t-test, P value = 0.0125. (C) Quantification of RNA levels for HOTAIRM1, MALAT1 and GAS5. Experiments were performed in triplicate technological measurements from three biological replicates and standard deviations are shown.

Simultaneous inhibition of NMD and miRISC does not sensitize HOTAIRM1

To investigate whether NMD and miRISC may be affecting HOTAIRM1's stability through a mechanism in which one destabilizing process sensitizes to the other, in other words a mechanism in which NMD and miRISC work hand-in-hand to destabilize the HOTAIRM1 transcript, we performed a double-knockdown of UPF1 and AGO2. We opted to use siUPF1.3 and not siUPF1.1 due to its slightly higher knockdown efficiency (Figure 14B). We verified the

success of the knockdowns by western blotting (Figure 16A) which we quantified relative to the stably expressed HuR protein to observe ~65% knockdown efficiencies for both genes (Figure 16B). We then quantified RNA levels of HOTAIRM1, GAS5 and MALAT1, as per our previously described UPF1 and AGO2 individual knockdowns. Similarly to the UPF1 individual knockdown, we observed a marked increase in GAS5 levels and no significant change in MALAT1 levels upon

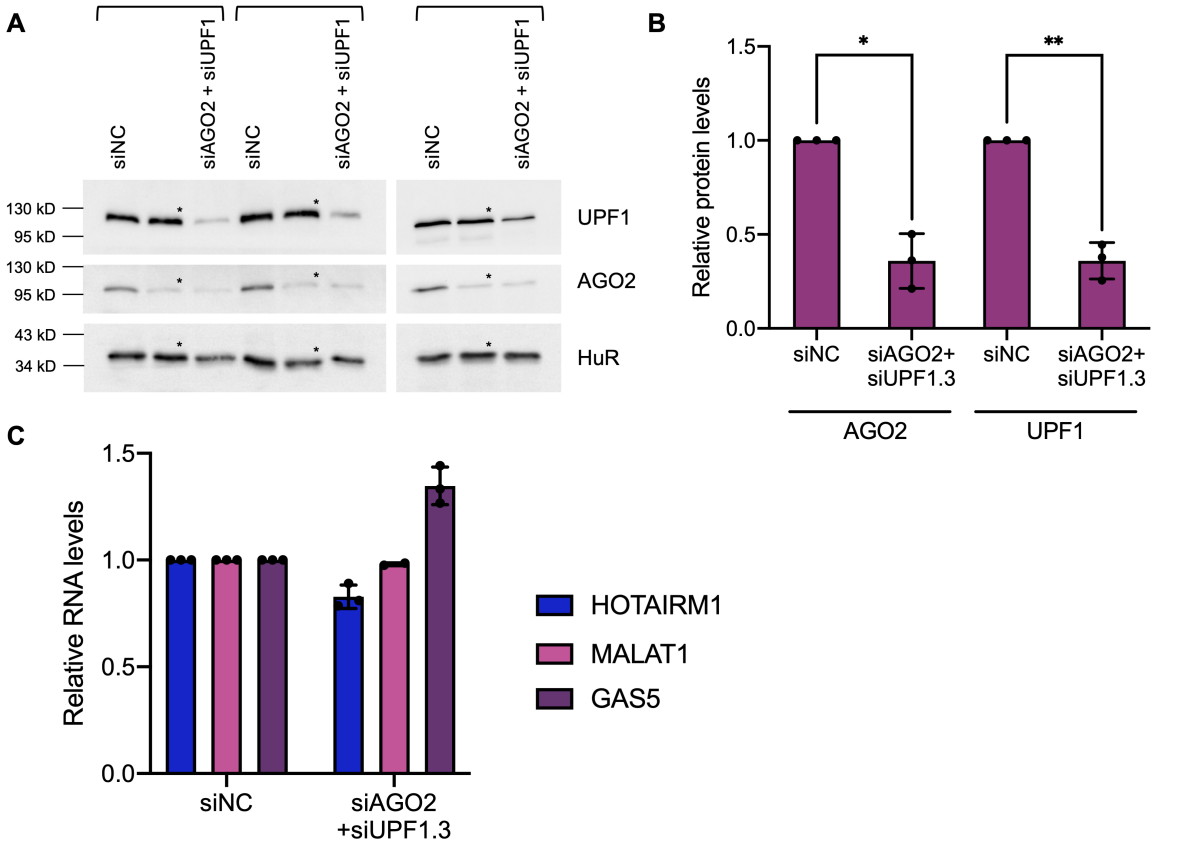

Figure 16. Simultaneous inhibition of NMD and miRISC does influence HOTAIRM1 levels. (A) Western blot confirmation of successful knockdown, comparing the non-coding siRNA control (siNC) to a condition with double-knockdown using siRNAs targeting AGO2 and UPF1 (siAGO2 + siUPF1). HuR is used as a control. (B) Quantification of AGO2 and UPF1 protein levels from the western blot, relative to HuR levels. Welch's t-test, P value = 0.0167 (AGO2) and P value = 0.0075 (UPF1). (C) Quantification of RNA levels for HOTAIRM1, NMD-sensitive GAS5, and NMD-insensitive MALAT1. *Bands marked with an asterisk are not relevant to this experiments. Experiments were performed in triplicate technological measurements from three biological replicates and standard deviations are shown.

UPF1 knockdown, indicating the success of the NMD inhibition (Figure 16C). We did not notice any significant increase in HOTAIRM1's levels, implying that its stability is not dependent on a collaborative mechanism involving both NMD and miRISC (Figure 16C). The potential mechanisms behind HOTAIRM1's translation-dependent destabilization, beyond NMD and miRISC, are further outlined in the discussion.

Exploration of HOTAIRM1-binding miRNAs

The last phase of this project consisted in examining the interactions between HOTAIRM1 and miRNAs, given that these interactions may be relevant if HOTAIRM1 is acting as a competing endogenous RNA (ceRNA) or if it is inducing target-directed miRNA degradation (TDMD, see discussion) of associated miRNAs. As such, three different methods were conducted to identify HOTAIRM1-binding miRNAs. First, the TarBase v8 database from DIANA tools, which comprises publicly available experimental data from CLIP-seq, RNA-seq and microarray experiments, was employed to reveal 55 hits (115). Next, miRcode, which is a map of putative miRNA target sites in the long non-coding transcriptome, was used to identify 24 hits (116). Finally, a literature search was conducted and it yielded 17 hits (117-124). Overall, a total of 82 miRNAs were identified by merging results from these three sources (Figure 17; Supplemental data 3). There was surprisingly little overlap between the miRNA hits obtained through each method, and only two miRNAs (miR-20a-5p and miR-17-5p) were identified as HOTAIRM1-binding using all three methods (Figure 17). These diverging results are further addressed in the discussion.

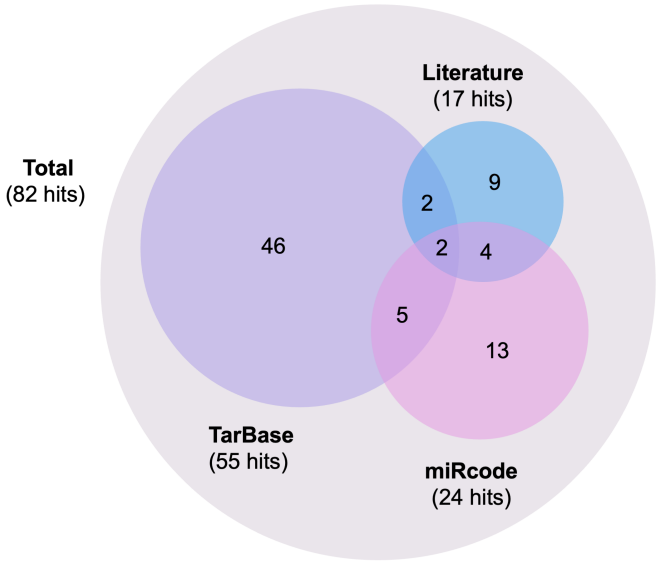

Figure 17. Experimental databases and prediction tools show diverging results regarding HOTAIRM1-miRNA interactions. The HOTAIRM1 miRNA interactome was assessed using 3 methods (miRcode, TarBase and publications), and hits were compared.

Out of the 82 candidate miRNAs examined, we then determined which ones specifically target HOTAIRM1's exon 2. These hold relevance as this exon is alternatively spliced, with some tissues and cell lines expressing higher levels of the HM123 isoform while others mostly express HM13. We found that 7 of them target exon 2, and then investigated how each of these relate to cancer, the results of which are summarized below (Table 2).

Table 2. Cancer involvement of the 7 miRNAs predicted to bind HOTAIRM1's exon 2.

miRNA	Publications	Mutations in TCGA?	HOTAIRM1 link?	Expression in NCCIT?
miR103	Colorectal cancer (125-128) Gastric cancer (129,130) Breast cancer (131,132) Glioma (133)	N/A	N/A	Yes (134)
miR135	Breast cancer (135-138) Gastric cancer (139,140) Prostate cancer (141) Pancreatic cancer (142)	Skin cutaneous melanoma Rectum adenocarcinoma Uterine corpus endometrial carcinoma Colon adenocarcinoma	N/A	Yes (134)
miR122	Colorectal cancer (143,144) Breast cancer (145) Gastric cancer (146,147)	Liver hepatocellular carcinoma Skin cutaneous melanoma Head and neck squamous cell carcinoma Uterine corpus endometrial carcinoma	N/A	N/A
miR216	Cervical cancer (148) Colorectal cancer (149) Pancreatic cancer (150) Gastric cancer (151) Acute myeloid leukemia (152) Breast cancer (153)	Skin cutaneous melanoma Uterine corpus endometrial carcinoma Pheochromocytoma and Paraganglioma Colon adenocarcinoma Bladder Urothelial Carcinoma Lung squamous cell carcinoma Brain Lower Grade Glioma	N/A	N/A
miR490	Gastric cancer (154-156) Bladder cancer (157) Prostate cancer (158) Colon cancer (159) Lung cancer (160) Ovarian cancer (161) Breast cancer (162)	N/A	N/A	N/A
miR107	Colorectal cancer (125,163-165) Penile cancer (166) Breast cancer (167,168) Papillary thyroid cancer (42) Lung cancer (169,170)	N/A	Yes (42)	Yes (134)
let7i	Breast cancer (171,172) Lung cancer (173) Prostate cancer (174) Ovarian cancer (175)	N/A	N/A	N/A

Discussion

This project began by investigating HOTAIRM1's isoforms in the cell lines of interest, to set the foundation for further study. We found that HOTAIRM1 is spliced alternatively and with cell-type specificity, specifically that HMs is largely predominant in HEK293T cells, while there is a drastic increase in HOTAIRM1 levels upon treatment with retinoic acid (RA) in NCCIT cells and overall higher levels of HMu. We then determined the half-lives of HOTAIRM1 isoforms and found that HMs is more stable than HMu, with half-lives approximately 10 hours and 1.5 hours, respectively, and that splicing inhibition using isoginkgetin (isoG) stabilizes HOTAIRM1, with half-lives increasing to over 24 hours and around 2 hours, respectively. Following cycloheximide-mediated translational inhibition, HOTAIRM1 levels increased, indicating that HOTAIRM1's stability is influenced by translation. We thus sought to determine which translation-dependent process is responsible for these observed changes. For this, we started by verifying that the exon-junction complex (EJC) is deposited onto HOTAIRM1. Through individual knockdowns of UPF1 and AGO2, we then showed that this is not due to nonsense-mediated decay (NMD) nor miRNA-induced silencing (miRISC), respectively. We also performed a double-knockdown of UPF1 and AGO2 and found that simultaneous inhibition of NMD and miRISC does not affect HOTAIRM1's levels. Finally, we explored HOTAIRM1-binding miRNAs and identified 82 candidates, including 7 which are predicted to bind HOTAIRM1's alternatively spliced exon 2 and which have all been implicated in cancers.

Diversity in the expression of HOTAIRM1 isoforms

Comparably to many lncRNAs, HOTAIRM1 exists as an unspliced isoform (HMu) as well as alternatively spliced isoforms (HM123 and HM13), depending on the tissue type or cell line. As such, most studies on HOTAIRM1 include an investigation of the predominant variant in the model of interest. In NB4 and HL-60 acute promyelocytic leukemia cell lines and in neutrophil cell lines,

the HM13 isoform predominates, with minor amounts of HMu and HM123 present (31,46,176). The NT2-D1 pluripotent embryonal carcinoma cell line mainly exhibits the HM123 spliced isoform, as well as comparable amounts of HMu (46). The HK-2, ACHN and CAKI-1 kidney cell lines mostly express HMu, with some HM123 and trace amounts of HM13 (43). In the T98G glioblastoma cell line, HM123 is the predominant isoform (177). The SHY5Y neuroblastoma cell line expresses the HM123 variant prior to induction and both HM123 and HM13 after induction (178). In breast cancer models, HM13 was identified as the predominant isoform (179). As part of this study, we explored the expression of HOTAIRM1 variants in our models. We revealed that, in the HEK293T cell line, HMs is the major isoform compared to HMu. We also showed that, in the NCCIT cell line, there is a drastic increase in HOTAIRM1 levels upon treatment with RA, with HMu being the major isoform compared to HMs. Therefore, our research adds to prior endeavors which aim to establish a comprehensive map of the expression of HOTAIRM1 isoforms across cell lines.

To assess the expression HOTAIRM1 isoforms, this study relied on RT-qPCR of an amplicon within exon 3 for total HOTAIRM1 levels, an amplicon spanning the junction between exons 2 and 3 for HM123 levels, and an amplicon within intron 1 for HMu levels. Unfortunately, HM13 could not be measured by RT-qPCR as the junction between exons 1 and 3 is extremely GC-rich, rendering the design of suitable primer pairs virtually impossible, as determined via thorough primer pair efficiency testing. Instead, Northern blotting or RNA sequencing would allow us to precisely determine the HOTAIRM1 isoforms expressed in our cell lines of interest (180,181).

In NCCIT, a human pluripotent cell line known to differentiate into neuronal lineages in response to RA, we observed a stark increase in HOTAIRM1 levels upon RA treatment (107). The literature supports our observations as HOTAIRM1 is located within the *HOXA* gene cluster, which is highly implicated in development, thus it seems logical that HOTAIRM1's expression would be repressed in pluripotent cells and induced in differentiating cells (33).

HMu is abundantly found in some cell lines, such as NCCIT. The question of whether this is due to deliberate and active retention in the unspliced form or due instead to high transcription

rates coupled with low RNA processing rates remains to be addressed and would be an intriguing avenue for future investigation.

Cellular localization of varying HOTAIRM1 isoforms

Cellular localization of macromolecules such as proteins or RNAs plays a major role in their ability to perform their cellular roles (182). Thus, in-depth comprehension of HOTAIRM1's localization within the NCCIT cell line, more precisely the localization of the spliced versus unspliced forms, would allow us to better understand where the splicing occurs, how much of each isoform is retained in the nucleus versus how much is exported to the cytoplasm, where these different isoforms localize specifically within the cytoplasm in relation to organelles, granules or membranes, and generally provide insight into HOTAIRM1's cellular roles. This could be achieved by performing small molecule fluorescent in situ hybridization (smFISH), probing for areas within introns to assess HMu localization, areas within exons to determine total HOTAIRM1 localization, and performing a comparison to assess the localization of HMs. This could also be achieved by performing cellular fractionation to separate nuclei from cytoplasm, followed by RT-qPCR in the resulting fractions, though this approach would yield less precise information (183).

Although studies looking into the cellular localization of HOTAIRM1 have never been conducted in the NCCIT cell line, they have been performed in select cell lines. A study by Hamilton et al. looking at the NT2-D1 pluripotent embryonal carcinoma cell line and a study by Wang et al. investigating multiple renal proximal tubule cell lines found that, in these models, HMu preferentially localized to the nucleus while HMs preferentially localized to the cytoplasm (43,46). A study by Han et al. looking at glioblastoma cell lines U87MG, T98G and A172 using the cellular fractionation approach found that HM123 is largely located in the cytoplasm while HM13 is primarily cytoplasmic with slight amounts of nuclear localization (177). The same study then performed FISH exclusively in T98G cells to confirm their observations (177). Since this study

identified HMs in the nucleus, it would be interesting to investigate whether it is exported to the cytoplasm and then imported back into the nucleus, or whether there is active nuclear retention.

Interestingly, it was demonstrated that lncRNAs which encode micropeptides tend to localize in the cytoplasm, while lncRNAs which do not undergo translation are mostly located in the nucleus (66). Hence, the primarily cytoplasmic localization of HMs in investigated cell lines reveals that it may indeed be undergoing translation, while the primarily nuclear localization of HMu indicates that it likely does not undergo such translation, though this requires further investigation.

Relationship between the EJC and HOTAIRM1

This study demonstrates the presence of core EJC components EIF4A3, MAGOH and RBM8A on HOTAIRM1. However, the question of which peripheral EJC factors bind HOTAIRM1 was not addressed. Given that specific EJC composition can affect RNA processing, learning more about the EJC factors that make up HOTAIRM1's distinct EJC would prove insightful (81). A recent study by Chuang et al. using biotinylated antisense DNA oligonucleotide probes identified HOTAIRM1-binding proteins through mass spectrometry and found enrichment of core EJC factors EIF4A3 and RBM8A, as well as peripheral EJC factors CASC3, PYM1, UPF1 and UPF3B (involved in NMD), among other targets (67). Likewise, recent unpublished data from our lab investigating the protein interactome of HOTAIRM1 revealed that EIF4A3, RBM8A and PYM1, but not MAGOH nor CASC3, may be binding HOTAIRM1. However, both of these analyses were performed without biological replication, and the authors recommend verification of identified factors by additional methods (67).

Regarding EJC deposition onto HOTAIRM1, current literature indicates that this is highly likely to occur during the process of splicing, though it is important to note that we did not show concurrence between splicing and EJC deposition in this study. Regarding EJC removal from HOTAIRM1, current literature indicates this likely occurs during translation, either through ribosome- or PYM1-mediated displacement. Evidence presented in the introduction leads us to

believe that HOTAIRM1 may be undergoing small amounts of translations, which would be enough to cause EJC removal (89). Hence, it would be interesting to investigate whether the EJC is removed from HOTAIRM1, and if so, the step of RNA processing at which this occurs. This could include performing cellular fractionation followed by RNA immunoprecipitation experiments similar to the ones presented in this study, to explore whether EJC factors are bound to HOTAIRM1 in nuclear and cytoplasmic fractions. If HOTAIRM1 remains EJC-bound in both fractions, then we may wonder which mechanisms HOTAIRM1 is employing to avoid degradation by NMD despite translation and the presence of EJCs downstream from termination codons.

Many groups have attempted to obtain complete crystal structures of the EJC (87,184-186). Although these structures provide insight on the way EJC components interact with one another and with RNA, none of the groups were able to obtain a reliable structure for the N terminus of RBM8A, as all models are missing the first ~60 amino acids. In this way, although our data seems to show successful pulldown of RBM8A tagged at the N terminus with a 3xFLAG, we cannot ascertain that the N terminus is indeed accessible.

While exogenous RIPs using transfected tagged proteins and tag-specific antibodies are instrumental in the exploration of RNA-protein interactions, endogenous RIPs using antibodies directly targeting the protein of interest have the advantage of targeting these RNA-protein (RNP) complexes in a cellular context (113). One major setback to this technique is that commercially available IP-grade antibodies are rare. Although multiple antibodies targeting EJC factors were tested in this study, few were successful in pulling down the desired proteins, as showcased by immunoblotting (Figure 13B), and even fewer were able to generate reproducible RNA data. The most successful pulldown from this study employed the clone 4C4 anti-RBM8A antibody and showed co-IP of core EJC factors EIF4A3 and MAGOH. This result is in line with other studies performing endogenous RIP of EJC factors, in which they exclusively show evidence of RBM8A pulldown (67).

In addition to the exogenous 3xFLAG-tagged and endogenous RIP experiments performed in this study, it would be interesting to perform crosslinking immunoprecipitation (CLIP) experiments. While RIP techniques purify RNP complexes under native conditions (187,188), CLIP techniques rely on ultraviolet (UV) irradiation of cells, which induces irreversible covalent binding between RNAs and proteins (189). This allows for more stringent purification steps in the protocol and is hence beneficial for result validation and the removal of false-positive hits. In this way, we recommend performing CLIP to confirm the interaction between core EJC factors and HOTAIRM1.

HOTAIRM1 half-life: measurements and perspectives

Transcriptional inhibitors such as actinomycin-D (ActD) used in this study have long been the gold standard for determining RNA stability and are still considered as a reliable way of measuring half-life (190). However, there are some drawbacks to using transcriptional inhibitors, notably their toxicity, as their large-scale impacts on cellular physiology may affect precision when measuring RNA decay rates, especially during extended treatments (77). Hence, newer methods based on metabolic pulse labelling of RNA transcripts using uridine analogs are emerging as alternatives to transcriptional inhibitors (191). During the pulse, uridine analogs become incorporated into all nascent RNA transcripts, and cell extracts are collected at sequential time points following removal of uridine analogs from the cellular environment (192,193). The half-life is then estimated by determining the decrease in metabolically labeled RNA over time (190). These metabolic labeling techniques have the advantage of being less toxic to cells, and are thus preferred, especially for RNAs with long half-lives (74). In the case of HOTAIRM1, whose spliced isoform has a half-life exceeding 24 hours upon isoG treatment, cellular toxicity of ActD is a major issue as the experiment could not be carried out for an extended period of time (194). In this case, metabolic labeling techniques such as 5′-BrU immunoprecipitation (BRIC) would be preferred (191). A recent study by Han et al. performed BRIC in the A172 glioma cell line and found that HM123 has a half-life around 11 hours while HM13's half-life is around 12 hours, which not only

shows the success of the BRIC technique for our RNA of interest, but is also in line with our findings that the half-life of spliced HOTAIRM1 is around 10 hours in NCCIT cells (177).

Given that lncRNAs have a median half-life of 3.5 hours and a mean half-life of 4.8 hours, ranging from less than 30 minutes to over 48 hours, this places HMs in the category of the most stable lncRNAs and HMu in the category of the least stable lncRNAs (74). When compared to mRNAs, which are generally considered as more stable with a median half-life of 5.1 hours and a mean half-life of 7.7 hours, spliced HOTAIRM1 can still be regarded as a highly stable transcript (74). It is generally considered that RNAs with shorter half-lives have regulatory roles within the cell, as high turnover means they can be expressed sporadically in response to specific stimuli, while RNAs with longer half-lives perform maintenance roles, as they need to be constantly expressed and low turnover is thus advantageous (74). Our findings regarding HMs' high transcript stability indicate that it may be playing an essential role in NCCIT cells, while HMu's low stability hints at a more regulatory role, though this deserves further investigation.

In support of the idea that HM123 and HM13 may also exhibit different half-lives, a study by 't Hoen et al. looking at RNA stability in proliferating and differentiated myogenic cells showed that splice variants that include alternatively spliced internal exons may differ in stability (195). This contradicts the widespread idea that the 3' UTR is the lone determinant of transcript stability (73).

A study by Chen showed major differences in the nucleocytoplasmic distribution of splice variants, and showed that this can be at least partially attributed to differences between nuclear and cytoplasmic RNA degradation mechanisms (196). This link between RNA cellular localization and stability would be particularly interesting to explore for HOTAIRM1 given our previously discussed point that its isoforms have been shown to localize differentially.

N6-methyladenosine (m6A) is an abundant modification in RNAs which is directed by a methyltransferase "writer" complex containing METTL3, among other factors (197). m6A can be removed by demethylase "erasers" such as FTO and ALKBH5 (198). m6A modifications can be bound by "readers" from the YTHDF and IGF2BP families of proteins which regulate many

aspects of RNA post-transcriptional processes, such as translation and stability (199). A recent study by Wu et al. showed that METTL3 and IGF2BP2 are both upregulated in glioma tissues and cell lines, and that HOTAIRM1 functions as an oncogene in glioma progression (197). Interestingly, they also showed that METTL3-dependent m6A modification enhanced HOTAIRM1's stability, via IGFBP2 binding to HOTAIRM1 (197). In addition, two recent publications highlighted that the specificity of m6A deposition onto RNA transcripts is mediated by exon architecture via the EJC (200,201). Therefore, it is important to consider the influence of the EJC and RNA modifications like m6A on the stability of HOTAIRM1 when investigating its post-transcriptional regulation.

Suggested pathways for translation-dependent destabilization of HOTAIRM1

We have shown that translation destabilizes HOTAIRM1, but that this does not occur through the translation-related RNA-destabilizing mechanisms of NMD and miRISC, nor through a cooperative action between these two processes. Hence, the specific translation-dependent mechanism by which this occurs remains a topic of open investigation. Here, we suggest multiple avenues for such exploration.

We hypothesize that this may be occurring through no-go decay (NGD) (202,203). NGD occurs in RNAs in which translation elongation stalls, and it results in endonucleolytic cleavage, ultimately leading to both 5' to 3' and 3' to 5' decay (204-207). Thus, we suggest knocking down core components of the NGD machinery and seeing whether this affects HOTAIRM1 levels.

Alternatively, this may be occurring through non-stop decay (NSD) (202,203). NSD occurs in RNAs lacking an in-frame termination codon, as ribosomes stalled at the 3' end recruit multiple factors, for instance 3' to 5' exonucleases, ultimately leading to the degradation of the transcript (208-212). In this way, we also suggest knocking down core components of the NSD machinery and observing the effects on HOTAIRM1's stability.

Interestingly, it has been suggested that micropeptides encoded by short ORFs from lncRNAs may be interacting with the decapping protein complex that removes the m^7G cap from RNAs to promote 5' to 3' decay (213). This alternative mechanism by which HOTAIRM1 may be destabilized by translation constitutes another an area that we recommend investigating in.

Finally, translation has been shown to affect RNA stability in a codon-dependent manner, where specific codons, as opposed to specific nucleotide sequences, are associated with transcript stability (214). The number of ribosomes loaded onto a transcript modulates this codon-mediated effect on gene expression (214). This RNA-destabilizing mechanism has been termed codon optimality-mediated RNA decay (COMD) and could be another way in which translation may be affecting HOTAIRM1's post-transcriptional regulation.

Effect of isoginkgetin on HOTAIRM1 levels

The rationale behind the use of isoG in our RNA stability determination time courses was to use it as a splicing inhibitor to ensure that the half-lives we were observing for HMu and HMs were accurate. Indeed, we were concerned that the lower HMu half-life and the higher HMs half-life observed may in fact represent conversion from the unspliced to the spliced form upon transcriptional inhibition. The finding that both HMu and HMs are stabilized by isoG raised a new question, that HOTAIRM1 may be destabilized by a splicing-dependent mechanism. However, doubts remain considering the selectivity of isoG as a splicing inhibitor. Indeed, neither the Luciferase assay nor the examination of GAPDH splice variants were able to confirm the selectivity of this small molecule in inhibiting splicing. Both in the presence and absence of isoG, the intron-containing Luc-i gene produced higher luminescence than the intronless Luc gene, which is consistent with the knowledge that splicing aids in expression (215). For future uses of isoG as a splicing inhibitor, we recommend titrating the isoG concentration to determine if specificity increases.

HOTAIRM1-miRNA interactome

Considerable effort has been made to determine RNA-RNA interactions as this is a key step to understanding their roles, especially in the case of ncRNAs (216). This includes algorithmic *in silico* approaches and experimental *in vivo* and *in vitro* approaches. Algorithmic predictions provide a solid foundation for the discovery of such interactions by providing a list of potential binding partners, but are notorious for providing false-positive results (216). Experimental identification and validation of predicted interactions is hence crucial to overcome a growing issue in the field whereby many published RNA-RNA interactions cannot be validated (216). For our study, this includes all predicted HOTAIRM1-binding miRNAs identified exclusively from miRcode. Additionally, our finding that only 2 out of the 82 miRNAs were identified as HOTAIRM1-binding using all three methods (miRcode, TarBase and publications) raises further concerns regarding the reliability of miRNA-based experiments. In this way, we urge readers to perform experimental validation with adequate controls of any putative miRNA-lncRNA interaction. Recent unpublished data from our lab investigating the miRNA interactome of HOTAIRM1 revealed that miR-3196, miR-3960, miR-4508 and miR-4516 may be binding HOTAIRM1, in addition to the 82 miRNAs provided in this study. miR-3960 is particularly interesting as it was previously identified as a HOTAIRM1-binding partner by Xin et al. (124).

Most miRNAs exhibit high stability when bound to Argonaute proteins such as AGO2, and little is known regarding how these small RNAs are degraded (217). While base pairing between miRNAs and RNA using exclusively the seven-nucleotide seed sequence induces degradation of the RNA target, there is increasing evidence that extensive base pairing can instead trigger miRNA turnover (218,219). This mechanism, termed target-directed miRNA degradation (TDMD), has changed the way the field thinks about miRNA and RNA stability (219). Instead of miRNAs destabilizing RNAs, it is the RNAs which destabilize miRNAs (219). The suggested mechanism involves structural conformation changes in the Argonaute proteins, though further research is required to support this claim (220,221). Due to the abundance of predicted HOTAIRM1-binding

miRNAs, it would be interesting to investigate whether HOTAIRM1 is responsible for the TDMD-mediated decay of a subset of these miRNAs. It would not be surprising to find that it does, as lncRNAs are generally longer than mRNAs, and HOTAIRM1 is no exception with HMu exhibiting an impressive length of 4 kb while HM123 and HM13 are 1 kb and 0.8 kb long, respectively.

From a single-gene to a multi-gene approach

This project utilized a single-gene approach, looking at HOTAIRM1 specifically in order to discover intriguing post-transcriptional mechanisms affecting its stability and RNA processing. It would also be interesting to perform a multi-gene approach, to explore whether any of these mechanisms can be widely generalized to lncRNAs. For instance, we could perform RNA sequencing as an alternative to RT-qPCR, to investigate multiple genes in parallel. Nevertheless, in the age of high-throughput studies, single-gene approaches remain invaluable as they allow for more focused experimental designs and can act as stepping stones for subsequent multi-gene studies.

Conclusion and Summary

In conclusion, we addressed multiple aspects of HOTAIRM1's post-transcriptional regulation, in an effort to understand more about this lncRNA which was shown to be involved in multiple cancers, both as an oncogene and as a tumor suppressor.

Aim 1: Determine HOTAIRM1's stability and half-life

We found that HMs is overall a highly stable transcript, which may hint at a maintenance role for this lncRNA. By contrast, HMu is a lot less stable, which may hint at a more regulatory role. In the context of cancer, where different cell lines and tissues express different HOTAIRM1 isoforms, this means that HOTAIRM1 may not only exhibit vastly different stabilities, but also that it may be performing different cellular functions, depending on cancer type. This may contribute to its intriguing alternative role in either promoting or preventing cancer.

Aim 2: Investigate destabilizing mechanisms affecting HOTAIRM1

We showed that translation destabilizes HOTAIRM1, and that this cannot be attributed to NMD, but rather to a separate translation-dependent mechanism which remains to be determined. We also found that the miRISC does not seem to be affecting HOTAIRM1 levels, neither independently from nor jointly with NMD. We suggest further investigation into HOTAIRM1-destabilizing mechanisms and recommend focusing on Non-Stop Decay (NSD) and No-Go Decay (NGD). This will help better understand HOTAIRM1's post-transcriptional regulation, which may prove useful for downstream applications such as targeting it in cancers in which it is implicated.

Aim 3: Elucidate potential links between HOTAIRM1 and miRNAs

We investigated the links between HOTAIRM1 and miRNAs, paying particular attention to miRNAs involved in cancer and those binding HOTAIRM1's alternatively spliced exon 2, and obtained a shortlist of 7 miRNAs warranting further investigation. Following experimental

confirmation of interactions between these RNAs in our models, it may be interesting to look into the functional implications of such binding, for instance if HOTAIRM1 is acting as a ceRNA or if it is inducing TDMD of associated miRNAs.

Overall, context-dependent alternative splicing of HOTAIRM1 and available miRNA pool may affect HOTAIRM1's half-life and post-transcriptional regulation through various RNA destabilizing mechanisms, which could potentially explain its compelling duality in cancer as oncogene and tumor suppressor.

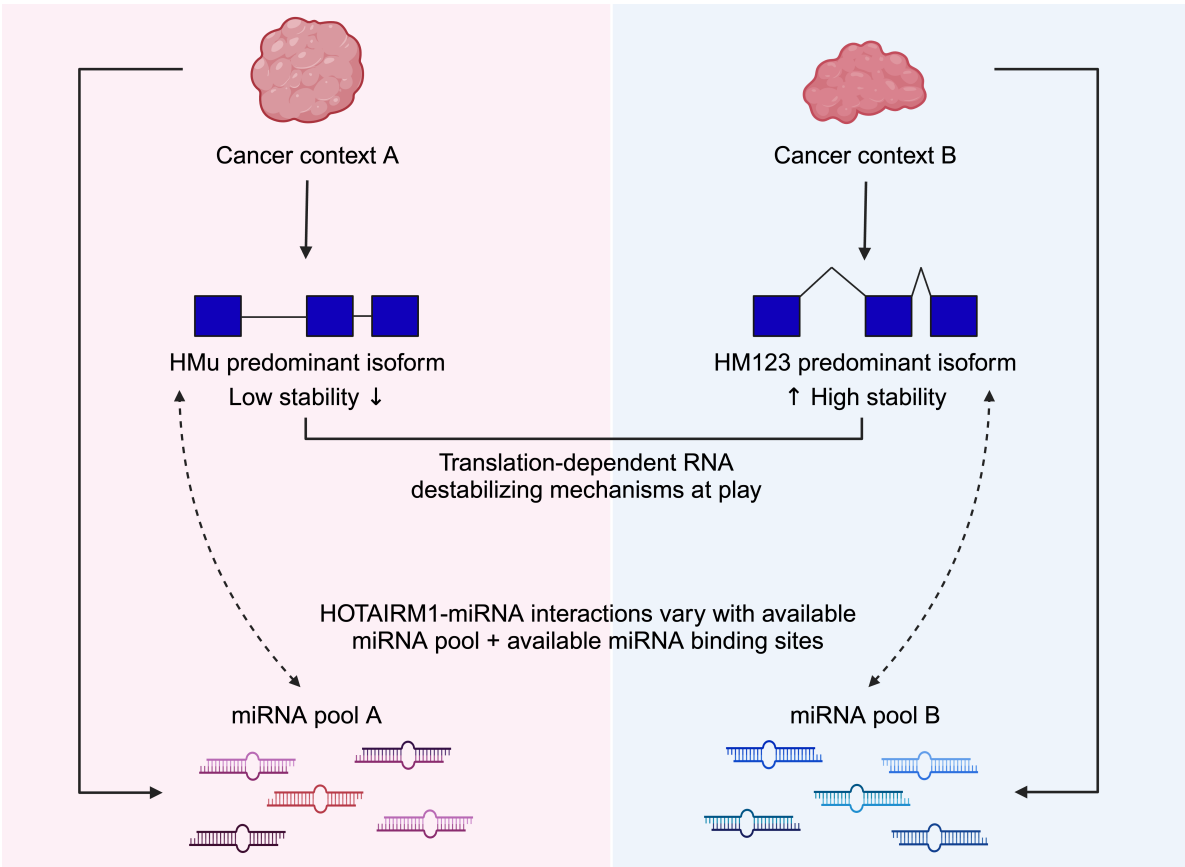

Figure 18. Current model for the post-transcriptional regulation of the lncRNA HOTAIRM1 involved in cancer. Depending on the specific cancer context, different HOTAIRM1 isoforms are expressed. These exhibit different half-lives, in a translation-dependent manner. In addition, cancer context affects the pool of miRNAs expressed which can interact with HOTAIRM1. These interactions depend not only on the available miRNAs, but also on HOTAIRM1's available binding sites, which are themselves determined by the HOTAIRM1 isoform expressed and the RNA-binding proteins expressed which may hinder miRNA-binding (7).

References

1. Crick, F., Barnett, L., Brenner, S., and Watts-Tobin, R. J. (1961) General nature of the genetic code for proteins. *Nature* **192**
2. Pachnis, V., Belayew, A., and Tilghman, S. M. (1984) Locus unlinked to alpha-fetoprotein under the control of the murine raf and Rif genes. *Proceedings of the National Academy of Sciences* **81**, 5523-5527
3. Jarroux, J., Morillon, A., and Pinskaya, M. (2017) History, Discovery, and Classification of lncRNAs. *Long Non Coding RNA Biology*, 1-46
4. Griffiths-Jones, S. (2007) Annotating noncoding RNA genes. *Annu. Rev. Genomics Hum. Genet.* **8**, 279-298
5. Eddy, S. R. (2001) Non–coding RNA genes and the modern RNA world. *Nature Reviews Genetics* **2**, 919-929
6. Joshi, M., and Rajender, S. (2020) Long non-coding RNAs (lncRNAs) in spermatogenesis and male infertility. *Reproductive Biology and Endocrinology* **18**, 1-18
7. Created with BioRender (2024).
8. Brown, C. J., Hendrich, B. D., Rupert, J. L., Lafreniere, R. G., Xing, Y., Lawrence, J., and Willard, H. F. (1992) The human XIST gene: analysis of a 17 kb inactive X-specific RNA that contains conserved repeats and is highly localized within the nucleus. *Cell* **71**, 527-542
9. Feil, R., Walter, J., Allen, N. D., and Reik, W. (1994) Developmental control of allelic methylation in the imprinted mouse Igf2 and H19 genes. *Development* **120**, 2933-2943
10. Bernstein, B., Birney, E., Dunham, I., Green, E., Gunter, C., and Snyder, M. Project Consortium ENCODE (2012) An integrated encyclopedia of DNA elements in the human genome. *Nature* **489**, 57-74

11. Feingold, E., Good, P., Guyer, M., Kamholz, S., Liefer, L., Wetterstrand, K., Collins, F., Gingeras, T., Kampa, D., and Sekinger, E. (2004) The ENCODE (ENCyclopedia of DNA elements) project. *Science* **306**, 636-640

12. Landt, S. G., Marinov, G. K., Kundaje, A., Kheradpour, P., Pauli, F., Batzoglou, S., Bernstein, B. E., Bickel, P., Brown, J. B., and Cayting, P. (2012) ChIP-seq guidelines and practices of the ENCODE and modENCODE consortia. *Genome research* **22**, 1813-1831

13. Kapranov, P., Willingham, A. T., and Gingeras, T. R. (2007) Genome-wide transcription and the implications for genomic organization. *Nature Reviews Genetics* **8**, 413-423

14. Pauli, A., Rinn, J. L., and Schier, A. F. (2011) Non-coding RNAs as regulators of embryogenesis. *Nature Reviews Genetics* **12**, 136-149

15. Niu, L., Lou, F., Sun, Y., Sun, L., Cai, X., Liu, Z., Zhou, H., Wang, H., Wang, Z., and Bai, J. (2020) A micropeptide encoded by lncRNA MIR155HG suppresses autoimmune inflammation via modulating antigen presentation. *Science advances* **6**, eaaz2059

16. Cai, B., Li, Z., Ma, M., Wang, Z., Han, P., Abdalla, B. A., Nie, Q., and Zhang, X. (2017) LncRNA-Six1 encodes a micropeptide to activate Six1 in Cis and is involved in cell proliferation and muscle growth. *Frontiers in physiology* **8**, 230

17. Wu, S., Guo, B., Zhang, L., Zhu, X., Zhao, P., Deng, J., Zheng, J., Li, F., Wang, Y., and Zhang, S. (2022) A micropeptide XBP1SBM encoded by lncRNA promotes angiogenesis and metastasis of TNBC via XBP1s pathway. *Oncogene* **41**, 2163-2172

18. Li, M., Shao, F., Qian, Q., Yu, W., Zhang, Z., Chen, B., Su, D., Guo, Y., Phan, A.-V., and Song, L.-s. (2021) A putative long noncoding RNA-encoded micropeptide maintains cellular homeostasis in pancreatic β cells. *Molecular Therapy-Nucleic Acids* **26**, 307-320

19. Spencer, H. L., Sanders, R., Boulberdaa, M., Meloni, M., Cochrane, A., Spiroski, A.-M., Mountford, J., Emanueli, C., Caporali, A., and Brittan, M. (2020) The LINC00961 transcript and its encoded micropeptide, small regulatory polypeptide of amino acid response, regulate endothelial cell function. *Cardiovascular Research* **116**, 1981-1994

20. Shatkin, A. (1976) Capping of eucaryotic mRNAs. *Cell* **9**, 645-653

21. Statello, L., Guo, C.-J., Chen, L.-L., and Huarte, M. (2021) Gene regulation by long non-coding RNAs and its biological functions. *Nature reviews Molecular cell biology* **22**, 96-118

22. Zhang, X., Wang, W., Zhu, W., Dong, J., Cheng, Y., Yin, Z., and Shen, F. (2019) Mechanisms and functions of long non-coding RNAs at multiple regulatory levels. *International journal of molecular sciences* **20**, 5573

23. Jin, J., Xie, S., Sun, Q., Huang, Z., Chen, K., Guo, D., Rao, X., Deng, Y., Liu, Y., and Li, S. (2020) Upregulation of BCAM and its sense lncRNA BAN are associated with gastric cancer metastasis and poor prognosis. *Molecular Oncology* **14**, 829-845

24. Li, L., Wang, Y., Song, G., Zhang, X., Gao, S., and Liu, H. (2019) HOX cluster-embedded antisense long non-coding RNAs in lung cancer. *Cancer letters* **450**, 14-21

25. Salagierski, M., Verhaegh, G. W., Jannink, S. A., Smit, F. P., Hessels, D., and Schalken, J. A. (2010) Differential expression of PCA3 and its overlapping PRUNE2 transcript in prostate cancer. *The Prostate* **70**, 70-78

26. Prensner, J. R., Iyer, M. K., Balbin, O. A., Dhanasekaran, S. M., Cao, Q., Brenner, J. C., Laxman, B., Asangani, I., Grasso, C., and Kominsky, H. D. (2011) Transcriptome sequencing identifies PCAT-1, a novel lincRNA implicated in prostate cancer progression. *Nature biotechnology* **29**, 742

27. Ma, Y., Zhang, J., Wen, L., and Lin, A. (2018) Membrane-lipid associated lncRNA: a new regulator in cancer signaling. *Cancer Letters* **419**, 27-29

28. Paraskevopoulou, M. D., and Hatzigeorgiou, A. G. (2016) Analyzing miRNA–lncRNA interactions. *Long non-coding RNAs: methods and protocols*, 271-286

29. Atianand, M. K., and Fitzgerald, K. A. (2014) Long non-coding RNAs and control of gene expression in the immune system. *Trends in molecular medicine* **20**, 623-631

30. Cheng, J.-T., Wang, L., Wang, H., Tang, F.-R., Cai, W.-Q., Sethi, G., Xin, H.-W., and Ma, Z. (2019) Insights into biological role of LncRNAs in epithelial-mesenchymal transition. *Cells* **8**, 1178

31. Zhang, X., Lian, Z., Padden, C., Gerstein, M. B., Rozowsky, J., Snyder, M., Gingeras, T. R., Kapranov, P., Weissman, S. M., and Newburger, P. E. (2009) A myelopoiesis-associated regulatory intergenic noncoding RNA transcript within the human HOXA cluster. *Blood* **113**, 2526-2534

32. Consortium, G. (2020) The GTEx Consortium atlas of genetic regulatory effects across human tissues. *Science* **369**, 1318-1330

33. Zhang, X., Lian, Z., Padden, C., Gerstein, M. B., Rozowsky, J., Snyder, M., Gingeras, T. R., Kapranov, P., Weissman, S. M., and Newburger, P. E. (2009) A myelopoiesis-associated regulatory intergenic noncoding RNA transcript within the human HOXA cluster. *Blood, The Journal of the American Society of Hematology* **113**, 2526-2534

34. Kim, C. Y., Oh, J. H., Lee, J.-Y., and Kim, M. H. (2020) The LncRNA HOTAIRM1 Promotes Tamoxifen Resistance by Mediating HOXA1 Expression in ER+ Breast Cancer Cells. *J Cancer* **11**, 3416-3423

35. Zhang, L., Zhang, J., Li, S., Zhang, Y., Liu, Y., Dong, J., Zhao, W., Yu, B., Wang, H., and Liu, J. (2021) Genomic amplification of long noncoding RNA HOTAIRM1 drives anaplastic thyroid cancer progression via repressing miR-144 biogenesis. *RNA biology* **18**, 547-562

36. Li, X., Pang, L., Yang, Z., Liu, J., Li, W., and Wang, D. (2019) LncRNA HOTAIRM1/HOXA1 axis promotes cell proliferation, migration and invasion in endometrial cancer. *OncoTargets and therapy* **12**, 10997

37. Liang, Q., Li, X., Guan, G., Xu, X., Chen, C., Cheng, P., Cheng, W., and Wu, A. (2019) Long non-coding RNA, HOTAIRM1, promotes glioma malignancy by forming a ceRNA network. *Aging* **11**, 6805

38. Shi, T., Guo, D., Xu, H., Su, G., Chen, J., Zhao, Z., Shi, J., Wedemeyer, M., Attenello, F., and Zhang, L. (2020) HOTAIRM1, an enhancer lncRNA, promotes glioma proliferation by regulating long-range chromatin interactions within HOXA cluster genes. *Molecular biology reports* **47**, 2723-2733

39. Li, Q., Dong, C., Cui, J., Wang, Y., and Hong, X. (2018) Over-expressed lncRNA HOTAIRM1 promotes tumor growth and invasion through up-regulating HOXA1 and sequestering G9a/EZH2/Dnmts away from the HOXA1 gene in glioblastoma multiforme. *Journal of Experimental & Clinical Cancer Research* **37**, 1-15

40. Lu, R., Zhao, G., Yang, Y., Jiang, Z., Cai, J., Zhang, Z., and Hu, H. (2019) Long noncoding RNA HOTAIRM1 inhibits cell progression by regulating miR-17-5p/PTEN axis in gastric cancer. *Journal of cellular biochemistry* **120**, 4952-4965

41. Chao, H., Zhang, M., Hou, H., Zhang, Z., and Li, N. (2020) HOTAIRM1 suppresses cell proliferation and invasion in ovarian cancer through facilitating ARHGAP24 expression by sponging miR-106a-5p. *Life Sciences* **243**, 117296

42. Li, D., Chai, L., Yu, X., Song, Y., Zhu, X., Fan, S., Jiang, W., Qiao, T., Tong, J., and Liu, S. (2020) The HOTAIRM1/miR-107/TDG axis regulates papillary thyroid cancer cell proliferation and invasion. *Cell death & disease* **11**, 1-14

43. Hamilton, M. J., Young, M., Jang, K., Sauer, S., Neang, V. E., King, A. T., Girke, T., and Martinez, E. (2020) HOTAIRM1 lncRNA is downregulated in clear cell renal cell carcinoma and inhibits the hypoxia pathway. *Cancer letters* **472**, 50-58

44. Wan, L., Kong, J., Tang, J., Wu, Y., Xu, E., Lai, M., and Zhang, H. (2016) HOTAIRM1 as a potential biomarker for diagnosis of colorectal cancer functions the role in the tumour suppressor. *Journal of Cellular and Molecular Medicine* **20**, 2036-2044

45. Ren, T., Hou, J., Liu, C., Shan, F., Xiong, X., Qin, A., Chen, J., and Ren, W. (2019) The long non-coding RNA HOTAIRM1 suppresses cell progression via sponging endogenous

miR-17-5p/B-cell translocation gene 3 (BTG3) axis in 5-fluorouracil resistant colorectal cancer cells. *Biomedicine & Pharmacotherapy* **117**, 109171

46. Wang, X. Q., and Dostie, J. (2017) Reciprocal regulation of chromatin state and architecture by HOTAIRM1 contributes to temporal collinear HOXA gene activation. *Nucleic acids research* **45**, 1091-1104
47. Segal, D., Coulombe, S., Sim, J., and Dostie, J. (2023) A conserved HOTAIRM1-HOXA1 regulatory axis contributes early to neuronal differentiation. *RNA biology* **20**, 1523-1539
48. Desmet, F.-O., Hamroun, D., Lalande, M., Collod-Béroud, G., Claustres, M., and Béroud, C. (2009) Human Splicing Finder: an online bioinformatics tool to predict splicing signals. *Nucleic acids research* **37**, e67-e67
49. Wang, H., Li, H., Jiang, Q., Dong, X., Li, S., Cheng, S., Shi, J., Liu, L., Qian, Z., and Dong, J. (2021) HOTAIRM1 promotes malignant progression of transformed fibroblasts in glioma stem-like cells remodeled microenvironment via regulating miR-133b-3p/TGFβ axis. *Frontiers in Oncology* **11**, 603128
50. Hao, Y., Li, X., Chen, H., Huo, H., Liu, Z., and Chai, E. (2020) Over-expression of long noncoding RNA HOTAIRM1 promotes cell proliferation and invasion in human glioblastoma by up-regulating SP1 via sponging miR-137. *Neuroreport* **31**, 109-117
51. Xie, P., Li, X., Chen, R., Liu, Y., Liu, D., Liu, W., Cui, G., and Xu, J. (2021) Upregulation of HOTAIRM1 increases migration and invasion by glioblastoma cells. *Aging* **13**, 2348
52. Chen, D., Li, Y., Wang, Y., and Xu, J. (2021) LncRNA HOTAIRM1 knockdown inhibits cell glycolysis metabolism and tumor progression by miR-498/ABCE1 axis in non-small cell lung cancer. *Genes & Genomics* **43**, 183-194
53. Gu, D., Tong, M., Wang, J., Zhang, B., Liu, J., Song, G., and Zhu, B. (2023) Overexpression of the lncRNA HOTAIRM1 promotes lenvatinib resistance by downregulating miR-34a and activating autophagy in hepatocellular carcinoma. *Discover Oncology* **14**, 66

54. Yu, X., Duan, W., Wu, F., Yang, D., Wang, X., Wu, J., Zhou, D., and Shen, Y. (2023) LncRNA-HOTAIRM1 promotes aerobic glycolysis and proliferation in osteosarcoma via the miR-664b-3p/Rheb/mTOR pathway. *Cancer Science* **114**, 3537-3552

55. Tang, Z., Li, C., Kang, B., Gao, G., Li, C., and Zhang, Z. (2017) GEPIA: a web server for cancer and normal gene expression profiling and interactive analyses. *Nucleic acids research* **45**, W98-W102

56. Weinstein, J. N., Collisson, E. A., Mills, G. B., Shaw, K. R., Ozenberger, B. A., Ellrott, K., Shmulevich, I., Sander, C., and Stuart, J. M. (2013) The cancer genome atlas pan-cancer analysis project. *Nature genetics* **45**, 1113-1120

57. Simms, C. L., Thomas, E. N., and Zaher, H. S. (2017) Ribosome-based quality control of mRNA and nascent peptides. *Wiley Interdisciplinary Reviews: RNA* **8**, e1366

58. Dever, T. E. (2002) Gene-specific regulation by general translation factors. *Cell* **108**, 545-556

59. Mars, J.-C., Ghram, M., Culjkovic-Kraljacic, B., and Borden, K. L. (2021) The cap-binding complex CBC and the eukaryotic translation factor eIF4E: co-conspirators in cap-dependent RNA maturation and translation. *Cancers* **13**, 6185

60. Pan, J., Wang, R., Shang, F., Ma, R., Rong, Y., and Zhang, Y. (2022) Functional micropeptides encoded by long non-coding RNAs: a comprehensive review. *Frontiers in molecular biosciences* **9**, 817517

61. Ruiz-Orera, J., Messeguer, X., Subirana, J. A., and Alba, M. M. (2014) Long non-coding RNAs as a source of new peptides. *elife* **3**, e03523

62. Ruiz-Orera, J., Villanueva-Cañas, J. L., and Albà, M. M. (2020) Evolution of new proteins from translated sORFs in long non-coding RNAs. *Experimental cell research* **391**, 111940

63. Pueyo, J. I., Magny, E. G., and Couso, J. P. (2016) New peptides under the s (ORF) ace of the genome. *Trends in biochemical sciences* **41**, 665-678

64. Richter, J. D., and Sonenberg, N. (2005) Regulation of cap-dependent translation by eIF4E inhibitory proteins. *Nature* **433**, 477-480

65. Zhao, J., Li, Y., Wang, C., Zhang, H., Zhang, H., Jiang, B., Guo, X., and Song, X. (2020) IRESbase: a comprehensive database of experimentally validated internal ribosome entry sites. *Genomics, proteomics & bioinformatics* **18**, 129-139

66. Ji, Z., Song, R., Regev, A., and Struhl, K. (2015) Many lncRNAs, 5'UTRs, and pseudogenes are translated and some are likely to express functional proteins. *elife* **4**, e08890

67. Chuang, T.-W., Su, C.-H., Wu, P.-Y., Chang, Y.-M., and Tarn, W.-Y. (2023) LncRNA HOTAIRM1 functions in DNA double-strand break repair via its association with DNA repair and mRNA surveillance factors. *Nucleic Acids Research* **51**, 3166-3184

68. Rombel, I. T., Sykes, K. F., Rayner, S., and Johnston, S. A. (2002) ORF-FINDER: a vector for high-throughput gene identification. *Gene* **282**, 33-41

69. Michel, A. M., Fox, G., M. Kiran, A., De Bo, C., O'Connor, P. B., Heaphy, S. M., Mullan, J. P., Donohue, C. A., Higgins, D. G., and Baranov, P. V. (2014) GWIPS-viz: development of a ribo-seq genome browser. *Nucleic acids research* **42**, D859-D864

70. Houseley, J., and Tollervey, D. (2009) The many pathways of RNA degradation. *Cell* **136**, 763-776

71. Deshmukh, M. V., Jones, B. N., Quang-Dang, D.-U., Flinders, J., Floor, S. N., Kim, C., Jemielity, J., Kalek, M., Darzynkiewicz, E., and Gross, J. D. (2008) mRNA decapping is promoted by an RNA-binding channel in Dcp2. *Molecular cell* **29**, 324-336

72. LaCava, J., Houseley, J., Saveanu, C., Petfalski, E., Thompson, E., Jacquier, A., and Tollervey, D. (2005) RNA degradation by the exosome is promoted by a nuclear polyadenylation complex. *Cell* **121**, 713-724

73. Vasudevan, S., and Steitz, J. A. (2007) AU-rich-element-mediated upregulation of translation by FXR1 and Argonaute 2. *Cell* **128**, 1105-1118

74. Clark, M. B., Johnston, R. L., Inostroza-Ponta, M., Fox, A. H., Fortini, E., Moscato, P., Dinger, M. E., and Mattick, J. S. (2012) Genome-wide analysis of long noncoding RNA stability. *Genome research* **22**, 885-898

75. Preker, P., Nielsen, J., Kammler, S., Lykke-Andersen, S., Christensen, M. S., Mapendano, C. K., Schierup, M. H., and Jensen, T. H. (2008) RNA exosome depletion reveals transcription upstream of active human promoters. *Science* **322**, 1851-1854

76. Lugowski, A., Nicholson, B., and Rissland, O. S. (2018) Determining mRNA half-lives on a transcriptome-wide scale. *Methods* **137**, 90-98

77. Bensaude, O. (2011) Inhibiting eukaryotic transcription. Which compound to choose? How to evaluate its activity? Which compound to choose? How to evaluate its activity? *Transcription* **2**, 103-108

78. Wilkinson, M. E., Charenton, C., and Nagai, K. (2020) RNA splicing by the spliceosome. *Annual review of biochemistry* **89**, 359-388

79. Deveson, I. W., Brunck, M. E., Blackburn, J., Tseng, E., Hon, T., Clark, T. A., Clark, M. B., Crawford, J., Dinger, M. E., and Nielsen, L. K. (2018) Universal alternative splicing of noncoding exons. *Cell Systems* **6**, 245-255. e245

80. Zuckerman, B., and Ulitsky, I. (2019) Predictive models of subcellular localization of long RNAs. *Rna* **25**, 557-572

81. Woodward, L. A., Mabin, J. W., Gangras, P., and Singh, G. (2017) The exon junction complex: a lifelong guardian of mRNA fate. *Wiley Interdisciplinary Reviews: RNA* **8**, e1411

82. Le Hir, H., Moore, M. J., and Maquat, L. E. (2000) Pre-mRNA splicing alters mRNP composition: evidence for stable association of proteins at exon–exon junctions. *Genes & development* **14**, 1098-1108

83. Le Hir, H., Izaurralde, E., Maquat, L. E., and Moore, M. J. (2000) The spliceosome deposits multiple proteins 20–24 nucleotides upstream of mRNA exon–exon junctions. *The EMBO journal* **19**, 6860-6869

84. Chan, C. C., Dostie, J., Diem, M. D., Feng, W., Mann, M., Rappsilber, J., and Dreyfuss, G. (2004) eIF4A3 is a novel component of the exon junction complex. *Rna* **10**, 200-209

85. Ferraiuolo, M. A., Lee, C.-S., Ler, L. W., Hsu, J. L., Costa-Mattioli, M., Luo, M.-J., Reed, R., and Sonenberg, N. (2004) A nuclear translation-like factor eIF4AIII is recruited to the mRNA during splicing and functions in nonsense-mediated decay. *Proceedings of the National Academy of Sciences* **101**, 4118-4123

86. Kataoka, N., Diem, M. D., Kim, V. N., Yong, J., and Dreyfuss, G. (2001) Magoh, a human homolog of Drosophila mago nashi protein, is a component of the splicing-dependent exon–exon junction complex. *The EMBO journal* **20**, 6424-6433

87. Bono, F., Ebert, J., Lorentzen, E., and Conti, E. (2006) The crystal structure of the exon junction complex reveals how it maintains a stable grip on mRNA. *Cell* **126**, 713-725

88. Merz, C., Urlaub, H., Will, C. L., and Lührmann, R. (2007) Protein composition of human mRNPs spliced in vitro and differential requirements for mRNP protein recruitment. *Rna* **13**, 116-128

89. Dostie, J., and Dreyfuss, G. (2002) Translation is required to remove Y14 from mRNAs in the cytoplasm. *Current Biology* **12**, 1060-1067

90. Diem, M. D., Chan, C. C., Younis, I., and Dreyfuss, G. (2007) PYM binds the cytoplasmic exon-junction complex and ribosomes to enhance translation of spliced mRNAs. *Nature structural & molecular biology* **14**, 1173-1179

91. Gehring, N. H., Lamprinaki, S., Kulozik, A. E., and Hentze, M. W. (2009) Disassembly of exon junction complexes by PYM. *Cell* **137**, 536-548

92. Nasif, S., Contu, L., and Mühlemann, O. (2018) Beyond quality control: The role of nonsense-mediated mRNA decay (NMD) in regulating gene expression. *Seminars in cell & developmental biology* **75**, 78-87

93. Lewis, B. P., Green, R. E., and Brenner, S. E. (2003) Evidence for the widespread coupling of alternative splicing and nonsense-mediated mRNA decay in humans. *Proceedings of the National Academy of Sciences* **100**, 189-192

94. Wery, M., Descrimes, M., Vogt, N., Dallongeville, A.-S., Gautheret, D., and Morillon, A. (2016) Nonsense-mediated decay restricts LncRNA levels in yeast unless blocked by double-stranded RNA structure. *Molecular cell* **61**, 379-392

95. Tani, H., Torimura, M., and Akimitsu, N. (2013) The RNA degradation pathway regulates the function of GAS5 a non-coding RNA in mammalian cells. *PloS one* **8**, e55684

96. Hwang, H. J., Park, Y., and Kim, Y. K. (2021) UPF1: from mRNA surveillance to protein quality control. *Biomedicines* **9**, 995

97. Bartel, D. P. (2018) Metazoan micrornas. *Cell* **173**, 20-51

98. Eulalio, A., Huntzinger, E., and Izaurralde, E. (2008) Getting to the root of miRNA-mediated gene silencing. *Cell* **132**, 9-14

99. Jin, H. Y., and Xiao, C. (2015) MicroRNA mechanisms of action: what have we learned from mice? *Frontiers in genetics* **6**, 328

100. Naeli, P., Winter, T., Hackett, A. P., Alboushi, L., and Jafarnejad, S. M. (2023) The intricate balance between microRNA-induced mRNA decay and translational repression. *The FEBS Journal* **290**, 2508-2524

101. Kuzuoğlu-Öztürk, D., Bhandari, D., Huntzinger, E., Fauser, M., Helms, S., and Izaurralde, E. (2016) mi RISC and the CCR 4–NOT complex silence mRNA targets independently of 43S ribosomal scanning. *The EMBO journal* **35**, 1186-1203

102. Bazzini, A. A., Lee, M. T., and Giraldez, A. J. (2012) Ribosome profiling shows that miR-430 reduces translation before causing mRNA decay in zebrafish. *Science* **336**, 233-237

103. Iwakawa, H.-o., and Tomari, Y. (2015) The functions of microRNAs: mRNA decay and translational repression. *Trends in cell biology* **25**, 651-665

104. Gu, S., and Kay, M. A. (2010) How do miRNAs mediate translational repression? *Silence* **1**, 1-5

105. Seidman, C. E., Struhl, K., Sheen, J., and Jessen, T. (1997) Introduction of plasmid DNA into cells. *Current protocols in molecular biology* **37**, 1-8

106. Schneider, C. A., Rasband, W. S., and Eliceiri, K. W. (2012) NIH Image to ImageJ: 25 years of image analysis. *Nature methods* **9**, 671-675

107. Damjanov, I., Horvat, B., and Gibas, Z. (1993) Retinoic acid-induced differentiation of the developmentally pluripotent human germ cell tumor-derived cell line, NCCIT. *Laboratory investigation; a journal of technical methods and pathology* **68**, 220-232

108. Abelson, H., Johnson, L., Penman, S. t., and Green, H. (1974) Changes in RNA in relation to growth of the fibroblast: II. The lifetime of mRNA, rRNA, and tRNA in resting and growing cells. *Cell* **1**, 161-165

109. O'Brien, K., Matlin, A. J., Lowell, A. M., and Moore, M. J. (2008) The biflavonoid isoginkgetin is a general inhibitor of Pre-mRNA splicing. *Journal of Biological Chemistry* **283**, 33147-33154

110. Younis, I., Berg, M., Kaida, D., Dittmar, K., Wang, C., and Dreyfuss, G. (2010) Rapid-response splicing reporter screens identify differential regulators of constitutive and alternative splicing. *Molecular and cellular biology* **30**, 1718-1728

111. Terpe, K. (2003) Overview of tag protein fusions: from molecular and biochemical fundamentals to commercial systems. *Applied microbiology and biotechnology* **60**, 523-533

112. Berman, H. M., Westbrook, J., Feng, Z., Gilliland, G., Bhat, T. N., Weissig, H., Shindyalov, I. N., and Bourne, P. E. (2000) The protein data bank. *Nucleic acids research* **28**, 235-242

113. Wheeler, E. C., Van Nostrand, E. L., and Yeo, G. W. (2018) Advances and challenges in the detection of transcriptome-wide protein–RNA interactions. *Wiley Interdisciplinary Reviews: RNA* **9**, e1436

114. Gutschner, T., Hämmerle, M., and Diederichs, S. (2013) MALAT1—a paradigm for long noncoding RNA function in cancer. *Journal of molecular medicine* **91**, 791-801

115. Karagkouni, D., Paraskevopoulou, M. D., Chatzopoulos, S., Vlachos, I. S., Tastsoglou, S., Kanellos, I., Papadimitriou, D., Kavakiotis, I., Maniou, S., and Skoufos, G. (2018) DIANA-TarBase v8: a decade-long collection of experimentally supported miRNA–gene interactions. *Nucleic acids research* **46**, D239-D245

116. Jeggari, A., Marks, D. S., and Larsson, E. (2012) miRcode: a map of putative microRNA target sites in the long non-coding transcriptome. *Bioinformatics* **28**, 2062-2063

117. Hamilton, M. P., Rajapakshe, K. I., Bader, D. A., Cerne, J. Z., Smith, E. A., Coarfa, C., Hartig, S. M., and McGuire, S. E. (2016) The Landscape of microRNA Targeting in Prostate Cancer Defined by AGO-PAR-CLIP. *Neoplasia* **18**, 356-370

118. Lipchina, I., Elkabetz, Y., Hafner, M., Sheridan, R., Mihailovic, A., Tuschl, T., Sander, C., Studer, L., and Betel, D. (2011) Genome-wide identification of microRNA targets in human ES cells reveals a role for miR-302 in modulating BMP response. *Genes Dev* **25**, 2173-2186

119. Choudhury, Y., Tay, F. C., Lam, D. H., Sandanaraj, E., Tang, C., Ang, B. T., and Wang, S. (2012) Attenuated adenosine-to-inosine editing of microRNA-376a* promotes invasiveness of glioblastoma cells. *J Clin Invest* **122**, 4059-4076

120. Gillen, A. E., Yamamoto, T. M., Kline, E., Hesselberth, J. R., and Kabos, P. (2016) Improvements to the HITS-CLIP protocol eliminate widespread mispriming artifacts. *BMC Genomics* **17**, 338

121. Shahab, S. W., Matyunina, L. V., Mezencev, R., Walker, L. D., Bowen, N. J., Benigno, B. B., and McDonald, J. F. (2011) Evidence for the complexity of microRNA-mediated regulation in ovarian cancer: a systems approach. *PLoS One* **6**, e22508

122. Chen, Z., Bian, C., Huang, J., Li, X., Chen, L., Xie, X., Xia, Y., Yin, R., and Wang, J. (2022) Tumor-derived exosomal HOTAIRM1 regulates SPON2 in CAFs to promote progression of lung adenocarcinoma. *Discover Oncology* **13**, 92

123. Imig, J., Brunschweiger, A., Brümmer, A., Guennewig, B., Mittal, N., Kishore, S., Tsikrika, P., Gerber, A. P., Zavolan, M., and Hall, J. (2015) miR-CLIP capture of a miRNA targetome uncovers a lincRNA H19–miR-106a interaction. *Nature chemical biology* **11**, 107-114

124. Xin, J., Li, J., Feng, Y., Wang, L., Zhang, Y., and Yang, R. (2017) Downregulation of long noncoding RNA HOTAIRM1 promotes monocyte/dendritic cell differentiation through competitively binding to endogenous miR-3960. *OncoTargets and therapy* **10**, 1307-1315

125. Chen, H. Y., Lang, Y. D., Lin, H. N., Liu, Y. R., Liao, C. C., Nana, A. W., Yen, Y., and Chen, R. H. (2019) miR-103/107 prolong Wnt/β-catenin signaling and colorectal cancer stemness by targeting Axin2. *Sci Rep* **9**, 9687

126. Wang, D. S., Zhong, B., Zhang, M. S., and Gao, Y. (2018) Upregulation of serum miR-103 predicts unfavorable prognosis in patients with colorectal cancer. *Eur Rev Med Pharmacol Sci* **22**, 4518-4523

127. Nonaka, R., Miyake, Y., Hata, T., Kagawa, Y., Kato, T., Osawa, H., Nishimura, J., Ikenaga, M., Murata, K., Uemura, M., Okuzaki, D., Takemasa, I., Mizushima, T., Yamamoto, H., Doki, Y., and Mori, M. (2015) Circulating miR-103 and miR-720 as novel serum biomarkers for patients with colorectal cancer. *Int J Oncol* **47**, 1097-1102

128. Ye, S., Lu, Y., Ru, Y., Wu, X., Zhao, M., Chen, J., Xu, M., Huang, Q., Wang, Y., Shi, S., Bu, S., and Xi, Y. (2020) LncRNAs GACAT3 and LINC00152 regulate each other through miR-103 and are associated with clinicopathological characteristics in colorectal cancer. *J Clin Lab Anal* **34**, e23378

129. Wei, F., Wang, Y., Zhou, Y., and Li, Y. (2021) Long noncoding RNA CYTOR triggers gastric cancer progression by targeting miR-103/RAB10. *Acta Biochim Biophys Sin* **53**, 1044-1054

130. Zheng, J., Liu, Y., Qiao, Y., Zhang, L., and Lu, S. (2017) miR-103 Promotes Proliferation and Metastasis by Targeting KLF4 in Gastric Cancer. *Int J Mol Sci* **18**, 910

131. Kanabe, B. O., Ozaslan, M., Aziz, S. A., Al-Attar, M. S., Kılıç İ, H., and Khailany, R. A. (2021) Expression patterns of LncRNA-GAS5 and its target APOBEC3C gene through miR-103 in breast cancer patients. *Cell Mol Biol* **67**, 5-10

132. Xiong, B., Lei, X., Zhang, L., and Fu, J. (2017) miR-103 regulates triple negative breast cancer cells migration and invasion through targeting olfactomedin 4. *Biomed Pharmacother* **89**, 1401-1408

133. Chen, L. P., Zhang, N. N., Ren, X. Q., He, J., and Li, Y. (2018) miR-103/miR-195/miR-15b Regulate SALL4 and Inhibit Proliferation and Migration in Glioma. *Molecules* **23**, 29-38

134. Port, M., Glaesener, S., Ruf, C., Riecke, A., Bokemeyer, C., Meineke, V., Honecker, F., and Abend, M. (2011) Micro-RNA expression in cisplatin resistant germ cell tumor cell lines. *Molecular cancer* **10**, 1-8

135. Jiang, D., Zhou, B., Xiong, Y., and Cai, H. (2019) miR-135 regulated breast cancer proliferation and epithelial-mesenchymal transition acts by the Wnt/β-catenin signaling pathway. *Int J Mol Med* **43**, 1623-1634

136. Yang, W., Feng, W., Wu, F., Gao, Y., Sun, Q., Hu, N., Lu, W., and Zhou, J. (2020) MiR-135-5p inhibits TGF-β-induced epithelial-mesenchymal transition and metastasis by targeting SMAD3 in breast cancer. *J Cancer* **11**, 6402-6412

137. Liu, Q., and Dong, H. (2021) EIF4A3-mediated hsa_circ_0088088 promotes the carcinogenesis of breast cancer by sponging miR-135-5p. *J Biochem Mol Toxicol* **35**, e22909

138. Taipaleenmäki, H., Browne, G., Akech, J., Zustin, J., van Wijnen, A. J., Stein, J. L., Hesse, E., Stein, G. S., and Lian, J. B. (2015) Targeting of Runx2 by miR-135 and miR-203 Impairs Progression of Breast Cancer and Metastatic Bone Disease. *Cancer Res* **75**, 1433-1444

139. Yin, L., Xu, G., Zhu, Y., and Wang, Y. (2019) Expression of miR-23a and miR-135 and tumor markers in gastric cancer patients and the significance in diagnosis. *Oncol Lett* **18**, 5853-5858

140. Han, W., Bu, X., Liu, Y., Liu, F., Ren, Y., Cui, Y., and Kong, S. (2021) Clinical value of miR-135 and miR-20a combined with multi-detector computed tomography in the diagnosis of gastric cancer. *World J Surg Oncol* **19**, 283

141. He, W., He, H., Zhang, N., Rui, W., Wang, X., Zhu, Y., and Xie, X. (2020) Associations between the expressions of MiR-135 and MiR-92a and pathogenesis of prostate cancer and analysis of their clinical significance. *J buon* **25**, 1619-1624

142. Yang, Y., Ishak Gabra, M. B., Hanse, E. A., Lowman, X. H., Tran, T. Q., Li, H., Milman, N., Liu, J., Reid, M. A., Locasale, J. W., Gil, Z., and Kong, M. (2019) MiR-135 suppresses glycolysis and promotes pancreatic cancer cell adaptation to metabolic stress by targeting phosphofructokinase-1. *Nat Commun* **10**, 809

143. Wang, X., Zhang, H., Yang, H., Bai, M., Ning, T., Deng, T., Liu, R., Fan, Q., Zhu, K., Li, J., Zhan, Y., Ying, G., and Ba, Y. (2020) Exosome-delivered circRNA promotes glycolysis to induce chemoresistance through the miR-122-PKM2 axis in colorectal cancer. *Mol Oncol* **14**, 539-555

144. Sendi, H., Yazdimamaghani, M., Hu, M., Sultanpuram, N., Wang, J., Moody, A. S., McCabe, E., Zhang, J., Graboski, A., Li, L., Rojas, J. D., Dayton, P. A., Huang, L., and Wang, A. Z. (2022) Nanoparticle Delivery of miR-122 Inhibits Colorectal Cancer Liver Metastasis. *Cancer Res* **82**, 105-113

145. Fong, M. Y., Zhou, W., Liu, L., Alontaga, A. Y., Chandra, M., Ashby, J., Chow, A., O'Connor, S. T., Li, S., Chin, A. R., Somlo, G., Palomares, M., Li, Z., Tremblay, J. R., Tsuyada, A., Sun, G., Reid, M. A., Wu, X., Swiderski, P., Ren, X., Shi, Y., Kong, M., Zhong, W., Chen, Y., and Wang, S. E. (2015) Breast-cancer-secreted miR-122 reprograms glucose metabolism in premetastatic niche to promote metastasis. *Nat Cell Biol* **17**, 183-194

146. Jiao, Y., Zhang, L., Li, J., He, Y., Zhang, X., and Li, J. (2021) Exosomal miR-122-5p inhibits tumorigenicity of gastric cancer by downregulating GIT1. *Int J Biol Markers* **36**, 36-46

147. Meng, L., Chen, Z., Jiang, Z., Huang, T., Hu, J., Luo, P., Zhang, H., Huang, M., Huang, L., Chen, Y., Lu, M., Xu, A. M., and Ying, S. (2020) MiR-122-5p suppresses the proliferation, migration, and invasion of gastric cancer cells by targeting LYN. *Acta Biochim Biophys Sin* **52**, 49-57

148. Zhu, H., Zeng, Y., Zhou, C. C., and Ye, W. (2018) SNHG16/miR-216-5p/ZEB1 signal pathway contributes to the tumorigenesis of cervical cancer cells. *Arch Biochem Biophys* **637**, 1-8

149. Cai, Z., Suo, L., and Huang, Z. (2021) Isoflurane Suppresses Proliferation, Migration, and Invasion and Facilitates Apoptosis in Colorectal Cancer Cells Through Targeting miR-216. *Front Med* **8**, 658926

150. Azevedo-Pouly, A. C., Sutaria, D. S., Jiang, J., Elgamal, O. A., Amari, F., Allard, D., Grippo, P. J., Coppola, V., and Schmittgen, T. D. (2017) miR-216 and miR-217 expression is reduced in transgenic mouse models of pancreatic adenocarcinoma, knockout of miR-216/miR-217 host gene is embryonic lethal. *Funct Integr Genomics* **17**, 203-212

151. Chen, X., Zhang, L., Song, Q., and Chen, Z. (2020) MicroRNA-216b regulates cell proliferation, invasion and cycle progression via interaction with cyclin T2 in gastric cancer. *Anticancer Drugs* **31**, 623-631

152. Zhang, T. J., Wu, D. H., Zhou, J. D., Li, X. X., Zhang, W., Guo, H., Ma, J. C., Deng, Z. Q., Lin, J., and Qian, J. (2018) Overexpression of miR-216b: Prognostic and predictive value in acute myeloid leukemia. *J Cell Physiol* **233**, 3274-3281

153. Liu, T., Ye, P., Ye, Y., and Han, B. (2021) MicroRNA-216b targets HK2 to potentiate autophagy and apoptosis of breast cancer cells via the mTOR signaling pathway. *Int J Biol Sci* **17**, 2970-2983

154. Xia, Y., Lv, J., Jiang, T., Li, B., Li, Y., He, Z., Xuan, Z., Sun, G., Wang, S., Li, Z., Wang, W., Wang, L., and Xu, Z. (2021) CircFAM73A promotes the cancer stem cell-like properties of gastric cancer through the miR-490-3p/HMGA2 positive feedback loop and HNRNPK-mediated β-catenin stabilization. *J Exp Clin Cancer Res* **40**, 103

155. Li, J., Xu, X., Liu, C., Xi, X., Wang, Y., Wu, X., and Li, H. (2021) MiR-490-5p Restrains Progression of Gastric cancer through DTL Repression. *Gastroenterol Res Pract* **2021**, 2894117

156. Luo, M., and Liang, C. (2020) LncRNA LINC00483 promotes gastric cancer development through regulating MAPK1 expression by sponging miR-490-3p. *Biol Res* **53**, 14

157. Zhen, H., Du, P., Yi, Q., Tang, X., and Wang, T. (2021) LINC00958 promotes bladder cancer carcinogenesis by targeting miR-490-3p and AURKA. *BMC Cancer* **21**, 1145

158. Fan, H., and Zhang, Y. S. (2019) miR-490-3p modulates the progression of prostate cancer through regulating histone deacetylase 2. *Eur Rev Med Pharmacol Sci* **23**, 539-546

159. Qin, D., Wei, R., Zhu, S., Min, L., and Zhang, S. (2021) MiR-490-3p Silences CDK1 and Inhibits the Proliferation of Colon Cancer Through an LLPS-Dependent miRISC System. *Front Mol Biosci* **8**, 561678

160. Zhang, Z. Y., Gao, X. H., Ma, M. Y., Zhao, C. L., Zhang, Y. L., and Guo, S. S. (2020) CircRNA_101237 promotes NSCLC progression via the miRNA-490-3p/MAPK1 axis. *Sci Rep* **10**, 9024

161. Tian, J., Xu, Y. Y., Li, L., and Hao, Q. (2017) MiR-490-3p sensitizes ovarian cancer cells to cisplatin by directly targeting ABCC2. *Am J Transl Res* **9**, 1127-1138

162. Fan, H., Yuan, J., Li, X., Ma, Y., Wang, X., Xu, B., and Li, X. (2020) LncRNA LINC00173 enhances triple-negative breast cancer progression by suppressing miR-490-3p expression. *Biomed Pharmacother* **125**, 109987

163. Liang, Y., Zhu, D., Hou, L., Wang, Y., Huang, X., Zhou, C., Zhu, L., Wang, Y., Li, L., Gu, Y., Luo, M., Wang, J., and Meng, X. (2020) MiR-107 confers chemoresistance to colorectal cancer by targeting calcium-binding protein 39. *Br J Cancer* **122**, 705-714

164. Zhang, Q., and Chen, Z. (2020) lncRNA UASR1 sponges miR-107 in colorectal cancer to upregulate oncogenic CDK8 and promote cell proliferation. *Oncol Lett* **20**, 305

165. Fu, Y., Lin, L., and Xia, L. (2019) MiR-107 function as a tumor suppressor gene in colorectal cancer by targeting transferrin receptor 1. *Cell Mol Biol Lett* **24**, 31

166. Pinho, J. D., Silva, G. E. B., Teixeira Júnior, A. A. L., Belfort, M. R. C., Mendes, J. M., Cunha, I. W. D., Quintana, L. G., Calixto, J. R. R., Nogueira, L. R., Coelho, R. W. P., and Khayat, A. S. (2020) MIR-107, MIR-223-3P and MIR-21-5P Reveals Potential Biomarkers in Penile Cancer. *Asian Pac J Cancer Prev* **21**, 391-397

167. Wang, G., Ma, C., Shi, X., Guo, W., and Niu, J. (2019) miR-107 Enhances the Sensitivity of Breast Cancer Cells to Paclitaxel. *Open Med (Wars)* **14**, 456-466

168. Luo, Y., Hua, T., You, X., Lou, J., Yang, X., and Tang, N. (2019) Effects of MiR-107 on The Chemo-drug Sensitivity of Breast Cancer Cells. *Open Med (Wars)* **14**, 59-65

169. Jin, D., Guo, J., Wu, Y., Yang, L., Wang, X., Du, J., Dai, J., Chen, W., Gong, K., Miao, S., Li, X., and Sun, H. (2020) m(6)A demethylase ALKBH5 inhibits tumor growth and metastasis by reducing YTHDFs-mediated YAP expression and inhibiting miR-107/LATS2-mediated YAP activity in NSCLC. *Mol Cancer* **19**, 40

170. Wei, X., Lei, Y., Li, M., Zhao, G., Zhou, Y., Ye, L., and Huang, Y. (2020) miR-107 inhibited malignant biological behavior of non-small cell lung cancer cells by regulating the STK33/ERK signaling pathway in vivo and vitro. *J Thorac Dis* **12**, 1540-1551

171. Kotipalli, A., Banerjee, R., Kasibhatla, S. M., and Joshi, R. (2021) Analysis of H3K4me3-ChIP-Seq and RNA-Seq data to understand the putative role of miRNAs and their target genes in breast cancer cell lines. *Genomics Inform* **19**, e17

172. de Anda-Jáuregui, G., Espinal-Enríquez, J., Drago-García, D., and Hernández-Lemus, E. (2018) Nonredundant, Highly Connected MicroRNAs Control Functionality in Breast Cancer Networks. *Int J Genomics* **2018**, 9585383

173. Kryczka, J., Migdalska-Sęk, M., Kordiak, J., Kiszałkiewicz, J. M., Pastuszak-Lewandoska, D., Antczak, A., and Brzeziańska-Lasota, E. (2021) Serum Extracellular Vesicle-Derived miRNAs in Patients with Non-Small Cell Lung Cancer-Search for Non-Invasive Diagnostic Biomarkers. *Diagnostics* **11**, 425

174. Mahn, R., Heukamp, L. C., Rogenhofer, S., von Ruecker, A., Müller, S. C., and Ellinger, J. (2011) Circulating microRNAs (miRNA) in serum of patients with prostate cancer. *Urology* **77**, 9-16

175. Su, Z., Hou, X. K., and Wen, Q. P. (2014) Propofol induces apoptosis of epithelial ovarian cancer cells by upregulation of microRNA let-7i expression. *Eur J Gynaecol Oncol* **35**, 688-691

176. Zhang, X., Weissman, S. M., and Newburger, P. E. (2014) Long intergenic non-coding RNA HOTAIRM1 regulates cell cycle progression during myeloid maturation in NB4 human promyelocytic leukemia cells. *RNA biology* **11**, 777-787

177. Han, W., Wang, S., Qi, Y., Wu, F., Tian, N., Qiang, B., and Peng, X. (2022) Targeting HOTAIRM1 ameliorates glioblastoma by disrupting mitochondrial oxidative phosphorylation and serine metabolism. *iScience* **25**, 104823

178. Rea, J., Menci, V., Tollis, P., Santini, T., Armaos, A., Garone, M. G., Iberite, F., Cipriano, A., Tartaglia, G. G., and Rosa, A. (2020) HOTAIRM1 regulates neuronal differentiation by modulating NEUROGENIN 2 and the downstream neurogenic cascade. *Cell death & disease* **11**, 527

179. Kim, C. Y., Oh, J. H., Lee, J.-Y., and Kim, M. H. (2020) The LncRNA HOTAIRM1 promotes tamoxifen resistance by mediating HOXA1 expression in ER+ breast cancer cells. *J Cancer* **11**, 3416

180. Nicolae, M., Mangul, S., Măndoiu, I. I., and Zelikovsky, A. (2011) Estimation of alternative splicing isoform frequencies from RNA-Seq data. *Algorithms for molecular biology* **6**, 1-13

181. Leung, C. L., Zheng, M., Prater, S. M., and Liem, R. K. (2001) The BPAG1 locus: alternative splicing produces multiple isoforms with distinct cytoskeletal linker domains, including predominant isoforms in neurons and muscles. *The Journal of cell biology* **154**, 691-698

182. Ryder, P. V., and Lerit, D. A. (2018) RNA localization regulates diverse and dynamic cellular processes. *Traffic* **19**, 496-502

183. Chin, A., and Lécuyer, E. (2017) RNA localization: Making its way to the center stage. *Biochimica et Biophysica Acta (BBA)-General Subjects* **1861**, 2956-2970

184. Lau, C.-K., Diem, M. D., Dreyfuss, G., and Van Duyne, G. D. (2003) Structure of the Y14-Magoh core of the exon junction complex. *Current Biology* **13**, 933-941

185. Andersen, C. B., Ballut, L., Johansen, J. S., Chamieh, H., Nielsen, K. H., Oliveira, C. L., Pedersen, J. S., Séraphin, B., Hir, H. L., and Andersen, G. R. (2006) Structure of the exon junction core complex with a trapped DEAD-box ATPase bound to RNA. *Science* **313**, 1968-1972

186. Nielsen, K. H., Chamieh, H., Andersen, C. B., Fredslund, F., Hamborg, K., Le Hir, H., and Andersen, G. R. (2009) Mechanism of ATP turnover inhibition in the EJC. *Rna* **15**, 67-75

187. Lerner, M. R., and Steitz, J. A. (1979) Antibodies to small nuclear RNAs complexed with proteins are produced by patients with systemic lupus erythematosus. *Proceedings of the National Academy of Sciences* **76**, 5495-5499

188. Tenenbaum, S. A., Carson, C. C., Lager, P. J., and Keene, J. D. (2000) Identifying mRNA subsets in messenger ribonucleoprotein complexes by using cDNA arrays. *Proceedings of the National Academy of Sciences* **97**, 14085-14090

189. Ule, J., Jensen, K. B., Ruggiu, M., Mele, A., Ule, A., and Darnell, R. B. (2003) CLIP identifies Nova-regulated RNA networks in the brain. *Science* **302**, 1212-1215

190. Tani, H., and Akimitsu, N. (2012) Genome-wide technology for determining RNA stability in mammalian cells: historical perspective and recent advantages based on modified nucleotide labeling. *RNA biology* **9**, 1233-1238

191. Imamachi, N., Tani, H., Mizutani, R., Imamura, K., Irie, T., Suzuki, Y., and Akimitsu, N. (2014) BRIC-seq: a genome-wide approach for determining RNA stability in mammalian cells. *Methods* **67**, 55-63

192. Ideue, T., Adachi, S., Naganuma, T., Tanigawa, A., Natsume, T., and Hirose, T. (2012) U7 small nuclear ribonucleoprotein represses histone gene transcription in cell cycle-arrested cells. *Proceedings of the National Academy of Sciences* **109**, 5693-5698

193. Tani, H., Mizutani, R., Salam, K. A., Tano, K., Ijiri, K., Wakamatsu, A., Isogai, T., Suzuki, Y., and Akimitsu, N. (2012) Genome-wide determination of RNA stability reveals hundreds of short-lived noncoding transcripts in mammals. *Genome research* **22**, 947-956

194. Ayupe, A. C., and Reis, E. M. (2017) Evaluating the stability of mRNAs and noncoding RNAs. *Enhancer RNAs: Methods and Protocols*, 139-153

195. t Hoen, P. A., Hirsch, M., de Meijer, E. J., de Menezes, R. X., van Ommen, G. J., and den Dunnen, J. T. (2011) mRNA degradation controls differentiation state-dependent differences in transcript and splice variant abundance. *Nucleic Acids Res* **39**, 556-566

196. Chen, L. (2010) A global comparison between nuclear and cytosolic transcriptomes reveals differential compartmentalization of alternative transcript isoforms. *Nucleic acids research* **38**, 1086-1097

197. Wu, Z., Lin, Y., and Wei, N. (2023) N6-methyladenosine-modified HOTAIRM1 promotes vasculogenic mimicry formation in glioma. *Cancer Science* **114**, 129-141

198. Zheng, G., Dahl, J. A., Niu, Y., Fedorcsak, P., Huang, C. M., Li, C. J., Vågbø, C. B., Shi, Y., Wang, W. L., Song, S. H., Lu, Z., Bosmans, R. P., Dai, Q., Hao, Y. J., Yang, X., Zhao, W. M., Tong, W. M., Wang, X. J., Bogdan, F., Furu, K., Fu, Y., Jia, G., Zhao, X., Liu, J.,

Krokan, H. E., Klungland, A., Yang, Y. G., and He, C. (2013) ALKBH5 is a mammalian RNA demethylase that impacts RNA metabolism and mouse fertility. *Mol Cell* **49**, 18-29

199. Huang, H., Weng, H., Sun, W., Qin, X., Shi, H., Wu, H., Zhao, B. S., Mesquita, A., Liu, C., Yuan, C. L., Hu, Y. C., Hüttelmaier, S., Skibbe, J. R., Su, R., Deng, X., Dong, L., Sun, M., Li, C., Nachtergaele, S., Wang, Y., Hu, C., Ferchen, K., Greis, K. D., Jiang, X., Wei, M., Qu, L., Guan, J. L., He, C., Yang, J., and Chen, J. (2018) Recognition of RNA N(6)-methyladenosine by IGF2BP proteins enhances mRNA stability and translation. *Nat Cell Biol* **20**, 285-295

200. He, P. C., Wei, J., Dou, X., Harada, B. T., Zhang, Z., Ge, R., Liu, C., Zhang, L. S., Yu, X., Wang, S., Lyu, R., Zou, Z., Chen, M., and He, C. (2023) Exon architecture controls mRNA m(6)A suppression and gene expression. *Science* **379**, 677-682

201. Yang, X., Triboulet, R., Liu, Q., Sendinc, E., and Gregory, R. I. (2022) Exon junction complex shapes the m6A epitranscriptome. *Nature Communications* **13**, 7904

202. Powers, K. T., Szeto, J.-Y. A., and Schaffitzel, C. (2020) New insights into no-go, non-stop and nonsense-mediated mRNA decay complexes. *Current Opinion in Structural Biology* **65**, 110-118

203. Monaghan, L., Longman, D., and Cáceres, J. F. (2023) Translation-coupled mRNA quality control mechanisms. *The EMBO Journal* **42**, e114378

204. Doma, M. K., and Parker, R. (2006) Endonucleolytic cleavage of eukaryotic mRNAs with stalls in translation elongation. *Nature* **440**, 561-564

205. Tollervey, D. (2006) RNA lost in translation. *Nature* **440**, 425-426

206. Clement, S. L., and Lykke-Andersen, J. (2006) No mercy for messages that mess with the ribosome. *Nature structural & molecular biology* **13**, 299-301

207. Passos, D. O., Doma, M. K., Shoemaker, C. J., Muhlrad, D., Green, R., Weissman, J., Hollien, J., and Parker, R. (2009) Analysis of Dom34 and its function in no-go decay. *Molecular biology of the cell* **20**, 3025-3032

208. Van Hoof, A., Frischmeyer, P. A., Dietz, H. C., and Parker, R. (2002) Exosome-mediated recognition and degradation of mRNAs lacking a termination codon. *Science* **295**, 2262-2264

209. Frischmeyer, P. A., Van Hoof, A., O'Donnell, K., Guerrerio, A. L., Parker, R., and Dietz, H. C. (2002) An mRNA surveillance mechanism that eliminates transcripts lacking termination codons. *Science* **295**, 2258-2261

210. Wagner, E., and Lykke-Andersen, J. (2002) mRNA surveillance: the perfect persist. *Journal of Cell Science* **115**, 3033-3038

211. Anderson, J. S. J., and Parker, R. (1998) The 3′ to 5′ degradation of yeast mRNAs is a general mechanism for mRNA turnover that requires the SKI2 DEVH box protein and 3′ to 5′ exonucleases of the exosome complex. *The EMBO journal* **17**, 1497-1506

212. Schmid, M., and Jensen, T. H. (2008) The exosome: a multipurpose RNA-decay machine. *Trends in biochemical sciences* **33**, 501-510

213. D'Lima, N. G., Ma, J., Winkler, L., Chu, Q., Loh, K. H., Corpuz, E. O., Budnik, B. A., Lykke-Andersen, J., Saghatelian, A., and Slavoff, S. A. (2017) A human microprotein that interacts with the mRNA decapping complex. *Nature chemical biology* **13**, 174-180

214. Wu, Q., Medina, S. G., Kushawah, G., DeVore, M. L., Castellano, L. A., Hand, J. M., Wright, M., and Bazzini, A. A. (2019) Translation affects mRNA stability in a codon-dependent manner in human cells. *eLife* **8**, e45396

215. Jo, B.-S., and Choi, S. S. (2015) Introns: the functional benefits of introns in genomes. *Genomics & informatics* **13**, 112

216. Lai, D., and Meyer, I. M. (2016) A comprehensive comparison of general RNA–RNA interaction prediction methods. *Nucleic acids research* **44**, e61-e61

217. Wu, P.-H., and Zamore, P. D. (2021) To degrade a microRNA, destroy its argonaute protein. *Molecular Cell* **81**, 223-225

218. Cazalla, D., Yario, T., and Steitz, J. A. (2010) Down-regulation of a host microRNA by a Herpesvirus saimiri noncoding RNA. *Science* **328**, 1563-1566

219. Ameres, S. L., Horwich, M. D., Hung, J.-H., Xu, J., Ghildiyal, M., Weng, Z., and Zamore, P. D. (2010) Target RNA–directed trimming and tailing of small silencing RNAs. *Science* **328**, 1534-1539

220. Shi, C. Y., Kingston, E. R., Kleaveland, B., Lin, D. H., Stubna, M. W., and Bartel, D. P. (2020) The ZSWIM8 ubiquitin ligase mediates target-directed microRNA degradation. *Science* **370**, eabc9359

221. Han, J., LaVigne, C. A., Jones, B. T., Zhang, H., Gillett, F., and Mendell, J. T. (2020) A ubiquitin ligase mediates target-directed microRNA decay independently of tailing and trimming. *Science* **370**, eabc9546

Appendix (Supplemental data)

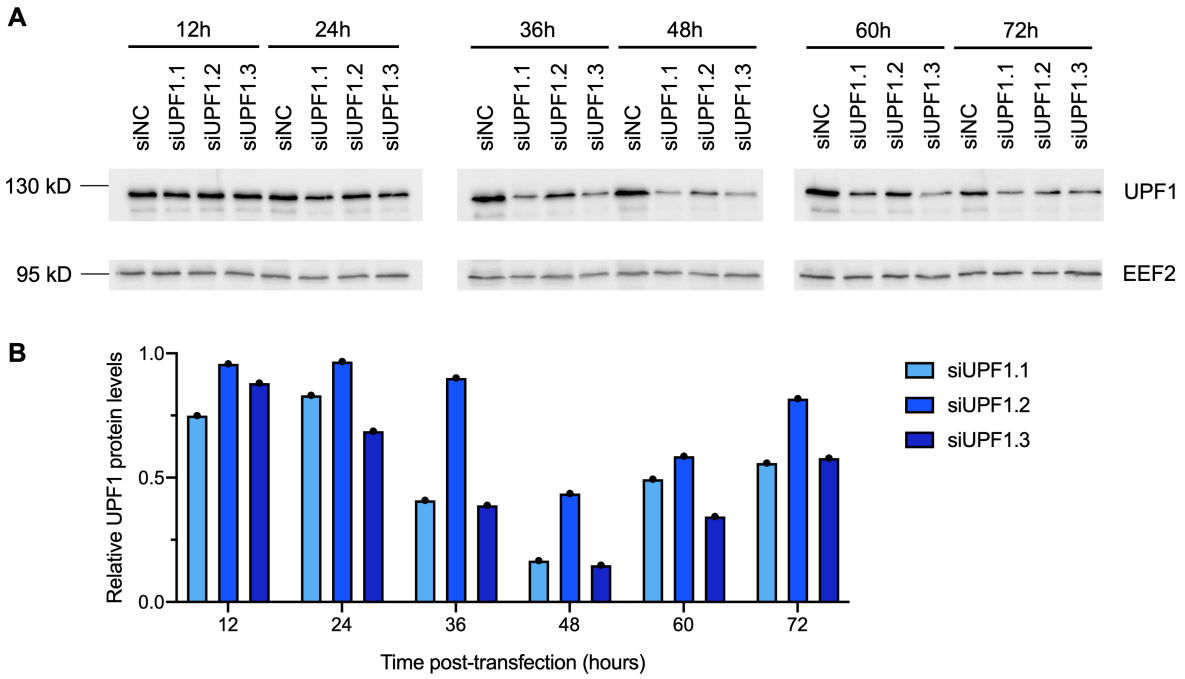

Supplemental data 1. Preliminary knockdown time course for optimization, testing three UPF1 siRNAs over six time points. (A) Western blot assessment of knockdown, comparing the non-coding siRNA control (siNC) to three UPF1-targeting siRNAs (siUPF1.1, siUPF1.2 and siUPF1.3). EEF2 is used as a control. (B) Quantification of UPF1 protein levels from the western blot, relative to siNC and to EEF2 levels. (n=1)

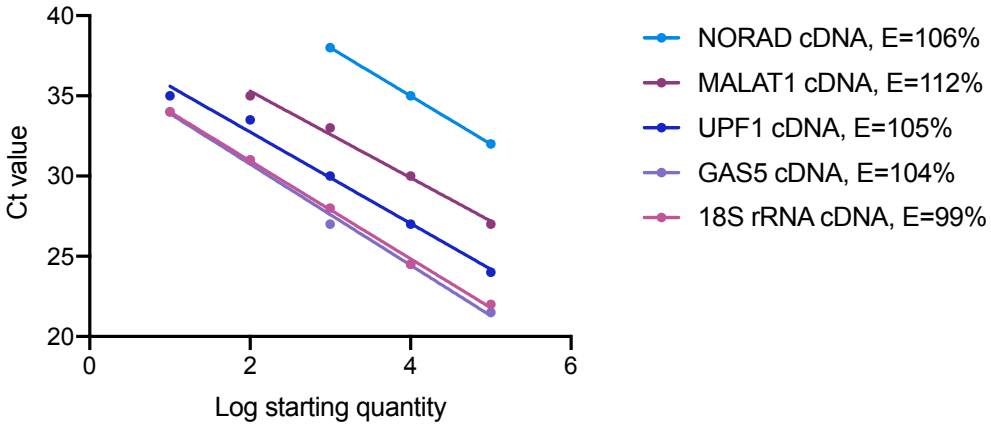

Supplemental data 2. Primer pair efficiency testing of novel NORAD, MALAT1, UPF1, GAS5 and 18S rRNA primer pairs. cDNA samples from total HEK293T cells were quantified using five 8-fold serial dilutions. Results were analyzed using CFX Manager and CFX Maestro software, validating primer pairs whose E-value is above 85% and below 115%.

Supplemental data 3. Comprehensive available list of HOTAIRM1-binding miRNAs.

miRNA	miRcode	TarBase v8	Literature
let-7b-5p		x	
let-7c-5p		x	
let-7d-5p		x	
let-7i-3p		x	
miR-103	x	x	
miR-106a-5p		x	x
miR-106b-5p		x	x
miR-107	x		x
miR-1179		x	
miR-122	x		
miR-125b			x
miR-1296-5p		x	
miR-129a-5p	x		x
miR-129b-5p	x		x
miR-130a-3p		x	
miR-130b-3p		x	
miR-132-3p		x	
miR-133b-3p			x
miR-135a	x		
miR-137	x		x
miR-148a-3p	x	x	
miR-148b-3p	x		
miR-150-5p	x		
miR-152	x		
miR-153-50			x
miR-15a-3p		x	
miR-17-5p	x	x	x
miR-181a-5p		x	
miR-181b-5p		x	
miR-181c-5p		x	
miR-181d-5p		x	
miR-182-5p			
miR-18a-5p		x	
miR-200b-3p		x	
miR-20a-5p	x	x	x
miR-20b-5p	x	x	
miR-212-3p		x	
miR-216a	x		
miR-216b-5p	x		
miR-22-3p	x	x	

miR-224-5p		x	
miR-25-3p		x	
miR-26a-5p		x	
miR-26b-5p		x	
miR-29a-3p		x	
miR-29b-3p		x	
miR-29c-3p		x	
miR-302a-3p		x	
miR-30e-3p		x	
miR-31-5p		x	
miR-3127-5p		x	
miR-3180-3p		x	
miR-320b		x	
miR-328-5p			x
miR-330-3p		x	
miR-335-3p		x	
miR-338-3p	x		
miR-34a			x
miR-376a-5p		x	
miR-3960			x
miR-423-3p		x	
miR-423-5p		x	
miR-424-5p		x	
miR-427	x		
miR-449a		x	
miR-449b-5p		x	
miR-4525		x	
miR-454-3p		x	
miR-490-3p	x		
miR-490-5p		x	
miR-495-3p			x
miR-498			x
miR-501-5p		x	
miR-5127	x		
miR-518a-3p	x		
miR-519d-3p	x		
miR-629-5p		x	
miR-664-30			x
miR-7-5p		x	
miR-93-5p	x	x	
miR-99a-3p		x	
miR-99b-3p		x	